Institute of Astronautics
Prof. Prof. h.c. Dr. Dr. h.c.
Ulrich Walter

Master's Thesis
W-band for CubeSat Applications

RT-MA-2016/15

Author:
Stefan Scheiblauer

Supervisor: Dr.-Ing. Martin Rott
Dipl.-Ing. (Univ.) Martin Langer
Institute of Astronautics
Technische Universität München

Declaration of Authorship

This thesis is a presentation of my original research work. Wherever contributions of others are involved, every effort is made to indicate this clearly, with due reference to the literature, and acknowledgement of collaborative research and discussions.

Munich, _____

_____

Author's signature

Abstract

The increasing data amount generated by current and future earth observation missions requires high data rate downlinks to avoid data loss. The large bandwidth available in the W-band (75–110 GHz) serves the need for the high throughput of scientific data but also allows a wide range of commercial broadcast and Internet services. Aside from the advantages of large bandwidth, reduced interference and decreased equipment size the impairments by the troposphere are insufficiently modeled as models are only validated up to 50 GHz. This stresses the need for spaceborne atmospheric attenuation measurements concurrent with rain measurements to enhance these models and set up statistics on the rain fades in W-band.
The objective of this phase 0/A feasibility study was to close this gap with a Cube-Sat W-band channel characterization mission. First a list of requirements for attenuation measurements and data transmission experiment shall be derived. The question how a first order payload concept and corresponding low earth orbit (LEO) satellite concepts look like shall be addressed.
From climate observations in Munich, for every month five distinct weather scenarios were selected. Based on these climate variables the tropospheric attenuation was simulated with the radio frequency propagation models recommended by the International Telecommunication Union (ITU). With the strongest attenuation occurring in July, 17.5 dB in zenith direction, the link calculations were performed for a beacon transmit power of 3.3 W. Binary phase-shift keying (BPSK) with a coding rate of 7/8 ensures at least a 1 Mb/s link for total losses below 197.6 dB and 10 Mb/s for total losses below 187.6 dB. The selected optimal conical horn fits in a 33 mm wide instrument and is supported by commercial off-the-shelf (COTS) subsystems. Utilizing the Space Mission Analysis and Design (SMAD) procedures resulted in three satellite concepts orbiting in a sun-synchronous repeat track at an altitude of 570 km. A magnetic torquer controls the attitude of the 1U satellite concept A, which comprises a nadir looking instrument. In concept B (1U) magnetic torquers point the instrument at the ground station. An integrated attitude control system points the satellite of concept C (1.5U).
During the study it became clear, that the selected power subsystem limits the mission life time to 2.2 years. Therefore, the planned step-wise measurement procedure comprising both, attenuation measurements and data transmission experiments is not realizable. The author suggests to further investigate two separate missions. The first mission dedicated to attenuation measurements and the second to data transmission. For concurrent attenuation measurements and rain observations a nadir pointing concept is sufficient to quantify atmospheric phenomena linked to the ground station location. For the data transmission it is inevitable to point at the ground station to maximize the transmission time.

Zusammenfassung

Die zunehmende Datenmenge, die durch aktuelle und künftige Erdbeobachtungsmissionen erzeugt wird, erfordert hohe Übertragungsraten, um Datenverlust zu vermeiden. Die hohe Bandbreite die im W-Band (75–110 GHz) zur Verfügung steht erlaubt nicht nur einen hohen Durchsatz von wissenschaftlichen Daten, sondern ermöglicht auch eine breite Palette von kommerziellen Rundfunk-und Internet-Diensten. Abgesehen von den Vorteilen der Bandbreite, reduzierter Interferenz und verringerter Baugröße der Instrumente ist die Signaldämpfung durch die Troposphäre unzureichend modelliert. Weiters sind die verfügbaren Modelle nur bis 50 GHz validiert. Dies unterstreicht die Notwendigkeit von satellitengestützten Dämpfungsmessungen der Atmosphäre mit gleichzeitigen Regenmessungen. Somit können Dämpfungsmodelle verbessert werden und Statistiken über die Dämpfung im W-band durch Regen erstellt werden.
Das Ziel dieser Machbarkeitsstudie war es, diese Lücke mit einer CubeSat W-Band Messkampagne zu schließen. Zunächst sollte eine Liste von Anforderungen für die Dämpfungsmessungen und Datenübertragungsexperimente erarbeitet werden. Die Frage, wie ein Payload-Entwurf und entsprechende Satelliten-Konzepte in einer erdnahen Umlaufbahn aussehen könnten wurde ebenfalls untersucht.
Aus Klimabeobachtungen in München, wurden für jeden Monat fünf verschiedene Wetterszenarien ausgewählt. Basierend auf diesen Klimavariablen wurde die troposphärische Dämpfung mit den Modellen der Internationale Fernmeldeunion (ITU) simuliert. Mit der stärksten Dämpfung im Juli, 17,5 dB in Zenith-Richtung, wurde die Leistungsübertragungsbilanz für eine Sendeleistung von 3,3 W berechnet. Die Binär-Phasenumtastung (BPSK) sorgt mit einer Informationsrate von 7/8 mindestens für eine 1 Mb/s-Verbindung bei Dämpfungen unter 197,6 dB und 10 Mb/s für Gesamtverluste kleiner 187,6 dB. Das ausgewählte optimale Kegelhorn paßt in ein 33 mm breites Instrument und wird von commercial off-the-shelf (COTS) Subsystemen versorgt. Anwenden der Space Mission Analysis and Design (SMAD) Methoden führte zu drei Satellitenkonzepten in einem sonnensynchronen Orbit in einer Höhe von 570 km. Ein Magnettorquer übernimmt die Lageregelung des 1U Satellitenkonzepts A, das einen nadir zeigenden Sender umfaßt. Im Konzept B (1U) wird das Instrument mit dem Magnettorquer auf die Bodenstation ausgerichtet. Im Konzepts C (1.5U) wird dies von einer vollintegrierten Lageregelung übernommen.
Während der Studie wurde deutlich, daß das gewählte Power-Subsystem die Missionslebesdauer auf 2,2 Jahre beschränkt. Daher ist der geplante schrittweise Experimentablauf, der sowohl Dämpfungsmessungen als auch Datenübertragungsexperimente beinhaltet, nicht realisierbar. Der Autor schlägt vor, zwei verschiedene Missionen weiter zu untersuchen. Der erste Mission soll auf Dämpfungsmessungen spezialisiert sein und die zweite auf Datenübertragung. Für gleichzeitige Dämpfungsmessungen und Regenmessungen ist ein nadir pointing Konzept ausreichend, um atmosphärische Phänomene, die mit dem Standort verbunden sind, zu quantifizieren. Für die Datenübertragung ist es unvermeidlich, den Sender auf die Bodenstation auszurichten, um die Übertragungszeit zu maximieren.

Contents

1 INTRODUCTION 1

1.1 Motivation of the thesis 3

1.2 Terminology 3

1.3 Current research 3

2 MISSION OVERVIEW 7

2.1 Background 7
2.1.1 Gaseous absorption by oxygen and water vapor 7
2.1.2 Cloud attenuation 8
2.1.3 Rain attenuation 9
2.1.4 Scintillation 9
2.1.5 Atmospheric noise 10
2.1.6 Atmosphere over Munich 10

2.2 Scientific objectives 11
2.2.1 Mission functional requirements 13
2.2.2 System requirements 13
2.2.3 Operation and ground segment 14

3 PROPAGATION SIMULATIONS 17

3.1 Gaseous attenuation 17

3.2 Attenuation by clouds 17

3.3 Attenuation by rain 18

3.4 Attenuation by scintillation 19

3.5 Total tropospheric attenuation 19

4 SIMULATION RESULTS 21

4.1 Orbit 21
4.1.1 Orbital life time 21
4.1.2 Contact times 22

4.2 Atmospheric attenuation 22

4.3 Discussion on simulation results 26

5 PAYLOAD INSTRUMENT AND SYSTEM CONCEPT 29

5.1 Concept of operations 29

5.2 Instrument design **30**
5.2.1 W-band transmission chain 31
5.2.2 Antenna parameter 32
5.2.3 Dimensions 37
5.2.4 Payload budgets 37

5.3 Satellite concept **38**
5.3.1 Satellite concept magnetic torquer (concept A, B) 39
5.3.2 Satellite concept ADCS (concept C) 40

5.4 Budgets **40**
5.4.1 Power 40
5.4.2 Communication 43
5.4.3 Mass 43

5.5 Identification of launch opportunities **43**

5.6 Discussion **44**

6 DATA PROCESSING AND VALIDATION CONCEPT **47**

6.1 Measurement and statistics **47**

6.2 Separation of multiple attenuation sources **50**

6.3 Discussion on data processing **53**

7 CONCLUSION **55**

7.1 Suggestions for further studies **56**

BIBLIOGRAPHY **56**

A FIRST APPENDIX **67**

A.1 Atmospheric simulations **67**
A.1.1 Gaseous attenuation 69
A.1.2 Cloud attenuation 70
A.1.3 Rain attenuation 71
A.1.4 Scintillation 73
A.1.5 Standard atmosphere 74

A.2 Payload design **77**
A.2.1 Link budget 77
A.2.2 Power Budget 79
A.2.3 Optimum conical horn 79
A.2.4 Estimated downlinked data volume 80
A.2.5 Bit error rate for BPSK 81

List of Figures

Fig. 1–1: Overview of the frequency allocations and nomenclature in the range from 60–110 GHz 4

Fig. 2–1: Specific gaseous attenuation in the EHF region 8
Fig. 2–2: Multiple sources of tropospheric attenuation. Parabolic antenna: mahorova-works, [Online]. Available: http://free-icon-rainbow.com, [acccessed: 09.01.2017] 10

Fig. 4–1: Total tropospheric attenuation in January as function of the elevation angle for five distinct weather scenarios 23
Fig. 4–2: Total tropospheric attenuation in July (worst month) for five distinct weather scenarios in dependence of the elevation angle 23
Fig. 4–3: Sky noise temperature in July (worst month) during clear sky and different cloud covers depending on elevation angle 24
Fig. 4–4: Individual sources of signal fades during heavy rain in July (worst month) 25
Fig. 4–5: Total tropospheric attenuation as function of outage time percentage and elevation angle in July 25

Fig. 5–1: Attitude during experimental mode. 1: nominal mode, transmitter on at 85° northern latitude; 2–4: orientation towards ground station, W-band experiments; 5: return to nominal mode, transmitter off at the equator Globe: MazeNL77, [Online]. Available: http://findicons.com, [accessed: 09.01.2017] 30
Fig. 5–2: The elements of the W-band transmission chain. 31
Fig. 5–3: Antenna gain for an optimal conical horn in dependence of the horn length. The right scale shows the required transmit power for an EIRP of 30 dBi at a given horn length aperture diameter respectively 33
Fig. 5–4: Maximum total loss (free space and tropospheric) for a 1 Mb/s and a 10 Mb/s link in January depending on the weather situation, EIRP of 30 dBi, E_b/N_0 of 10 dB 34
Fig. 5–5: Maximum total loss (free space and tropospheric) for a 1 Mb/s and a 10 Mb/s link in July depending on the weather situation, EIRP of 30 dBi, E_b/N_0 of 10 dB 35
Fig. 5–6: Maximum downlink data rate with EIRP of 30 dBi, E_b/N_0 of 10 dB in January 36
Fig. 5–7: Maximum downlink data rate with EIRP of 30 dBi, E_b/N_0 of 10 dB in July 36
Fig. 5–8: BER analysis for various coding rates 37
Fig. 5–9: Draft of a possible conic W-band horn within the 33 mm wide instrument (front panel removed), 3D CAD model 38
Fig. 5–10: Required torques to point the spacecraft concepts B, C at GS during the second cycle on Oct 4, 2016 39
Fig. 5–11: Power consumption during the second cycle on Oct 4, 2016 43

Fig. 5–12: Launch opportunities until end of 2020 to a sun-synchronous LEO in the range from 500 km to 600 km 45

Fig. 6–1: Map of operational WMO RAOB at 00:00 UTC and 12:00 UTC, the black dashed line shows the ground track. Cycle two passes over Munich (black diamond) at 11:48:22 UTC. The narrow blue swath indicates boundaries of the 0.5 dB beam the light blue of the 3 dB. 49

Fig. 6–2: Cross section along the ground track from AOS to LOS, RAOB are indicated by the dashed lines. Black lines indicate the carrier path through the atmospheric layers with different weighting and different optical depth τ 50

List of Tables

Tab. 2–1: Climate variables at TUM Garching for five distinct scenarios. Clear sky refers to 0/8 cloud cover and 0 mm precipitation. Under cloudy condition the values were derived for days with 8/8 cloud cover and zero precipitation, rainy days are characterized by 8/8 cloud cover and precipitation greater than 0 mm. 12

Tab. 3–1: Tropospheric attenuation models and their dependence on atmospheric variables 19

Tab. 4–1: Summary of the orbital parameters 21
Tab. 4–2: Two-line element set of the chosen orbit 22

Tab. 5–1: Selected subsystems, their TRL and estimated costs for the three satellite concepts. Subsystems of concept A, B are indicated with $^{(A,B)}$, subsystems of concept C are marked with $^{(C)}$, unmarked subsystems are used in any of the three concepts 41
Tab. 5–2: Power Budget 42
Tab. 5–3: Mass budgets of the 1U and 1.5U concept. Left column gives the estimated mass of the subsystem based on the manufacturers' data sheet. Margins depend on the maturity of the subsystem and the last column gives the mass including the margin 44

Tab. 6–1: ITU-R P.311 Part II, Slant path annual and monthly statistics of total attenuation, rain attenuation and rain rate 48

Tab. 7–1: Traceability Matrix: summary of the stated requirements and their modifications 57

Symbols and Formulas

Symbol	Unit	Description
η	[-]	antenna aperture efficiency
η_S	[-]	efficiency storage
λ	m	wavelength
Φ	°	elevation angle
ρ	g/m^3	liquid water density
Θ_{3dB}	°	half power beam width
A_C	dB	cloud attenuation
A_O	dB	oxygen absorption
A_R	dB	rain attenuation
A_S	dB	scintillation
A_T	dB	total tropospheric attenuation
A_{WV}	dB	water vapor absorption
B	Hz	occupied bandwidth
C_r	Wh	battery capacity
d	mm	horn diameter
D	Am^2	magnetic dipole moment
d_{GS}	m	ground station antenna diameter
DOD	%	depth of discharge
e_s	hPa	saturation pressure
f	Hz	frequency
G_R	dB	receiver gain
G_T	dBi	transmitter gain
h_{LCL}	m	height of lifting condensation level
I	kg m^2	moment of inertia
k	J/K	Boltzmann's constant
l	mm	horn length
$L_{depoint}$	dB	depointing losses
L_{FS}	dB	free space loss
n	[-]	refractive index
p_{outage}	%	outage
p_S	hPa	air pressure at ground station level
P_T	dBW	transmit power
R	mm/h	rain fall rate
R_b	s^{-1}	information bit rate
R_c	s^{-1}	channel bit rate
rH	%	relative humidity
T_d	°C	dew point temperature
t_{dur}	s	duration of slew manoeuvre
t_L	yr	mission life time
T_{LCL}	K	temperature at LCL
T_S	K	temperature at surface
T_{SM}	Nm	torque slew manoeuvre
T_{sys}	dBK	system temperature

Acronyms

ADCS attitude determination and control system

AOS acquisition of signal

BER bit error rate

BOL beginning of life

BPSK binary phase-shift keying

COTS commercial off-the-shelf

DOD depth of discharge

DWD Deutscher Wetterdienst

E_b/N_0 energy per bit to noise power spectral density ratio

EIRP equivalent isotropically radiated power

EOL end of life

ESA European Space Agency

Gb gigabit

GEO geostationary Earth orbit

GNSS global navigation satellite system

GS ground station

IF intermediate frequency

ITU International Telecommunication Union

LCL lifting condensation level

LEO low Earth orbit

LOS loss of signal

LRT Institute of Astronautics

LTAN local time of the ascending node

LWC liquid water content

Mb megabit

MB megabyte

MEO medium Earth orbit

MMW millimeter-wave

MOC mission operation center

n/a not applicable

PSK phase-shift keying

QPSK quadrature phase-shift keying

RAOB radiosonde observation

RF radio frequency

RTE radiative transfer equation

RTI radio tomographic imaging

SSO sun-synchronous orbit

STK Systems Tool Kit

tbd to be defined

TLE two-line element

TOA top of the atmosphere

TRL technology readiness level

TT&C telemetry, tracking and command

TUM Technische Universität München

UHF ultra high frequency

UTC Coordinated Universal Time

VHF very high frequency

WMO World Meteorological Organization

1 Introduction

Europe's current Earth observing programs with the Sentinel satellite constellation will generate daily a data volume of 20 terabytes by the end of 2017 [1]. This enormous data volume requires new broadband links to access the data. Also in future planetary explorer missions the need for high throughput communication will become more important. This is caused by a wider range of observed parameters and teleoperated landers or rovers. Therefore it is necessary to establish a gigabit space communication network for interplanetary missions to transmit data collected on the Moon, on Mars and beyond back to Earth [2]. In remote areas on Earth, like Antarctica, it is of concern to forward scientific data via satellite to the research facilities. This bypasses time consuming shipping of hard drives from Antarctica [3]. All mentioned scientific applications have in common that the increase in data volume requires higher transmission capacities than these available nowadays. Moving beyond X-band (8–12 GHz) and Ka-band (20–30 GHz) to less congested higher frequencies increases the available bandwidth [4, 5]. Broadband links at W-band (75-110 GHz) are essential to handle these data amounts [6] and avoid data loss due to limited on-board memory or data compression. Depending on the application the data will be forwarded and downliked directly from a low Earth orbit (LEO)-satellite to the ground station or transmitted via a geostationary Earth orbit (GEO) relay satellite [4, 7].

Further, a wide field of commercial services will benefit from high bandwidth communication links. Such applications are High Definition TeleVison (HDTV), high speed Internet and mobile telecommunication services. Currently, service providers like O3b deliver Internet access with its 12 satellite constellation. They offer up to 1.6 Gigabits of bandwidth per beam via Ka-band [8]. Intelsat's Epic network provides Internet in C-, Ku- and Ka-band and has to reuse frequencies to overcome the limited spectrum available [9]. The operators of the upcoming OneWeb constellation (648 -720 satellites) announced to be able to provide a capacity of > 5 Gb/s per satellite with a latency of $<$ 50 ms [10]. In November 2016 Space X published its plans to set up a constellation of 4425 satellites, providing Internet speeds of 1 Gb/s for a wide range of broadband and communications services [11]. Beyond Ka-band, the W-band provides mobile users with data comparable to wired Ethernet connection [6].

From a technical perspective using W-Band is advantageous because higher frequencies allow smaller equipment and consequently reduces the size of the satellite and launch vehicle. The high directivity and spatial resolution enables the reuse of frequency and prevent interference [5, 6, 12].

The challenge of using frequencies in the W-band is the atmospheric impact on the radio wave propagation. The main attenuation sources are located in the lowest 10–20 km, the troposphere. These are:

- Gaseous Absorption: In the frequency range 20–300 GHz oxygen and water vapor molecules absorb the electromagnetic radiation. Where the absorption due

to well mixed oxygen is weakly dependent on ground temperature and pressure the water vapor content varies in space and time. As the water vapor content changes during the day, season and the geographic location, the attenuation varies. The water vapor absorption increases monotonically in the 40–100 GHz range [12].

- Cloud Attenuation: In W-band the wavelength is larger than the suspended water droplets in the cloud leading to attenuation. The Rayleigh approximation gives an estimate of the extinction cross section and the attenuation which depends only on the liquid water content, droplet temperature and the frequency [12].

- Rain attenuation: In contrast to the cloud attenuation the wavelength is in the order of the size of the hydrometeor. The incident electromagnetic wave is absorbed and scattered causing significant fades. Absorption and scattering are the dominant loss mechanisms for frequencies above Ka-band and limit the availability of the signal in the presence of rain. It depends on the rain rate and the site [13].

- Scintillation: Atmospheric turbulences alter the refractive index of the troposphere. The refractive index of the troposphere decreases with altitude and is a function of the meteorological conditions [14]. These inhomogeneities in the refractive index occur in small temporal (0.5 s) and small spatial scales at the boundary layer and degrade the performance of the communication system [4].

- Depolarization: Non-spherical hydrometeor depolarize due to differential attenuation and differential phase shift a orthogonal polarized wave. This causes signal leakage from one polarization to an orthogonal polarization. This effect mainly occurs during rain events [4, 14].

- Group delay: An other limiting factor is the dispersion. Because of the different travel times of different frequency components the pulse widens and limits the use of the available spectrum [4].

- Atmospheric noise: This is the equivalent black body temperature of the atmosphere in the W-band [4]. It is sensitive to the surface water-vapor density [15].

- Wet or snow-covered antenna: Wet or snow covered antenna reduce the signal strength by several dB [4].

Current propagation models provide a reliable estimate, but the ITU-R models for prediction of attenuation have been validated only for frequencies up to 50 GHz [12]. It is essential to investigate the behavior of electromagnetic waves in W-band to improve existing models and validate them by independent measurements [16]. Reliable statistics help to mitigate signal degradation in satellite links and understand the effects of the atmosphere. This moreover important since there exist only feasibility studies by agencies world wide but no communication satellite operates in the W-band.

1.1 Motivation of the thesis

The aim is to close this gap and characterize the W-band channel for data downlink from LEO to a ground station (GS) in Munich, Germany. This is important since this is not only of scientific interest but directly influences the design of high throughput transmission chains. With radio frequency (RF) propagation simulations it is possible to derive requirements for the space-based transmitter and ground segment to cope with the signal fades.
This phase 0/A study will address the following questions:

What are the requirements for a payload concept accommodated in a CubeSat to perform W-band channel measurements?

How does a possible W-band transmitter design and CubeSat mission look like to perform these measurements?

How to measure tropospheric attenuation and to provide these collected data sets?

1.2 Terminology

In IEEE radar nomenclature the frequency range from 75–110 GHz is called W-band whereas in International Telecommunication Union (ITU) nomenclature the range from 30–300 GHz is refereed to the extremely high frequency (EHF). In the metric designation this corresponds to the millimeter wave [17]. In the context of Electronic Warfare Operators the EU-NATO-US-ECM Band designation labels the frequency range from 60–100 GHz as M-Band [18]. The Radio Society of Great Britain (RSGB) calls the range from 60–90 GHz E-Band [18]. This frequency range corresponds to the rectangular US waveguide dimensions WR12 or the UK equivalent WG26 [19].
In the following the frequency term W-Band will be used. According to [20] the frequency range 71–76 GHz is reserved for space to Earth links and the range 81–86 GHz for uplink. Amateur bands are included in both ranges, namely at 75.5–76 GHz for downlink and 81–81.5 GHz for uplink. Figure 1–1 compares the frequency bands with the most common nomenclature.

1.3 Current research

In Europe the ongoing research can be summarized as follows: The German Aerospace Center (DLR) performed a feasibility study on future multi-Gb/s connection in the project ”gigabit satellite links at millimeter-wave frequencies (GISALI)” [21]. It showed that a 5 Gb/s satellite-Earth link from a LEO satellite (orbital height 1414 km) is achievable in W-band. The calculations were performed for a satellite antenna diameter of 0.5 m and 1 m diameter. The proposed transmitter had a transmit power of 30 dBm at a frequency of 73.5 GHz. The presented theoretic link budgets were calculated based on ITU recommendations for a GS in located in Yebes, Spain with a dish diameter of 2 m, 4 m and 6 m. With a ground antenna diameter of 6 m and a satellite dish diameter of 1 m a data rate of 5.0 Gb/s is theoretically feasible [21]. This paper describes the applicable ITU guidelines to compute the attenuation and the link budget. The stated results enable to

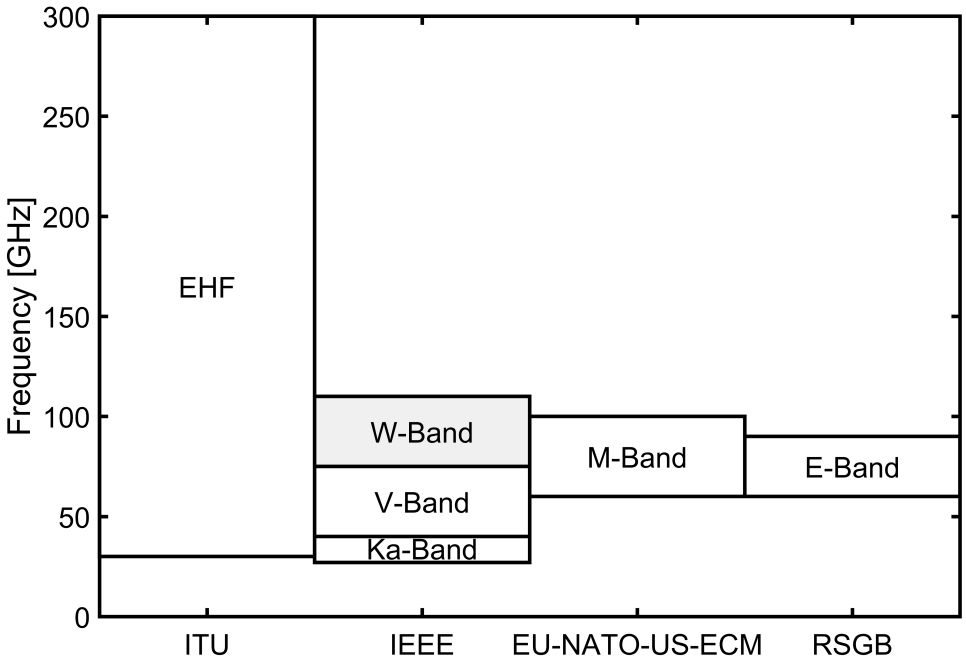

Fig. 1–1: Overview of the frequency allocations and nomenclature in the range from 60–110 GHz

compare the attenuation with the findings of this thesis, at least the order of magnitude of to be expected from a LEO downlink.
DAVID is Italy's study on DAta and Video Interactive Distribution to forward a data volume up to one gigabyte per satellite pass via W-band from remote locations to the Internet. The orbit is designed such that the satellite passes daily in sun-synchronous LEO at an altitude of 570.4 km over Northern Italy. Scientific data will be uplinked (94.5 GHz) from a ground station located in Antarctica to the satellite and downloaded in Italy via a 83.9 GHz link. This by passes the time consuming shipping of scientific data [3, 22, 23]. While the DAVID mission is focusing on data transmission the W-band Analysis and VErifcation project (WAVE) studies the tropospheric attenuation and the sky noise temperature in W-band. The satellite will be placed in a GEO and cover with three beams Northern Italy, central Italy and central Europe. [7] performed link calculations based on ITU recommendations for satellite antenna diameters of 0.9 m, 0.4 m and 0.25 m and diverse cloud types. The clouds differ in horizontal and vertical extent as well as in liquid water content expressed in g/m^3. With a receiver diameter of 0.3 m and under 90° elevation an attenuation of 5.6 dB can be expected in Spino D'Adda and 6.7 dB in Rome [7]. In the course of the study an experimental payload was flown on a high altitude aircraft to perform propagation experiments [24]. The next step was the development of a small satellite for In-Orbit Key-test and Validation of W-band (IKNOW) to characterize the channel attenuation [25]. The transmitter specifications show an equivalent isotropically radiated power (EIRP) of 28.9 dBW at a central frequency of 75.7 GHz. The antenna has a diameter of 110 mm and a minimum gain of 38 dBi [25]. The publications of the Italian researchers are a starting point for the orbit design with a daily revisit of Munich. In the papers they describe the effects of the

troposphere in detail as well as the corresponding models. The presented results allow to compare the attenuation to be expected at 76 GHz in a similar rain regime.
NASA's Glenn Research Center suggests to perform attenuation measurements at five fixed sites, each in a different rain or climate zone. [4] developed requirements for a transponder system in GEO and requirements for a receiver system operating at 76 GHz. For the spacecraft beacon they suggested an EIRP of 30 dBW. A ground station antenna diameter of 0.3 m was selected. The presented operation scheme stresses the importance of ancillary meteorological measurements like radiosonde observation (RAOB), weather radar and optical cloud monitoring [4]. [26] collected in a terrestrial measurement campaign data on gaseous and cloud attenuation. The authors claim that this three month experimental setup enables to get an first order estimate on rain attenuation avoiding costly spaceborne transmitters. These studies suggest detailed requirements for the spacecraft transmitter and GS receiver.
The above mentioned feasibility studies are stressing the need for a better understanding of the atmospheric propagation effects in W-band especially during rain. Currently no space borne W-band communication system is in operation to close this gap. In 2015 ESA published an invitation to tender for LEO CubeSat mission targeting at W-band channel measurements [27]. The aim is to develop and design beacons to enhance ITU-R models by measuring tropospheric scintillation, cloud, rain attenuation and depolarization due to ice. [27] noted that an atmosphere simulator will bridge the short LEO measurements to ensure statistical reliability.

In contrast to the above mentioned satellites a CubeSat is a standardized satellite bus with the dimensions 10x10x11 cm^3 refereed to as one unit (1U). It is scalable in three axes allowing spacecrafts up to typically 12U [28]. This standard was developed in 1999 by California Polytechnic State University, San Luis Obispo and Stanford University's Space Systems Development Lab. The operators are mainly universities (40.8%), companies (40.2%) and space agencies (6.7%) [29]. The large number of international launch services spurred the success of the CubeSat concept. According to [29] until January8, 2017 in total 580 CubeSats were launched. Applications range from astronomy, biology, Earth observation to technology demonstrator. CubeSats are considered as secondary payload and are deployed from adapter mostly to LEO [30]. To show the potential of CubeSats two examples should be mentioned.
The Microsized Microwave Atmospheric Satellite (MicroMAS) is a 3U satellite. Its payload, a passive microwave radiometers, detects the thermal emission near 118 GHz [31]. Measuring at nine different frequencies close to the absorption lines of water vapor and oxygen allows to retrieve temperature and moisture profiles of the atmosphere. This is of concern for prediction and a better understanding of the tropical cyclones and thunder storms on a global scale with an approximate 30 minute revisit. Therefore [31] suggest a 20 nanosatellites constellation to provide these data.
In the field of communication NASA's Optical Communications and Sensor Demonstration (OCSD) mission is scheduled to launch in late 2016. This mission will demonstrate a high throughput of 200 Mb/s with a laser link. To point the beam towards the ground station with an accuracy of 0.05 degrees the satellite has to rotate. On this mission also a new propulsion system will be tested using water as propellant. Small satellites

used as relay node for radar or hyperspectaral imaging missions or constellations will provide low-latency communication [32].
These missions highlight the potential and benefit of CubeSats to demonstrate new technology. Therefore it is consequent and cost efficient to test new W-band communication technology on board a small LEO satellite.

2 Mission overview

W-band satellite downlinks have the potential to transmit high data rates also in cloud covered areas. The first step in the design process is to estimate the total attenuation to derive the transmission power of the payload. The following section depicts the basics of radio wave propagation and its attenuation through the atmosphere. Then the atmosphere over Munich will be described, followed by the definition of the scientific objective. Based on the characteristics of the climate and the expected attenuating phenomena requirements will be derived allowing to model the atmosphere over Munich.

2.1 Background

In the far-field the emitted electromagnetic wave energy propagates out radially and its strength decreases proportional to the inverse distance squared. This free-space loss depends on the distance between transmitter and receiver and on the wavelength λ. In addition the carrier gets attenuated as it passes during up- and downlink through the atmosphere. In general the mechanisms causing signal degradation are absorption, scattering, refraction, reflection and diffraction. During absorption the RF energy is converted into internal energy, as the wave hits gas molecules or precipitation. Multiple reflections and bending on water vapor, precipitation or dust causes scattering. A change of the refractive index results in a bending of the microwaves, the so called refraction. If the wave hits a smooth surface, compared to its wave length, the signal undergoes reflection. Diffraction occurs if the wave bends around a physical obstacle [33].
In the W-band frequency range the four major contributions to signal degradation in the troposphere are distinguished. These are namely the gaseous attenuation, attenuation by clouds and rain and scintillation. The total signal attenuation depends on the specific attenuation and on the path length through the medium.
In the following paragraphs the sources will be discussed in detail. The impairments due to the ionosphere on the signal are neglected because they affect services below 12 GHz [34]. Figure 2–2 then depicts and summarizes the structure of atmospheric phenomena degrading the carrier propagation in the W-Band region.

2.1.1 Gaseous absorption by oxygen and water vapor

Oxygen and water vapor absorption are the main sources for gaseous attenuation in the 20–300 GHz frequency range under clear sky conditions. Ground temperature and atmospheric pressure weakly influence the oxygen attenuation. Therefore the variability of oxygen absorption A_O in time and space is small. The molecular absorption is a function of the frequency and the specific gaseous attenuation reaches at 60 GHz a value of 10 dB/km [12]. In the W-band the specific gaseous attenuation due to oxygen decreases from 0.26 dB/km at 70 GHz to 0.02 dB/km at 90 GHz [12].
Evapotranspiration is the main source of water vapor and depends on the available

amount of water and energy. The abundance depends on the surface cover and its moisture, so on the size of the reservoir for evaporation. The second driver is the sun as energy source. The water vapor distribution varies on different spatial and temporal scales. The evaporation and therefore the maximum water vapor content is reached between about 1 pm and 2 pm local time. With this 1–2 hour time lag after the maximum incident radiation the ground temperature reaches its diurnal maximum. According to the Clausius–Clapeyron [35] relation the saturation pressure increases with increasing temperature. The relation describes the capacity of an air parcel to hold water. On an annual basis the solar radiation varies due to Earth's orbit around the sun. The northern hemisphere receives the maximum flux in northern summer even tough the Earth is close to apogee. Therefore the water vapor attenuation A_{WV} depends on temperature, pressure and humidity. Water vapor absorption increases monotonically between 40 GHz and 100 GHz and causes a specific attenuation form 0.24 dB/km to 0.43 dB/km [12]. Due to the opposite dependence of oxygen and water vapor on frequency the specific gaseous attenuation ranges from 0.36 dB/km at 70 GHz and 0.5 dB/km at 95 GHz [4]. [12] states a range from 1–2.5 dB/km in V/W-band. Figure 2–1 visualizes the dependence of the specific gaseous attenuation (dB/km) on the frequency for a surface pressure of 1013 hPa, a temperature of 15°C for oxygen and a water vapor density of 7.5 g/m^3. The region for space to ground links (71–76 GHz) is marked with dots.

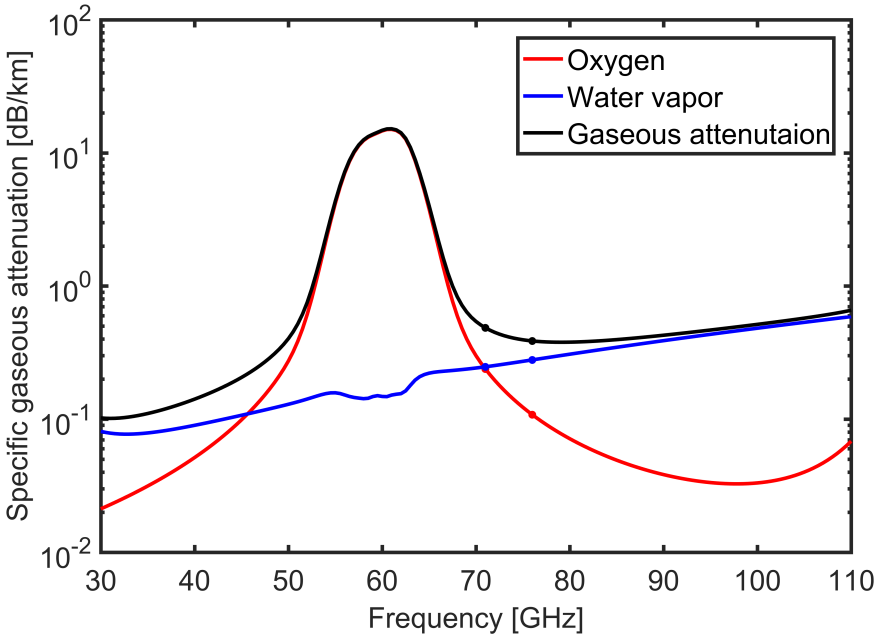

Fig. 2–1: Specific gaseous attenuation in the EHF region

2.1.2 Cloud attenuation

If the before mentioned water vapor content in an air parcel reaches a relative humidity of 100% the parcel is saturated and clouds form. A way to reach the saturation is by lifting the air parcel to its lifting condensation level (LCL). Here the air is saturated

with water vapor and it starts to condensate on condensation nuclei. Depending on the mechanism which caused the air parcel to rise two cloud forming processes can be distinguished. Firstly, rise of the air parcel by convection. According to the World Meteorological Organization (WMO) classification this would correspond to the low-level cumulus (Cu) clouds. If this cloud type keeps on growing the precipitation bearing multi-level cumulonimbus (Cb) cloud evolves [36]. This cloud types can be observed in central Europe in summer. The second process is advection. An air parcel is lifted to the LCL when it hits a barrier. This can be mountain ranges or a large dense air mass leading to stratiform clouds covers. The stratus (St) cloud has a uniform base and may produce drizzle [36]. The nimbostratus (Ns) forms is a gray cloud layer and brings constant precipitation with low visibility. It is thick enough to block the sun [36]. Depending on the origin of the air masses the clouds can be distinguished between continental and maritime clouds [35]. The droplet concentration in a marine cumulus clouds can reach a of maximum 200 droplets per cm^3 with a diameter ranging up to 20 µm. In contrast the droplet concentration in continental cumulus clouds can reach 1000 droplets per cm^3 but with a diameter up to 10 µm. The typical cloud droplet ranges from a diameter of 10 µm to 50 µm [35]. In relation to the millimeter-wave (MMW) the droplet size is small so that the Rayleigh approximation holds to compute the extinction cross section. Cloud attenuation depends on the liquid water content (LWC), on the temperature and on the frequency [12]. A visibility within the cloud or fog of about 300 m corresponds to a liquid water content of 0,05 g/m^3 and a visibility of roughly 50 m to 0.5 g/m^3 [37]. On these particles the incident carrier is evenly divided between forward and backward scattering [35, 37]. However, the precise estimation of the LWC in the atmosphere is still a problem [12].

2.1.3 Rain attenuation

When the cloud droplets reach the critical diameter of 100 µm they are considered as raindrops and can grow to a typical diameter of 1000 µm [35]. The diameter of the rain drop is in the range of the wave length causing pronounced forward scattering (Mie scattering). In this regime the absorption and scattering depends on the number density and on the diameter of the rain drops, summarized in the rain intensity R (mm/h). These parameters in turn depend on the cloud type and the development stage of the cloud [38] and on the RF. Precipitation is the predominant effect of signal degradation [14]. In the case of an orthogonal polarized wave the oblate rain drops cause depolarization because of the differential phase shift [14].

2.1.4 Scintillation

Small scale fluctuations of the refractive index along the slant path cause tropospheric scintillation. These inhomogeneities are induced by small-scale atmospheric turbulences and affect the satellite link above 10 GHz [12]. The refractive index is a function of the water vapor pressure and temperature in the boundary layer [39]. The boundary layer occupies the lower 1–2 km of the atmosphere. Scintillation occurs also inside rain caused by turbulences induced by the rain itself [12]. Ionospheric contributions to the

scintillation in W-band are negligible because it affects satellite services above 12 GHz [34].

2.1.5 Atmospheric noise

The blackbody flux density emitted by an atmospheric layer, mainly due to emissions from atmospheric gases and its hydrometeors within this layer, is given by the Stefan–Boltzmann law [35]. During clear sky conditions the brightness temperature in zenith direction in W-band is in the order of 50 K [40].

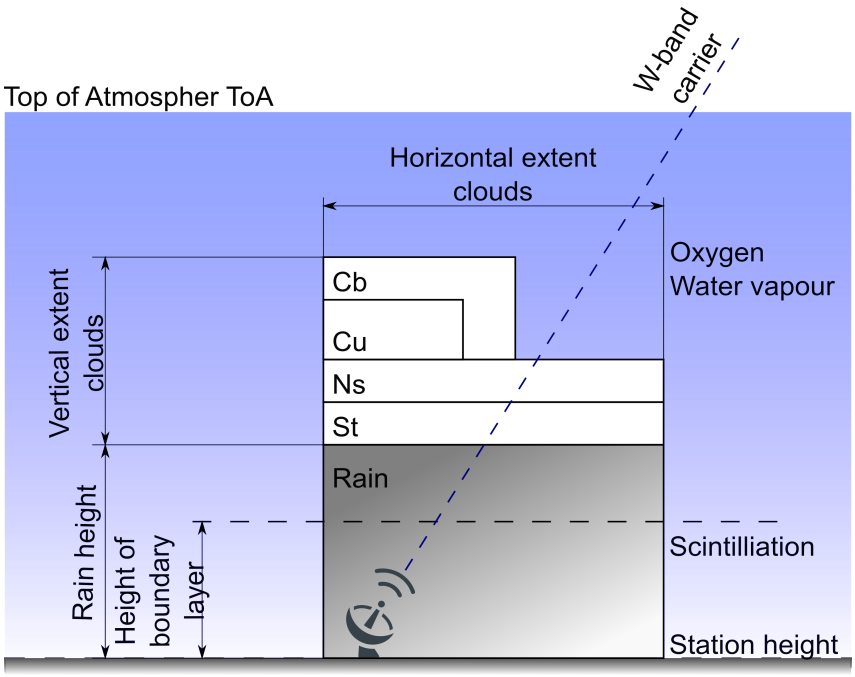

Fig. 2–2: Multiple sources of tropospheric attenuation. Parabolic antenna: mahorova-works, [Online]. Available: http://free-icon-rainbow.com, [acccessed: 09.01.2017]

2.1.6 Atmosphere over Munich

To perform the measurement experiments the Technische Universität München (TUM) Campus Garching was chosen as ground terminal. The antennas are mounted on the roof of the Institute of Astronautics (LRT) with the WGS 84 coordinates latitude 48.266 N, longitude 11.669 E and altitude of 476 m. Munich is located on the border between the oceanic climate and the humid continental climate according to Köppen climate classification scheme [41]. The climate in Munich derived from the 30 year average between 1971–2000 shows the lowest temperatures of -3.7°C in January [42]. The least amount of precipitation falls in the winter with 45.2 mm in February. In winter the atmosphere is stable layer suppressing convection. Therefore the precipitation is driven by characteristic stratiform clouds caused by advection. During July the maximum temperatures reach 23.1°C and the precipitation reaches its maximum with 131.6 mm in July [42]. In summer the atmospheric water vapor content raises due to

enhanced evaporation by the higher solar influx. This leads to an unstable layering of the atmosphere. In an unstable atmosphere convective uplift of humid air parcels form thunderstorms causing the maximum precipitation in summer. The number of days with rain reach its maximum in June with 13.8 days of rain [42].

Differences between the temperatures in Munich [42] and the TUM Garching, the closest Deutscher Wetterdienst (DWD) climate station in Oberschleißheim [43] can be attributed to the urban heat island [44]. The Oberschleißheim dataset (Tab. 2–1) was collected between April 1, 1976 and May 31, 2006 [43]. It was used to represent the climate at TUM Campus Garching assuming that the differences are negligible. Typical states of the summer and winter atmosphere over TUM Campus Garching are shown in table 2–1. Based on precipitation and cloud amount five distinct scenarios were selected. Clear sky was indicated by zero precipitation and 0/8 cloud cover. For the class cloud days with 8/8 cloud cover and zero precipitation were selected. The cloud types differ depending on the season in the horizontal and vertical extent as well as in the water density of the cloud. If 8/8 of the sky were covered by clouds and precipitation was measured the scenarios represented rainy conditions. As for the clouds, the rainy conditions depend on the season and differ in the rain rate. On a clear day in winter the radiation balance is often negative. Therefore the temperatures in January drop to -7.57°C. The cold and dense air masses cause the high pressure of 970.4 hPa. Additional the humidity is low since cool air can hold little amount of water vapor. A cloud cover blocks the outgoing infrared radiation of the ground and re-emits it. The temperature is -2.88°C. According to Clausius–Clapeyron relation this air masses can hold more water vapor than in January. Since water vapor is less dense than dry air the total air pressure drops to 965.2 hPa. Depending on the cloud type drizzle with 0.5 mm/h or a heavy rain fall of up to 40 mm/h can be generated [44].
In summer the temperature rise up to 19.3°C due to the surplus of solar radiation. Cloud cover reduce the solar in flux and decrease the temperatures to 12.6°C. Between the cloud type and and mean surface pressure is no clear connection because they are to small and short lived to influence the air pressure. Cumulus clouds can generate moderate rain with 5 mm/h and cumulonimbus bring up to 50 mm/h during a thunder storm [44].

2.2 Scientific objectives

The primary objective of this work is to provide a concept for W-band channel characterization. Firstly, to perform propagation experiments to measure the tropospheric attenuation under different climate conditions throughout a year. Therefore it is necessary to measure the sky noise temperature at W-band before any conclusions are drawn. The results of the measurements will allow to validate tropospheric attenuation models at the W-band frequency range.
Secondly, for utilization of available bandwidth a transmission experiments shall be carried out under near clear sky conditions. On board stored data sets shall be transmitted to access the quality of service of the data transmission. Based on these aims and the atmospheric characteristics at the TUM Garching site the following requirements are

Tab. 2–1: Climate variables at TUM Garching for five distinct scenarios. Clear sky refers to 0/8 cloud cover and 0 mm precipitation. Under cloudy condition the values were derived for days with 8/8 cloud cover and zero precipitation, rainy days are characterized by 8/8 cloud cover and precipitation greater than 0 mm.

Scenario	Temperature [°C]	Pressure [hPa]	Water vapor pressure [hPa]	Sky cover	Liquid water content [g/m³]	Vertical extent [km]	Horizontal extent [km]	Rainrate [mm/h]
Clear sky (Jan)	-7.6	970.4	2.9	0/8	0.0	0.0	0.0	0
Stratus (Jan)	-2.9	965.2	4.7	8/8	0.4	0.6	10.0	0
Nimbostratus (Jan)	-2.9	965.2	4.7	8/8	1.0	0.8	10.0	0
Moderate rain St (Jan)	0.1	957.7	5.8	8/8	0.4	0.6	10.0	5
Heavy rain Ns (Jan)	0.1	957.7	5.8	8/8	1.0	0.8	10.0	40
Clear sky (Jul)	19.3	962.2	13.6	0/8	0.0	0.0	0.0	0
Cumulus (Jul)	12.6	964.0	12.2	8/8	0.6	2.0	4.0	0
Cumulonimbus (Jul)	12.6	964.0	12.2	8/8	1.0	3.0	3.0	0
Moderate rain Cu (Jul)	14.1	959.3	14.6	8/8	0.6	2.0	4.0	5
Heavy rain Cb (Jul)	14.1	959.3	14.6	8/8	1.0	3.0	3.0	40

necessary to perform the attenuation measurements. The requirements are identified by the letter R for requirement or G for goal followed by three letters indicating the segment. MIS stands for mission functional requirements, SYS for system requirements, and OGS stands for operation and ground segment.

2.2.1 Mission functional requirements

R-MIS-001 To measure the total tropospheric attenuation in W-band (75–110 GHz) a beacon shall transmit a continuous unmodulated and unpolarized carrier RF. Preferably the frequency is located in the amateur band of 75.5–76 GHz [20]. Performing the measurements in this region reduces the costs for licenses and allows to integrate amateur receivers stations into the ground station network.

R-MIS-002 In the data transmission experiment on-board stored data shall be transmitted under nearly clear sky conditions with a data rate of 10 Mb/s [16].

R-MIS-003 The energy per bit to noise power spectral density ratio (E_b/N_0) shall be grater than 10 dB [14, 21] to ensure data rate at reception of 10 Mb/s.

R-MIS-004 The bit error rate (BER) shall be less than 10^{-6} [3, 14].

R-MIS-005 An EIRP of minimum 30 dB [4] shall maintain a 99% link availability under rainy conditions during attenuation measurements. (1% rain outage, see [45]). The EIRP has to be less than the maximum allowed 55 dBW [46].

R-MIS-006 To detect the scintillation effects with time scales less than 0.5 s [4] the sampling rate of the receiver has to be at minimum 10 Hz [4].

R-MIS-007 To ensure accurate measurements the power stability of the satellite transmitter has to be $<$0.3 dB/day (RMS) [4].

R-MIS-008 For reliable measurements the ground equipment shall have a receiver gain stability of $<$0.2 dB (10 minutes RMS) [4] and a power measurement accuracy of $<$0.1 dB (1 minute RMS) [4].

R-MIS-009 To find upper limit of the rain attenuation a horizontally polarized wave shall be assumed [47]. Due to the oblateness of the falling rain drop the fade in horizontal direction is larger than in vertical polarization.

R-MIS-010 The overall link availability shall be 99% [4, 12].

2.2.2 System requirements

R-SYS-001 To cover all seasons a mission life time of at least 14 months is required. This timespan includes two months for the commissioning phase followed by at least 12 consecutive months of routine science operations [48].

G-SYS-002 The goal is to extend the overall observation time to an integer multiple of 12 month [48], ideally in the range from 36 months to 60 months for

reasonable statistics [4, 7]. This can be reached by subsequent CubeSat missions or a constellation of three satellites [16].

R-SYS-003 The satellite shall pass daily over LRT at 12:00 Coordinated Universal Time (UTC) to be concurrent with the operational RAOB 10868 of Oberschleißheim.

R-SYS-004 The payload and the required subsystems shall fit into a one unit (1U) CubeSat bus and shall be compliant to the PC/104 specification [49].

G-SYS-005 A constellation shall consist of three identical 1U CubeSats [16].

R-SYS-006 The satellite orbit has to decay within 25 years [50] preferably without active measures.

2.2.3 Operation and ground segment

R-OGS-001 The mission operation center (MOC) and the science operations center (SOC) are located at LRT. The MOC performs telemetry, telecommand and tracking operations. It will uplink the mission plan and the telecommands in ultra high frequency (UHF). Telemetry and housekeeping data will be received in the very high frequency (VHF) at the GS. In both frequency ranges the bands assigned to amateur radio shall be used. The SOC runs the W-band propagation measurements and the data transmission experiment.

G-OGS-002 Integrating mobile W-band receiving stations along ground track into the ground segment allows to collect attenuation measurements under different weather conditions [7]. The stations shall be placed across Europe in different climate zones coordinated by the MOC. Besides the increased complexity this allows to cooperate with foreign institutions and enhances the reliability of the experiments [7].

R-OGS-003 The SOC shall be equipped with a total power radiometer to perform the power measurements of the sinusoidal wave. In addition a weather station has to be operated [4, 48]. The rain gage has to measure concurrent to the attenuation measurements with an integration interval of one minute [48].

R-OGS-004 An antenna dish diameter of 0.3 m to 0.5 m with an approximate beam width of 0.8° reduces the effect of satellite motion in the power measurement [4].

R-OGS-005 The receiver noise temperature shall be 1000 K or smaller. [16] reported that 1000 K for a 60 cm dish are realizable.

R-OGS-006 High sensitivity to mispointing requires precise antenna tracking of less then 0.1° [5].

In general this feasibility study aims to be compliant to the standards of the European Space Agency (ESA) in the margin philosophy, space debris mitigation and the use

of the technology readiness level (TRL). The frequency range was selected according to Electronic Communications Committee (ECC). For the payload design the physical dimensions according to [49] are applied. The link design follows the recommendations by the ITU.

3 Propagation simulations

To plan a satellite-ground link it is essential to assess the signal attenuation to be expected. Besides the free-space loss the major concern here is the signal degradation imposed by the troposphere. The ITU recommendation [45] summarizes the attenuations to be expected and shows how to compute the total attenuation and its individual components. Table 3–1 illustrates the dependence of the individual sources on weather variables. The input to these simulations are the climate data given in table 2–1. The simulations were programmed and performed in MATLAB [51]. The code is enclosed in the Appendix A. First the parameters of the receiving station were defined. The receiver station height of 500 m including an assumed building of 25 m was picked from the Bayern Atlas [52]. The physical diameter of the Earth-station antenna was set to 0.3 m similar to [4, 7]. The simulations were done for a time system availability of 99% (R-MIS-010) with elevations ranging form 10° to 90° and a frequency of 76 GHz. This frequency was chosen for maximum transponder utilization [4] and to enable a comparison with the results found by [7].

3.1 Gaseous attenuation

Before starting the simulation for the gaseous attenuation the vertical temperature profile $T(h)$ had to be defined. Based on ITU-R P.835 [53] standard atmospheres for summer and winter are distinguished in mid latitudes. The months April to September were treated as summer and October to March as winter (Appendix A.1.5). Based on the temperature profile $T(h)$, the pressure profile $p(h)$, the water vapor density profile $\rho(h)$ and the profile of the refractive index $n(h)$ was computed as a function of the altitude h. According to ITU-R P.676 [54] the atmospheric layers are represented accurately if the layer thickness increase from 10 cm at ground level to 1 km thickness at the top of the atmosphere (TOA) at an altitude of 100 km. For each of these layers the specific gaseous attenuation was computed with the function *gaspl* of the MATLAB built-in RF toolbox [51]. Multiplying the specific gaseous attenuation with the path length through the layer gave the attenuation in one layer. The path length depends on the elevation angle ϕ. The total gaseous attenuation A_G is the sum of all fades in the attenuating layers. The implemented equations [54] rely on the frequency f and are valid in the range 1–1000 GHz.

3.2 Attenuation by clouds

The attenuation by clouds A_C is subject to the cloud characteristics. This are on one hand the vertical and horizontal extent and on the other the LWC within the clouds. The cloud attenuation model ITU-R P.840-6 estimates the attenuation of the carrier that propagates through clouds and the used MATLAB function *fogpl* is based on it. Since the MATLAB built-in RF toolbox [51] is intended for terrestrial links the temperatures at cloud base level had to be computed. Following [55] the height of the LCL is the inverse

of the laps rate difference (0.122 K/km) times the temperature difference between the air temperature T_S and the dew point temperature T_d measured at 2 m above ground (Equ. 3–1).

$$h_{LCL} = 0.122(T_S - T_d) \tag{3–1}$$

The temperature at the LCL is the difference between the temperature at station height T_S and the difference between the height of the LCL and the ground station altitude times the dry-adiabatic laps rate of 9.8 K/km (Equ. 3–2).

$$T_{LCL} = T_S - (9.8h_{LCL}) \tag{3–2}$$

Depending on the cloud type various vertical extents have to be taken into consideration. In the simulations it is assumed that only one cloud type is present. The path length through the cloud varies with the cloud type (Tab. 2–1) and elevation angle ϕ. With the path length, the frequency f and the liquid water density the attenuation due to clouds was calculated with the MATLAB built-in RF toolbox [51]. Under clear sky condition the cloud attenuation is set to be zero.

3.3 Attenuation by rain

The rainy conditions were split depending on the rain rate into two regimes. During a moderate rain the fall rate lies between minimum 2.6 mm/h and 7.6 mm/h and the maximum rate no more than 7.6 mm in six minutes. Precipitation rates below are indicated as light rain. Rain intensities exceeding 76 mm/h or more 7.6 mm in six minutes are classified as heavy rain [44]. For the simulations a moderate rate of 5 mm/h was selected. According to [56] in 0.01% of the time in an average year the rain rate exceeds 40 mm/h in central Europe. The attenuation simulations are based on [45] which are only validated for the frequency range up to 55 GHz. The polarization is assumed to be horizontal (R-MIS-009) which reflects the worst case [47]. The height of the zero degree isotherm over Munich was bilinear interpolated using the data set provided by ITU R-P.839-4 [57]. It was at an altitude of 2.775 km. According to [57] the rain height is 0.36 km above the height of zero degree isotherm at 3.135 km. Dividing the difference between station height and rain height by the sine of the elevation angle resulted in the slant path through the rain. The horizontal projection of the slant path was obtained by multiplication with the cosine of the elevation angle. For the computation of the specific rain attenuation in dB/km the rainfall rate $R_{0.01}$ of 40 mm/h was extracted from the rain fall maps of ITU-R P.837 [56]. The specific rain attenuation itself was estimated with the MATLAB built-in function *rainpl* [51] for the two given rain rates. Afterwards the horizontal reduction factor and vertical adjustment factor was computed for the exceeding level of 0.01%. With this the effective path length was derived. The attenuation exceeding in 0.01% of an average year is predicted by multiplying the specific attenuation with the effective path length. The attenuations for a different outage percentage are obtained from the attenuation exceeding 0.01%. With the allowed outage of 1% the attenuation $A_R(p)$ was calculated, stating that in 1% of the time, in an average year the attenuation will exceed $A_R(p)$. For clear sky or just cloudy conditions as well as for the cases where the station is in the cloud the attenuation caused by rain is set to zero.

Tab. 3–1: Tropospheric attenuation models and their dependence on atmospheric variables

Attenuation	Recommendation	Dependence	Model limit
Gaseous	ITU-R P.676	$A_G(t, \phi, f, n_{(h)}, \rho_{(h)}, T_{(h)}, P_{(h)})$	1–1000 GHz
Cloud	ITU-R P.840	$A_C(h_S, f, \phi, T_s, T_d, cloud)$	10–200 GHz
Rain	ITU-R P.618	$A_R(f, \phi, \phi_S, R, h_R, h_S, p_{outage})$	f $\leq$ 55 GHz
Scintillation	ITU-R P.618	$A_S(T_S, e_S, f, \phi, d_{GS}, p_{outage})$	4-20 GHz $\phi \geq 5°$

3.4 Attenuation by scintillation

To estimate the attenuation by scintillation the ITU model [45] is applicable in the range from 4 GHz up to at least 20 GHz for elevation angles greater 5°. It depends on the surface temperature T_S and the relative humidity rH at station level. Since these variables change with seasons it is recommended to use monthly averages. In the simulations first the wet term of the radio refractivity according to [39] was computed with the mean water vapor pressure e_S, air pressure p and temperature T_S. The effective path length was derived with the assumed height of the boundary layer of 1 km. The effective antenna diameter was computed for a conservative antenna efficiency of $\eta = 0.5$. The antenna diameter varied between 0.3 m and 0.5 m (R-OGS-004). Afterwards the antenna averaging factor and the standard deviation of the signal path was calculated. With standard deviation of the signal and time percentage factor finally the fade depth for $A_S(p)$ was computed.

3.5 Total tropospheric attenuation

Combining the above mentioned effects resulted in the total tropospheric attenuation A_T for a fixed time percentage p (Equ. 3–3). In p percent of the time the rainfall rate was exceeded and consequently a larger total attenuation had to be expected. For the planning of a satellite-ground link ITU-R P.618 [45] recommends to use the ”worst month” value with the same outage percentage. The ”worst month” is a concept to find the least favorable conditions in 12 consecutive months [58].

$$A_T(p) = A_O(p) + A_{WV}(p) + \sqrt{[A_R(p) + A_C]^2 + A_S^2(p)} \tag{3–3}$$

This method for the total attenuation was tested and show an r.m.s. error of about 35% in the probability range 0.001% to 1% [45].

4 Simulation results

4.1 Orbit

The orbit was designed based on the findings of [3] in Systems Tool Kit (STK) [59]. The simulation time span was one day, from Oct 4, 2016 10:00:00 to Oct 5, 2016 10:00:00. The satellite passed twice a day directly over Munich on a sun-synchronous repeat track at an altitude of 570.5 km. It took 15 orbital revolutions to revisit Munich. The orbital period was 96 minutes with an eclipse duration of 36 minutes. In table 4–1 the orbital parameters are shown and the corresponding two-line element (TLE) in table 4–2. The first pass was at 11:48 UTC which was 12 min before the operational RAOB in Oberschleißheim (R-SYS-003) and the second in the night at 22:30 UTC 1.5 h before the RAOB.

4.1.1 Orbital life time

The orbital life time was estimated for a 1U and a 1.5U CubeSat with Semi-analytic Tool for End of Life Analysis (STELA) by CNES [60] and STK [59]. In both software tools the same TLE (Tab. 4–2) derived in STK and the same empirical atmospheric model NRLMSISE-00 were applied. For the 1U satellite a mass of 1.2 kg, a drag area of 0.01 m^2 and a reflecting area of 0.05 m^2 was assumed. The 1.5U satellite was represented by a mass of 2.0 kg, a drag area of 0.02 m^2 and a reflecting area of 0.05 m^2. The reflectivity coefficient was set to 1.5.
In STELA the variable drag coefficient and mean solar activity was used, resulting in a life time of 7.59 years for the 1U concept and in 6.57 years for concept 1.5U.
In STK a constant drag coefficient with 2.2 was applied. The life time analysis showed with the same orbital parameters different results. The 1U satellite concept had a life time of 5.2 years and in the case of the 1.5U satellite of 5.0 years (R-SYS-001). In any case the satellite will de-orbit within 25 years (R-SYS-006).

Tab. 4–1: Summary of the orbital parameters

Type of orbit	Sun synchronous repeat track
Approximate Altitude [km]	570.5
Inclination [°]	97.64
Lon. od first Ascending Node [°]	95.65
Number of Rev. to Repeat	15
Local time of ascending node	00:00:00.000 UTC
Orbital period [s]	5760
Eclipse Time[s]	2132

Tab. 4–2: Two-line element set of the chosen orbit

```
1 99999U          16278.41666667  .00000130  00000-0  10247-4 0 00006

2 99999 097.6350 013.5276 0010671 271.6864 178.3125 15.00938211000018
```

4.1.2 Contact times

The contact times of the W-band payload and UHF antenna were estimated in STK. The maximum W-band contact time was reached when the satellite was pointing at the ground station as it passed over Munich. The ground terminal tracked the satellite from a minimum elevation of 10° onward. The rotation of the satellite was constraint to a rotation about the cross-track axis resulting in two contact windows with a total contact time of roughly 25 minutes per day. The first started in cycle two at Oct 4, 2016 11:41:59 and ended on Oct 4, 2016 at 11:54:45. In cycle nine the second contact window was from Oct 4, 2016 22:32:03 to Oct 4, 2016 22:44:49.
For a nadir pointing payload concept the contact time shrank to 13.9 s during the mid-day pass and to 10.0 s during the night for a antenna half angle of 5° summing up to 23.9 s in total over Munich.
For the telemetry, tracking and command (TT&C) communication in UHF frequency the contact times were extended compared to the payload times due to the omnidirectional transmission pattern of the antenna. This allowed contact also in the cycle before (cycle 1 and 8) and right after the direct over head pass (cycle 3 and 10). A total contact for TT&C of 62 minutes per day was realized.

4.2 Atmospheric attenuation

The simulations were performed for an outage percentage of p=1%. The in the following presented examples of the attenuation values are for an elevation angle of 90° if not marked otherwise. Throughout the year the tropospheric attenuation depended heavily on the elevation angle (Fig. 4–1,4–2). To demonstrate the impact of the troposphere the optimum conditions in January are compared to the unfavorable conditions in July. The five winter scenarios (Fig. 4–1) differ by the magnitude of the attenuation. The attenuation under clear sky condition (black lines) was smallest with 0.4 dB. Under an elevation of 90°. The attenuation caused by stratus clouds was 1 dB and 2.4 dB for nimbostratus clouds. The strongest fades occurred during rain and increased with rain fall intensity. During moderate rain 2.9 dB are reached and during heavy rain 11.5 dB could be expected.
In summer (Fig. 4–2) the gaseous attenuation had increased to 0.8 dB. Under cloudy conditions the attenuation had risen to 3.9 dB (cumulus) and to 9.5 dB during cumulonimbus cloud cover. Moderate rain attenuated the carrier by 5.2 dB and heavy rain by 17.5 dB. These values represented only the signal degradation due to atmospheric effects. The free space loss due to the distance was not considered here.

Depending on weather the brightness temperature of the atmosphere varied. Figure 4–3 depicts the sky noise temperature. During clear skies the brightness temperature

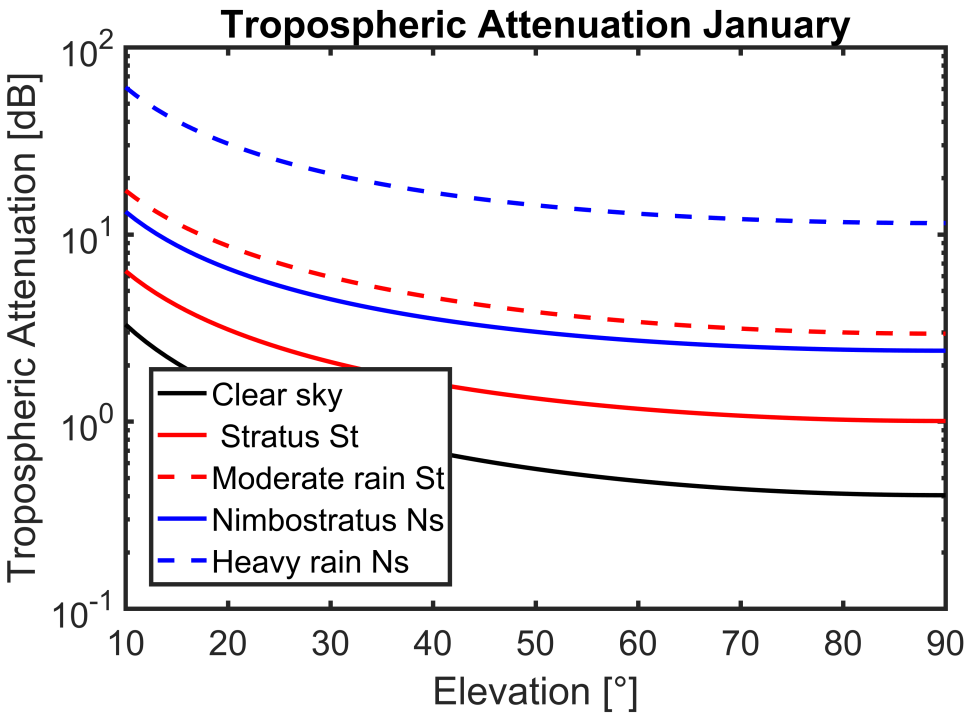

Fig. 4–1: Total tropospheric attenuation in January as function of the elevation angle for five distinct weather scenarios

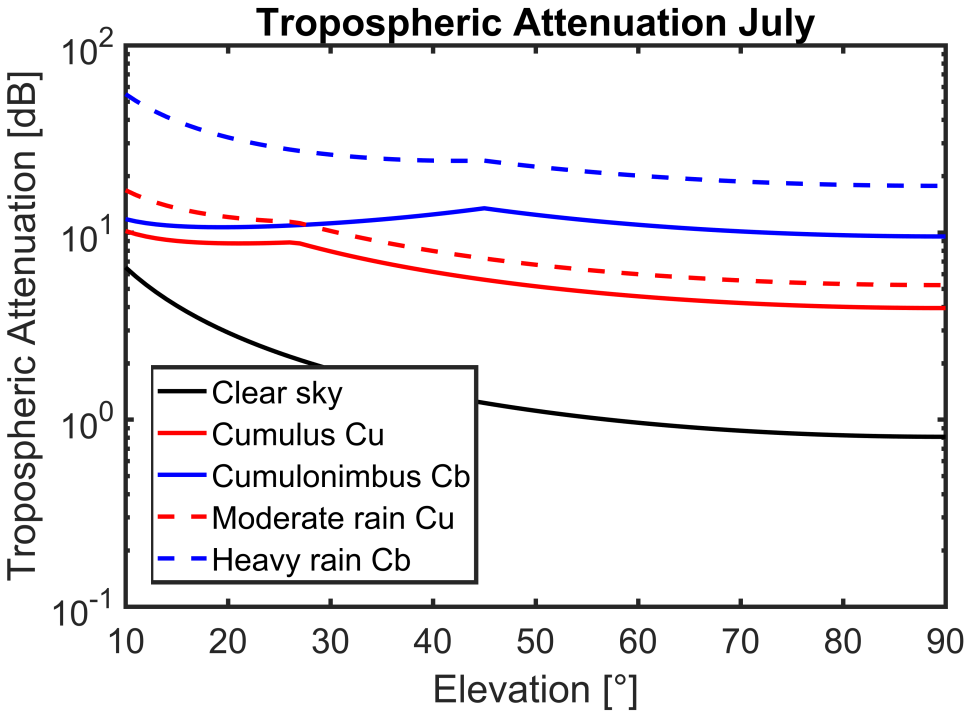

Fig. 4–2: Total tropospheric attenuation in July (worst month) for five distinct weather scenarios in dependence of the elevation angle

decreased monotonically from 51.6 K to 12.0 K. The brightness temperature in zenith direction was 160 K under a cumulus cloud and 238.8 K under a cumulonimbus cloud. According to [45] the prediction model is not applicable to rainy conditions. As above mentioned the impact of the horizontal extent was clearly visible.

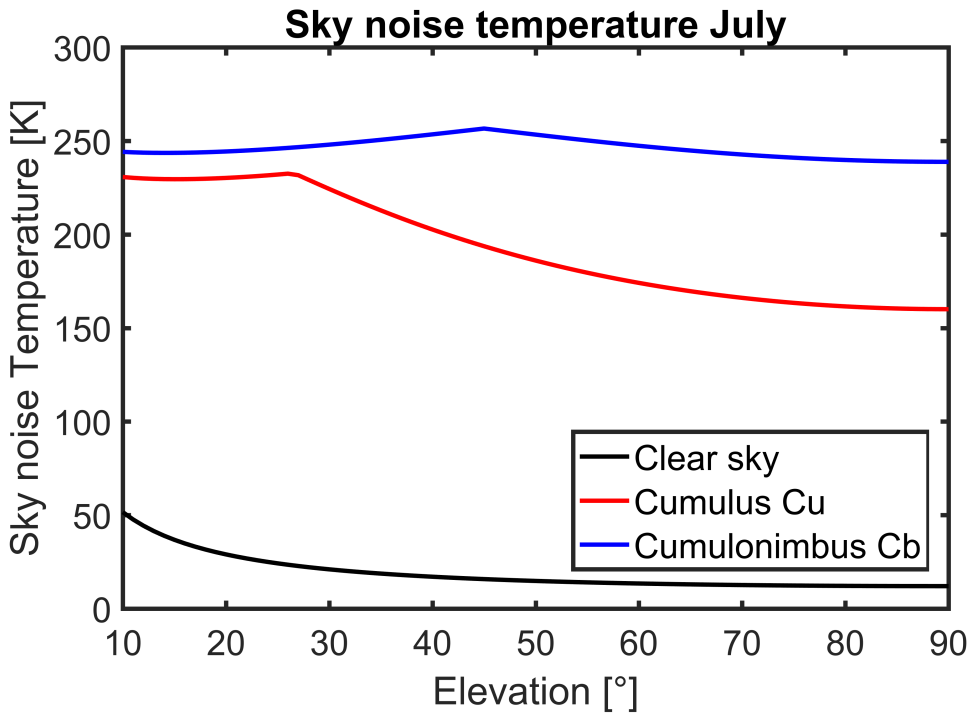

Fig. 4–3: Sky noise temperature in July (worst month) during clear sky and different cloud covers depending on elevation angle

Since the strongest attenuation were found during heavy rain in summer the sources were further analyzed (Fig. 4–4). The gaseous attenuation in the worst month, July, decreased monotonically from 0.9 dB at an elevation of 10° to 0.15 dB at zenith. In the same way as the gaseous attenuation the scintillation decreased from 6 dB at 10° elevation to 0.7 dB at 90°. An order of magnitude larger was the impact of clouds. At the lowest elevation the simulated fade was 9 dB. The maximum attenuation occurred at an elevation of 45°. Here the path length trough the cloud reached it maximum and caused the maximum attenuation of 12.6 dB. With increasing elevation, the effect of the cloud attenuation decreased to 8.9 dB at zenith. The dominant impact was found for the rain. The maximum attenuation occurred at the lowest elevation with 44.5 dB and decreased monotonically to 8.6 dB at 90° elevation. The total tropospheric attenuation has its maximum at 10° elevation with 54.9 dB. At the intermediate peak at 45° elevation the values show 24.2 dB decreasing further to 17.7 dB at an elevation of 90°. It has to be noted that the total attenuation was computed as given by equation 3–3.

The link availability constrains the attenuation to be expected. If a link availability of 99.9% for instance is required in 0.1% of the time in an average year the attenuation will be exceeding the values depicted in red (Fig. 4–5). The higher the allowed time percent outage the smaller are the occurring signal degradation A_p.

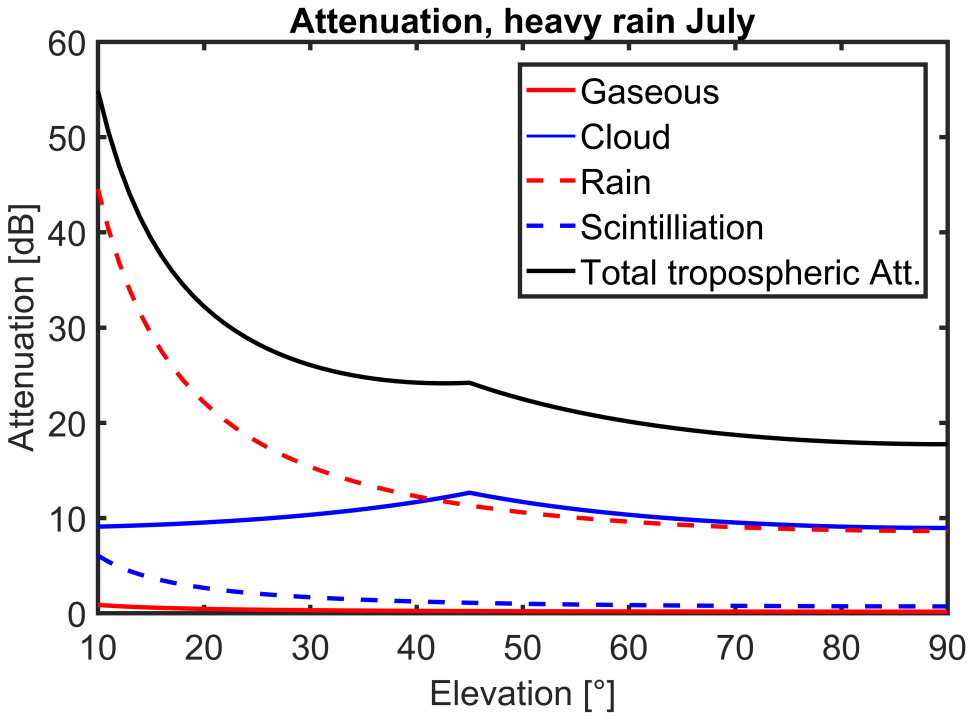

Fig. 4–4: Individual sources of signal fades during heavy rain in July (worst month)

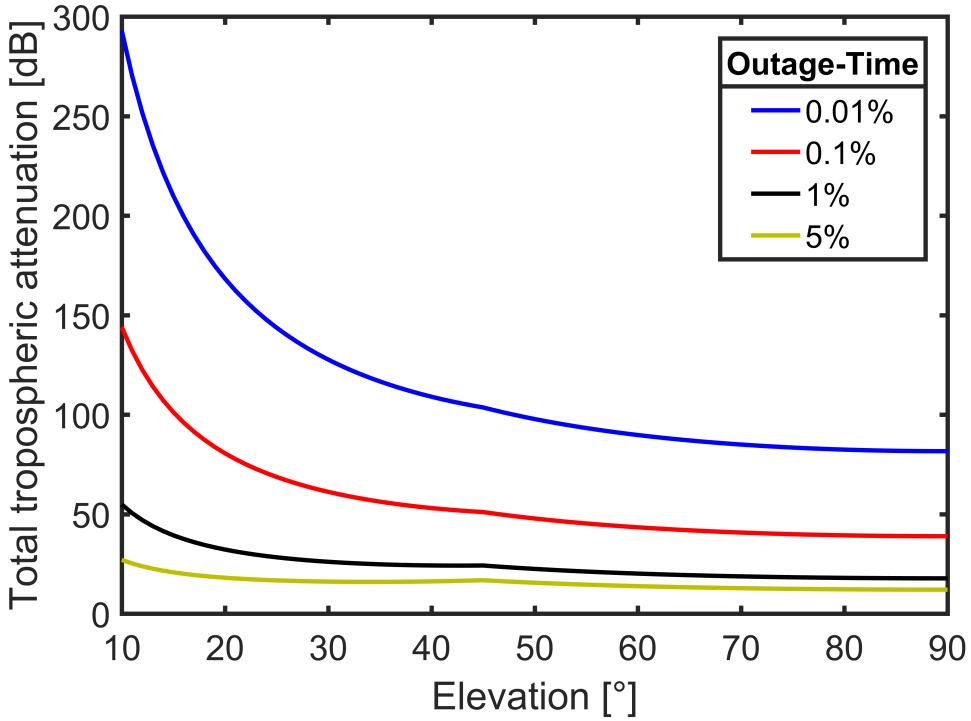

Fig. 4–5: Total tropospheric attenuation as function of outage time percentage and elevation angle in July

4.3 Discussion on simulation results

The first fly by will be at 11:48 which is 12 min before the RAOB in Oberschleißheim. In the 12 minutes time span only micro scale weather phenomena smaller than 1 km and shorter than one hour can occur like turbulences and phenomena in the boundary layer [61]. In the night at 22:30 the satellite passes again 1,5 hours before the RAOB at 00:00 UTC. This duration is in the temporal scale of mesoscale weather phenomena like thunderstorms or fronts. Mesoscale phenomena have a characteristic horizontal length of 1 - 1000 km and the characteristic time scale ranges from 1 hour to one day. Since thermal convection is suppressed during night the change between the satellite measurement and the RAOB can be assumed to be negligible. If a front passes the assumption does not hold. It is important that the atmospheric state remains unchanged between the attenuation measurement and the RAOB to enable a retrieval procedure. The required life time of 14 months (R-SYS-001) can be guaranteed. If the equipment outlasts 60 mouths also the extended mission life time can be realized (G-SYS-002). With the selected orbit the atmosphere is dense enough to de-orbit the satellite within 25 years (R-SYS-006).

Due to the higher humidity in summer the gaseous absorption is more pronounced in summer (0.8 dB). For overcast sky the difference can be explained by the cloud types and their extent. This is visible by the peak occurring at 26° for cumulus clouds and at 45° for cumulonimbus clouds (Fig. 4–2). This peak indicates the maximum path length through the cloud. The cumulus cloud type is smaller than a cumulonimbus cloud and bears less LWC. This is reflected by the signal fades. 3.9 dB can be expected for a cumulus cloud and 5.9 dB for a cumulonimbus cloud. For elevations below 26° respectively 45°, the beam is to shallow to pass through the cloud. For larger elevations right of the peak the beam has to pass through the cloud and even the rain causing fades in the order of 9.5 dB and 17.7 dB. This phenomena is not noticeable in winter since the horizontal extent is larger compared to the cloud types in summer. Stratus clouds are thinner and bear droplets with smaller diameter leading less attenuation compared to nimbostratus clouds with the same horizontal extent. The impact of the water density and the rain rate is clearly visible in both months.
The impact of the ground station antenna diameter is negligible for the attenuation simulations. Under heavy rain in July the total attenuation with an elevation of 90° is 17.74 dB with a dish diameter of 0.3 m and an antenna diameter of 0.6 m results in a total attenuation of 17.73 dB in down link. According to ITU the worst month has to be used for the link budget calculations. Based on the climate in Munich in July the largest attenuations can be expected due to heavy rain. The individual sources are depicted in 4–4. Gaseous attenuation is the smallest contributor with 0.2 dB under 90° elevation. Fluctuations of the refractive index cause fades in the order of 0.7 dB. For elevations larger 45° rain attenuation and cloud attenuation are in the same order of magnitude. For example at 90° elevation 8.6 dB during heavy rain and 8.9 dB within the cloud. Below 45° elevation the carrier passes just through the rain and not through the cloud explaining the different behavior of the attenuation. This indicates the difficulties to predict the attenuation due to the geometry of the clouds and their individual parameters.
The comparison of the finding with existing results is challenging since the input pa-

rameter are a function of the location, climate, elevation angle, frequency and outage percentage. [21] simulated for a center frequency of 73.5 GHz, a time outage of 5% and a rain fall intensity of 26.8 mm/h an attenuation of 18 dB with an elevation of 10° for a GS in Spain. The difference to the 27 dB found in figure 4–5 (green line) is due to the difference in the rain rate. Comparing the findings for an outage of 1% (black line) and a frequency of 76 GHz at zenith with the graphs in [7] for Rome shows that the results are in the same range of 18 dB. According to the ITU rain rate maps the same order of magnitude in rain fall rate (40 mm/h) can be expected in Munich. Anyhow, the comparison is only a rough check of the results because the resolution of the displayed graphs and maps is coarse. During the worst month the sky noise temperature to be expected is shown in figure 4–3. The general pattern of the sky radiometric temperature is in agreement with the observations stated in [15]. The highest values occur during rain followed by cloud covered skies. Under clear sky condition where the transmission experiment shall be performed the noise temperature ranges from 12–52 K. These results are in agreement with the 10–40 K stated by [4] for the V-band (50–75 GHz).

5 Payload instrument and system concept

5.1 Concept of operations

Tropospheric propagation measurements and transmission experiments require repetitive coverage of the Northern hemisphere. Under the assumption that the atmosphere is symmetric about the Intertropical Convergence Zone and the climate can be characterized by temperature and precipitation it is sufficient to measure just in the northern hemisphere. This reduces the power consumption to one forth of the orbit. One satellite is proposed to fly in a sun synchronous repeat track. The orbit will be optimized so that the satellite approximately passes over LRT GS at 12:00 UTC. An overhead pass at 00:00 UTC is desirable.
The first mission phase out of three is the commissioning phase. During this time all solar panels and antennas are deployed. In this phase the satellite, the payload and the ground segment is being verified before moving into the second mission phase.
During the propagation measurements the transmitted known and unpolarized, unmodulated 76 GHz signal will be received in first place by the Munich LRT ground station. The satellite signal will be received by a dish antenna. In addition the station must operate a power radiometer to detect the signal reverence level and a rain gage. Before and after the satellite overpass the Munich LRT GS measures the noise temperature of the sky in flight path direction. During the overpass the satellite points towards the ground station to extend the link window. The overpass of the satellite is then concurrent with the operational radiosonde launch at Oberschleißheim. This key feature enables to simulate attenuation of the atmosphere according to ITU models and compare the results with the measurements. Details will follow in chapter 6. After the satellite passed Munich it will return to its nadir looking nominal mode. Thus station located in other climate zones along the repetitive ground track are able to receive the signal and contribute to the atmosphere characterization. This phase lasts ideally 12 months to cover all seasons in the northern hemisphere and to derive reliable statistics.
After the characterization of the atmosphere the third mission phase is concerned with the data transmission under varying weather conditions. On-board stored data sets will be repeatedly transmitted in the northern hemisphere. As in phase two the satellite will point during its pass in the Munich area towards the LRT ground station. After the pass it will return to nominal nadir pointing mode. Mobile stations along the ground track receive the repetitively sent data sets. At the ground station the BER and quality of service will be analyses.
A typical cycle is depicted in figure (fig 5–1). The local horizon coordinate system of the satellite is defined by the yaw axis pointing towards the center of gravity (nadir), the roll axis points in the direction of the velocity and the pitch axis is orthogonal to the orbital plane completing the right handed frame. The nominal pointing mode is nadir (fig 5–1, 1) and the W-band payload will be activated at 85° northern latitude. Before acquisition of the signal the satellite will orient itself towards the ground station (fig 5–1, 2). During the overhead pass the satellite points at the ground station and transmits the W-band signal and measurements are taken (fig 5–1, 1–4) on ground. After the pass

the satellite will rotate back to its nominal attitude (fig 5–1, 5) and turn the transmitter off at the equator. The maneuver is constraint to a pure rotation about the pitch axis. The presented concept of operations assumes that the orbital life time is long enough to fulfill all three phases. An alternative concept of operation with one spacecraft is to run the payload in both hemispheres covering all seasons in one pass and switch it of the following cycles to recharge the batteries. Small constellation of three identical CubeSats [16] is also an option to collect enough data to characterize the tropospheric attenuation within short time. In all presented concepts the atmospheric drag is sufficient to de-orbit the satellite with in 25 years.

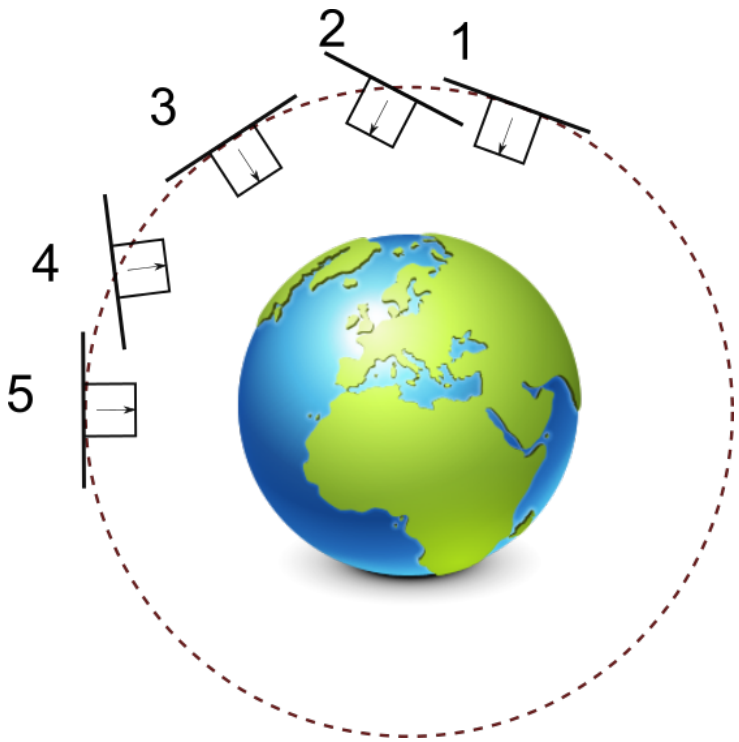

Fig. 5–1: Attitude during experimental mode. 1: nominal mode, transmitter on at 85° northern latitude; 2–4: orientation towards ground station, W-band experiments; 5: return to nominal mode, transmitter off at the equator
Globe: MazeNL77, [Online]. Available: http://findicons.com, [accessed: 09.01.2017]

5.2 Instrument design

In the next section a possible transmitter design is developed since no W-band transmitters are commercially available yet. First, the data rate will be estimated followed by the horn antenna dimensions. Both variables directly influence the link budget. The W-band payload is designed to be compliant to the PC/104 specification and fit in the limited space of 1U CubeSat.

5.2.1 W-band transmission chain

At the beginning of the transmission chain r redundant bits are added to the original data stream R_b of n bits (Fig. 5–2). The code rate ρ gives the ratio of the number of science data bits to the number of encoded bits.

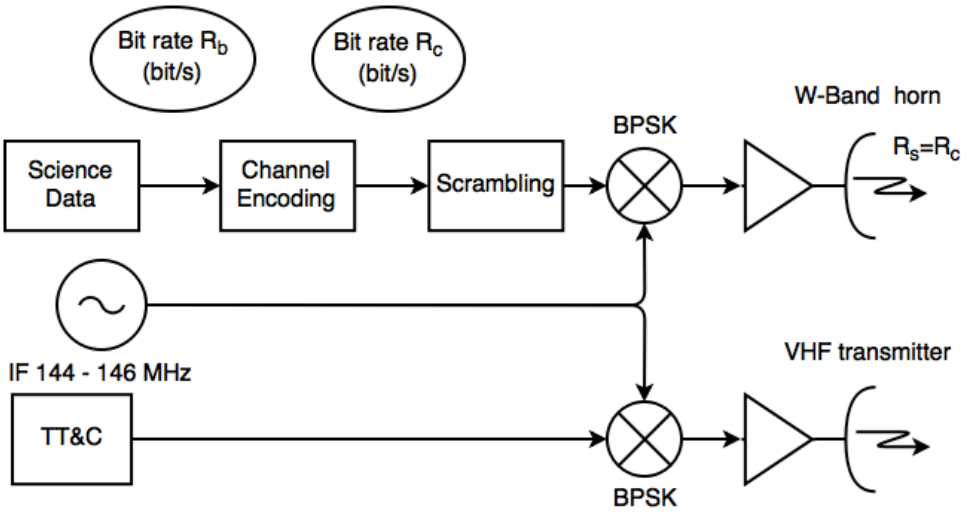

Fig. 5–2: The elements of the W-band transmission chain.

$$\rho = \frac{n}{n+r} \tag{5–1}$$

This forward error correction allows to detect and correct for errors [14]. After the encoding the bit rate has increased by a factor of $\frac{1}{\rho}$.

$$R_c = \frac{R_b}{\rho} \tag{5–2}$$

Since block encoding is less sensitive to fading conditions compared to the convolutional encoding block encoding technique was selected [14]. The selected code operates with a code rate of ρ = 7/8 and is a compromise between power demand and required bandwidth [14]. The repetitive transmission of on-board stored data leads to a repetitive bit stream causing lines in the spectrum of the modulated carrier. To avoid these peaks, ITU recommends to use energy dissipation techniques to limit the interference with other radio communication systems [14]. This is done with a method called scrambling. Scrambling introduces a known pseudo random bit stream and disperses the carrier power. In the next step the simplest and most robust modulation technique, the two-state phase-shift keying (PSK) is applied. The bit stream R_c is modulated onto an intermediate frequency (IF). The IF is located in the VHF amateur band in the range from 144.000 MHz to 144.025 MHz. The symbol rate (baud) R_s to be transmitted depends directly on the modulation scheme. In the case of the selected binary phase-shift keying (BPSK) the symbol rate is equal to R_c [14]. After the modulation, the IF is upconverted, amplified and transmitted (Fig. 5–2). The occupied bandwidth B is a

function of the spectral efficiency Γ (Equ. 5–3), which depends itself on the modulation type. In the case of BPSK Γ=0.7 bit s^{-1} Hz^{-1} [14].

$$B = \frac{R_c}{\Gamma} = \frac{R_b}{\rho\,\Gamma} \tag{5–3}$$

With the maximum available bandwidth of 2700 Hz [62] in the amateur band this results in an achievable data rate of 1890 b/s. To transmit at the required data rate of 1 Mb/s (R-MIS-002) a bandwidth of at least 1.43 MHz is necessary. Therefore the preferred amateur spectrum (R-MIS-001) is resigned and for the further analysis the full range of 71–76 GHz will be considered to transmit data rates R_c from 1 Mb/s to 10 Mb/s.

5.2.2 Antenna parameter

Due to the physical limitations an optimal conical horn antenna [63] was selected. The quadratic relation between the antenna diameter d and the length l (Equ. 5–4) is shown in figure 5–3. The maximum antenna gain only depends on the length of the horn and the wavelength λ of 3.9 mm (Equ. 5–5). On the right axis the transmit power in Watt is presented for the required EIRP of 30 dBi (R-MIS-004). To fit the horn into one unit cube the chosen diameter d of 30 mm corresponds to a length of 74 mm with an antenna gain of 24.8 dBW. Using the definition of EIRP (Equ. 5–6) this results in a transmit power of 5.2 dBW or 3.3 W.

$$d = \sqrt{3.127\,\lambda\,l} \tag{5–4}$$

$$G_T = 7.08 + 20\,log_{10}\left(\frac{d}{\lambda}\right) \tag{5–5}$$

$$EIRP = P_T + G_T \tag{5–6}$$

A measure for the directionality of the transmitted power is the angular beamwidth at 3 dB, $\Theta_{3\ dB}$. At this characteristic point the power intensity drops to one-half of the peak power. For the optimal conical horn antenna, the beam width at 3 dB (Equ. 5–7) for downlink is 8.4° in E-plane and 9.9° in the H-plane (Equ. 5–8). Supposing the link works with half of the signal strength, $\Theta_{3\ dB}$ defines the range of antenna pointing [33]. Nevertheless, it is practice to limit the alignment angle to that point where the signal drops by 0.5 dB [33]. Of course, this requires accurate attitude control. Assuming that for small angles the equation 5–9 holds the boresight angle for the 0.5 dB drop occurs at 1.7° in the E-plane and at 2° in the H-plane. For further considerations the stringent 1.7° will be used.

$$\Theta_{3\,dB\,E} = arcsin\left(\frac{0.5662\,\lambda}{d}\right) \tag{5–7}$$

$$\Theta_{3\,dB\,H} = arcsin\left(\frac{0.6639\,\lambda}{d}\right) \tag{5–8}$$

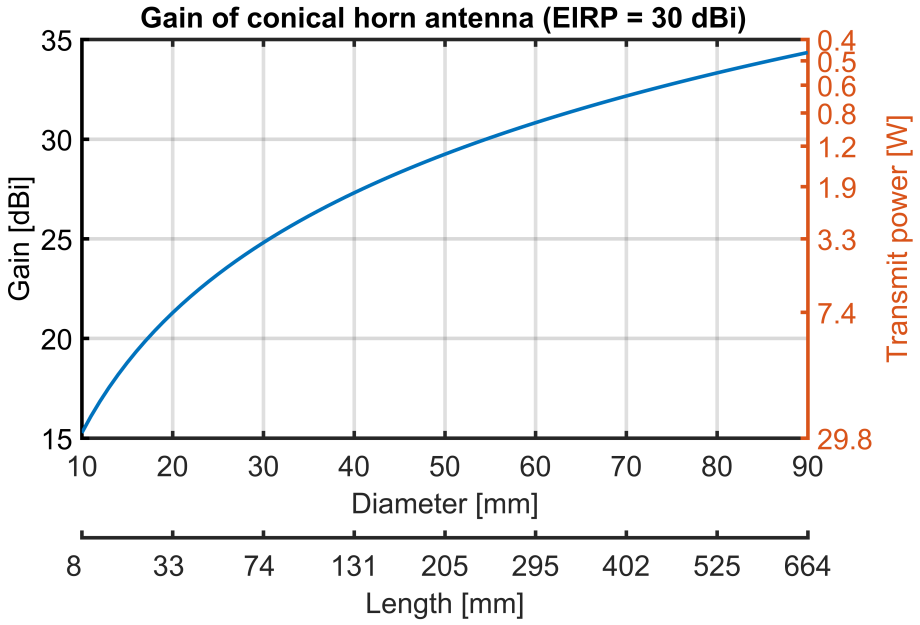

Fig. 5–3: Antenna gain for an optimal conical horn in dependence of the horn length. The right scale shows the required transmit power for an EIRP of 30 dBi at a given horn length aperture diameter respectively

$$G(\Theta)_{dBi} = G_{max,dBi} - 12\left(\frac{\Theta}{\Theta_{3\,dB}}\right)^2 \tag{5–9}$$

The overall link performance (Equ. 5–10) depends strongly on the distance between transmitter and receiver and the weather conditions. To overcome the impairments of the troposphere (A_T) it is recommended to use the attenuations occurring in the worst month [45]. During an overpass the distance decreases drastically from maximum 3000 km at 10° elevation to 570 km in zenith. This reduced distance lowers the free space loss (L_{FS}) and leads to an increase of the transmittable data rate R_c. The losses due to mispointing ($L_{depoint}$) are driven by the 3 dB beam width. These, in turn, depend on diameter of the antennas. At the ground station $\Theta_{3\,dB}$ decreases linearly with increasing diameter form 0.9° at 0.3 m to 0.6° at 0.5 m. Due to the high directivity of the beam the mispointing shall be less than 0.1° [5]. From the requirements the EIRP was set to 30 dB and E_b/N_0 to 10 dB. The system temperature T_{sys} is assumed to be 30 dBK (R-SGS-003). The Boltzmann constant k is -228 dBK and a overall margin of 3 dB [64] was applied.

$$P_T = \frac{E_b}{N_0} + A_T + L_{FS} + L_{depoint} + T_{sys} + R_c - G_T - G_R - k + 3 \tag{5–10}$$

The larger the diameter the narrower the beam and the more demanding are the requirements for the pointing mechanism. With the recommended margin of 2 dB [5] the loss due to misalignment $L_{depoint}$ sums up to 2.1 dB at a diameter of 0.3 m and to 2.4 dB for a diameter of 0.5 m. The depointing loss is assumed to be 2.4 dB. The selected dish antenna has a diameter of 0.3 m similar to that proposed by [4] with a gain of 45 dB.

Rearranging equation 5–10 and solving it for the critical total attenuation with the two required data rates of 1 Mb/s and 10 Mb/s shows that the lower data rate can cope with an attenuation up to 197.6 dB while for a 10 Mb/s link the limit is at 187.6 dB. These limits are indicated by the gray horizontal lines in figure 5–4 and 5–5. A transmit data rate of 1 Mb/s is realizable in all scenarios in January (Fig. 5–4), under clear sky conditions from a minimum elevation of 18° onward. Fof overcast sky the limit is 20° for stratus clouds and 29° for nimbostratus clouds. During moderate rain the lower limit is 26° and at heavy rain 72°. For a data rate of 10 Mb/s the limits are shifted to higher elevation angles. The minimum elevations are as follows: clear sky: 54°; stratus clouds: 60°; moderate rain: 84°; during nimbostratus clouds and heavy rain a 10 Mb/s connection is impossible.
In summer (Fig. 5–5) the attenuation are larger and also the smaller extent of the clouds is visible in the graphic showing the attenuation in dependence on the elevation angles. The minimum elevation angles to establish a 1 Mb/s link are: clear sky: 20°; cumulus clouds: 34°; cumulonimbus 59°; moderate rain 39°; no 1 Mb/s connection is possible during heavy rain . In July and during clear skies a 10 Mb/s connection can be expected to work at an elevation of 58° onward. In all other scenarios a 10 Mb/s is not reached.

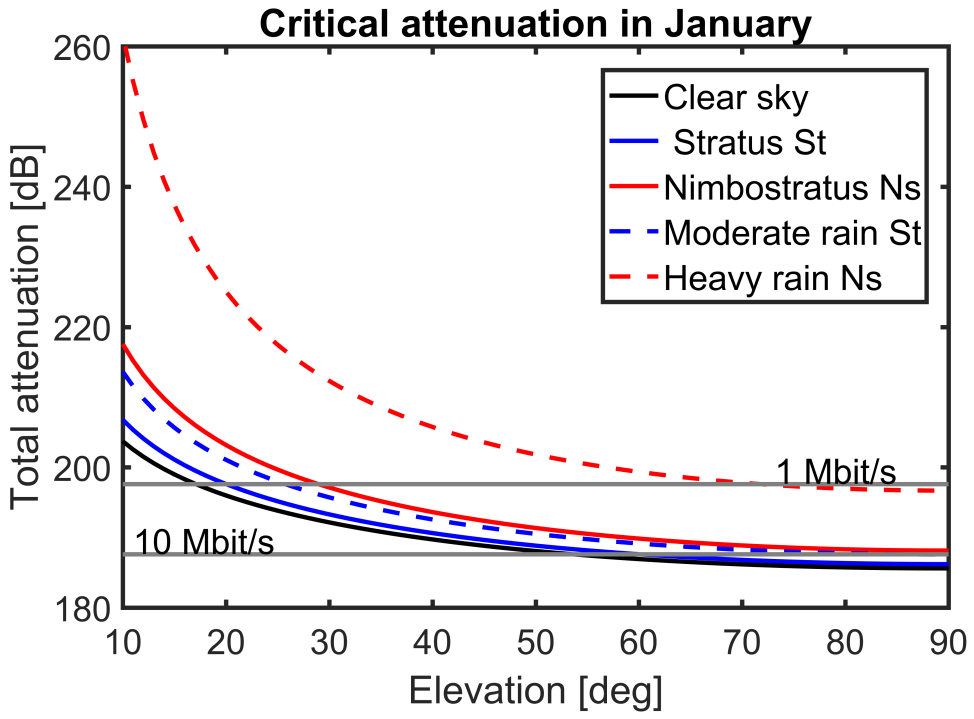

Fig. 5–4: Maximum total loss (free space and tropospheric) for a 1 Mb/s and a 10 Mb/s link in January depending on the weather situation, EIRP of 30 dBi, E_b/N_0 of 10 dB

Solving the link equation 5–10 for the realizable data rates reveals the effect of rain on the link performance. The smaller cloud and rain droplet diameters in January (Fig. 5–6) allow higher data rates, up to 15.8 Mb/s in zenith direction compared to July (Fig. 5–

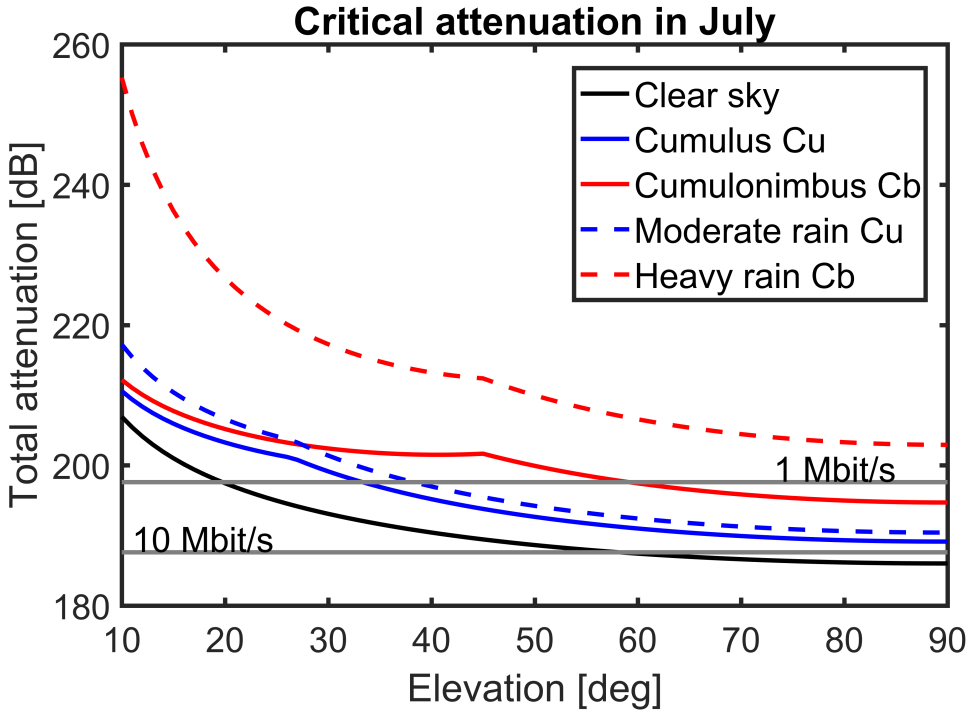

Fig. 5–5: Maximum total loss (free space and tropospheric) for a 1 Mb/s and a 10 Mb/s link in July depending on the weather situation, EIRP of 30 dBi, E_b/N_0 of 10 dB

7) where the droplet diameters are larger (14.4 Mb/s). Also the water vapor content due to the higher temperatures weakens the signal. It has to be mentioned again that the ITU simulations under rainy conditions are validated only up 50 GHz [45].

The transmitted data volume in one pass was estimated by multiplying the data rate function (Fig. 5–4 and Fig. 5–5) with the corresponding time interval and integrating over all elevation angles. The time interval of the GS antenna elevation function was 60 s and was derived in STK. In January under clear sky conditions 2.6 gigabit (Gb) can be downlinked in one pass. The volume decreases to 2.1 Gb at stratus cloud cover and to 1.2 Gb at nimbostratus clouds. Moderate rain allows to transmit a volume of 1.4 Gb, during heavy rain only 0.1 Gb can be sent. With the chosen coding rate of 7/8 this corresponds to an information data volume of 282.5 megabyte (MB); 233.8 MB; 129.5 MB; 156.3 MB and 13.5 MB. In July the data volume is 279 MB during clear skies and 113 MB. Moderate rain limits the transfer to 31 MB. The thicker cumulonimbus limits the data volume to 79 MB, during heavy rain the volume drops to 3 MB. In the case of a nadir pointing instrument and acquisition of signal (AOS) and loss of signal (LOS) at 80° the transmitted volume shrinks due to the contact time of 10 s to 156.1 megabit (Mb), 135.9 Mb, 86.7 Mb, 98.7 Mb and 12.0 Mb in January. In July a downlink can be established only during clear sky and cloudy conditions with a data volume of 141.8 Mb and 68.8 Mb. A purely nadir pointing instrument can transmit in the best case 18 MB in January and in July 16 MB. For the nadir pointing instrument the beam width was relaxed to 3 dB whereas in pointing mode the 0.5 dB beam width was applied.

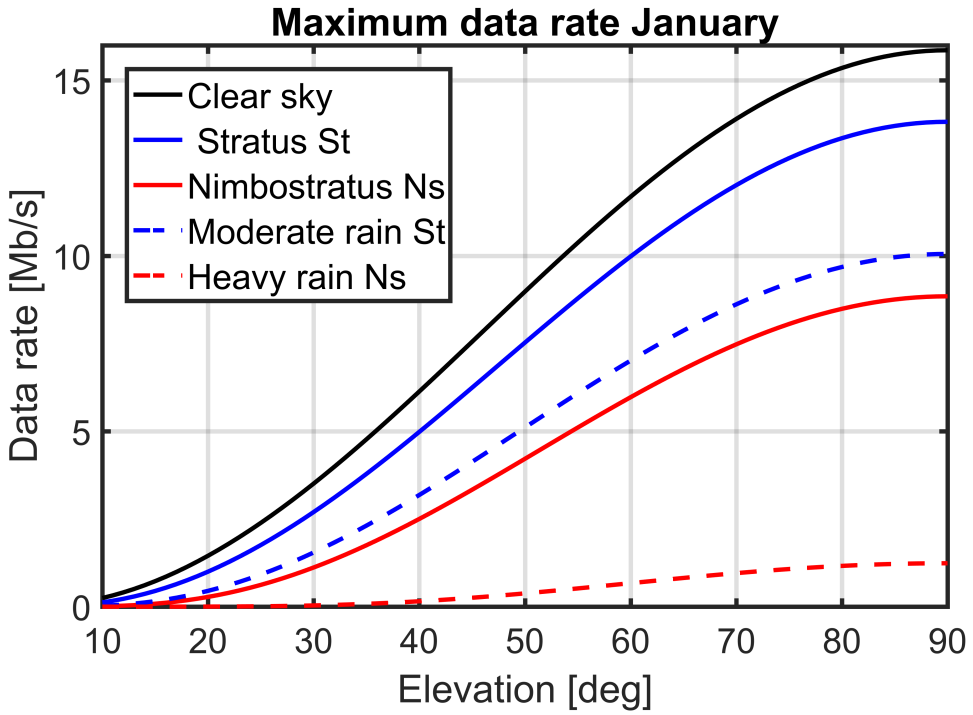

Fig. 5–6: Maximum downlink data rate with EIRP of 30 dBi, E_b/N_0 of 10 dB in January

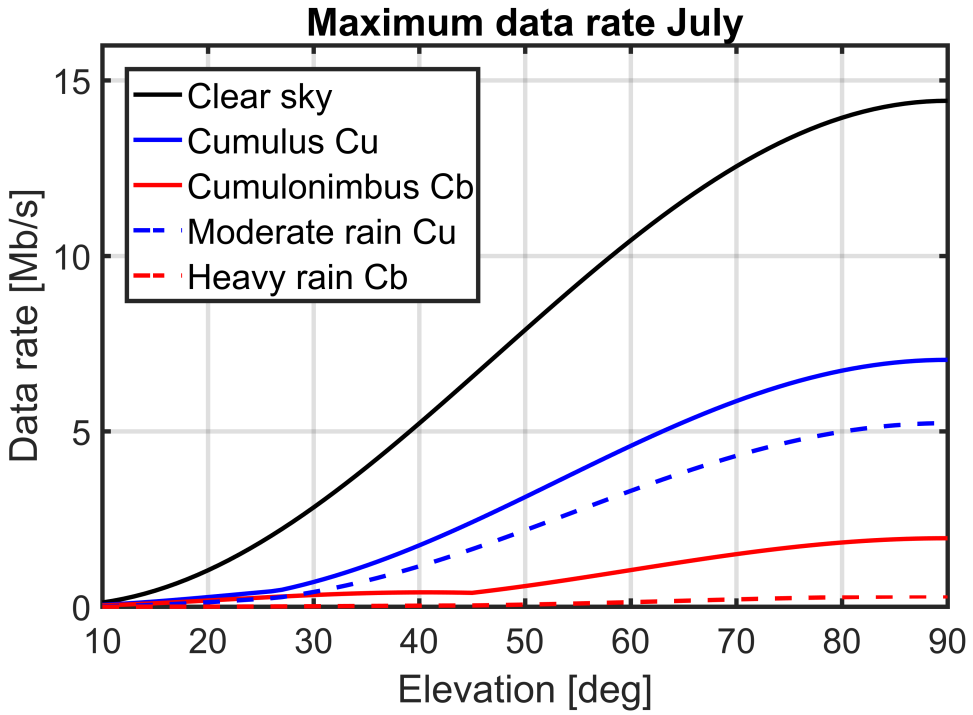

Fig. 5–7: Maximum downlink data rate with EIRP of 30 dBi, E_b/N_0 of 10 dB in July

Evaluating the complimentary error function for BPSK [14] for coding rates from 1 to 1/2 gave the expected BER for a defined E_b/N_0 (Fig. 5–8). To decode an uncoded message (ρ=1) with a BER of 10^{-6} an E_b/N_0 of at least 10.5 dB was required. To lower the E_b/N_0 one possibility was to tolerate a higher BER or to decrease the coding rate. A reduced E_b/N_0 is equal to a lower carrier power, but this reduction is achieved by an increased bandwidth B (Equ. 5–3).

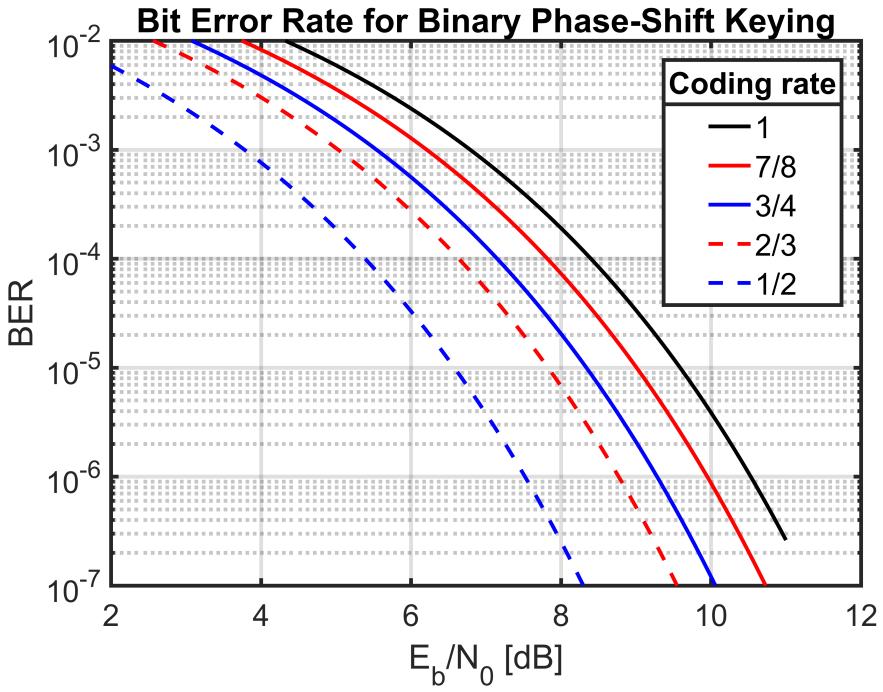

Fig. 5–8: BER analysis for various coding rates

5.2.3 Dimensions

Currently, no commercial off-the-shelf (COTS) W-Band satellite transmitter are available. The physical dimensions have to be compliant with the CubeSat-PC/104 standard boards. Its depth has to follow the form factor. For the estimation of the instrument volume and mass radar components from automotive applications were investigated. The three distance measurement radars operate at 94 GHz with dimensions of 78 x 42 x 28 mm mass of 160 g [65], at 77 GHz and dimensions of 120 x 90 x 46 mm and a mass of 500 g [66] and at 77 GHz and 91 x 59 x 21 mm [67]. [68] confirmed the first estimate of the payload dimensions of 2 Standard CubeSat-PC/104 boards of 90 x 96 x 33.2 mm including the 20% volumetric margin [64].

5.2.4 Payload budgets

Under the assumption of a power consumption of 3.3 W (Sec. 5.2.2) and an estimated efficiency of 0.6 the power consumption of the W-Band transmitter is 5.5 W. Applying a 20% maturity margin [64] results in an estimated power consumption of 6.6 W. Based

on the mass of the similar sized automotive 77 GHz distance radar and personal communication with [68] the estimated payload mass is 150 g. For a detailed analysis a 3D CAD model (Fig. 5–9) was created in CATIA [69]. Within this CAD software it is possible to assign material types to the components of the 3D model. The idea is to use time efficient 3D metal printing methods to plot the horn directly form the CAD model [70]. A conical horn antenna made of aluminum with a diameter of 30 mm a length of 74 mm and a wall thickness of 1 mm has an estimated mass of 21 g. The mass of the total instrument including electronic boards, spacer and screws is roughly 130 g.

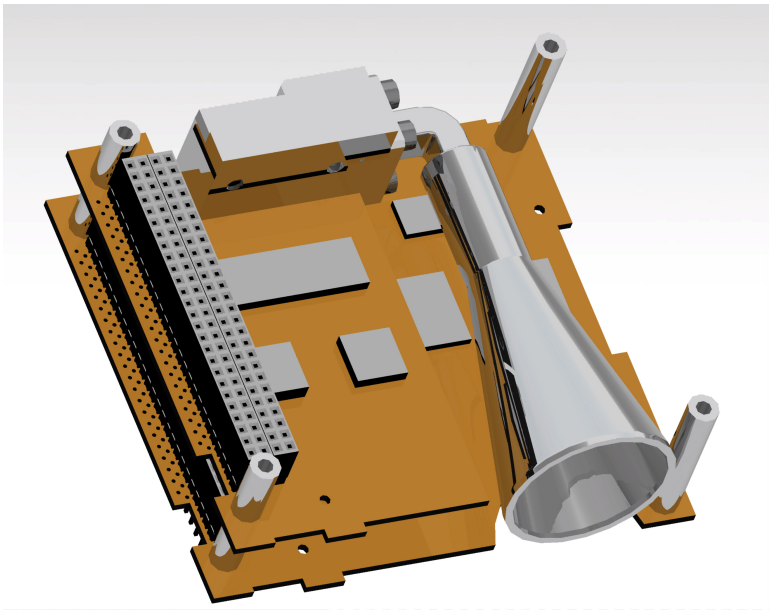

Fig. 5–9: Draft of a possible conic W-band horn within the 33 mm wide instrument (front panel removed), 3D CAD model

5.3 Satellite concept

A very basic concept (concept A) is to employ a nadir pointing payload and use magnetic torquer to maintain the attitude. But, the contact times of concept A are limited to roughly 10 s per flyby. For a sufficient link windows it is inevitable to point the instrument towards the TUM ground station. The instrument itself is permanently fixed to the structure without any steering mechanism. Therefore, two ADCS concepts were investigated to re-orientate the whole satellite. The first version is a 1U CubeSat (concept B). The satellite is actuated by magnetic torquers which are smaller in size compared to the fully integrated attitude determination and control system (ADCS) of concept C. Both concepts are designed to house the 33 mm wide payload. For each satellite concept the benchmark for the available payload volume was the 1U CubeSat Platform + ADCS by EnduroSat [71]. It comprises all subsystems and offers a payload compartment of 97 x 97 x 53 mm^3. It can support a payload mass of 453 g including a power supply of 521 mW. The pointing accuracy is at least 3 degree. Its important to mention that all concepts fit in a standard launch adapter.

5.3.1 Satellite concept magnetic torquer (concept A, B)

The nominal attitude of the 1U CubeSat is nadir pointing. At acquisition of signal the spacecraft is oriented towards the ground station with an attitude angle of + 66.5°. When it passes over Munich within 12 minutes (t_{dur}) the magnetic torquer will point the payload at TUM. The attitude angle at loss of signal will be -66.5°. For a rough estimate of the required torque the equation 5–11 provided in [72] was evaluated. To point the satellite with a mass m of 1.215 kg and a moment of inertia I of 0.0023 kgm^2 a torque T of 9.3×10^{-5} mNm has to be applied.

$$T = \frac{4\Theta I}{t_{dur}^2} \tag{5–11}$$

$$D = \frac{T}{B} \tag{5–12}$$

With a magnetic field B of 4.5×10^{-5} T the resulting dipole moment D is 0.0021 Am^2 (Equ. 5–12). A detailed analysis of the angular velocity and angular acceleration rates during the slew maneuverer shows that equation 5–11 underestimates the required torque (Fig. 5–10, red line). With the angular rates exported from STK the maximum required torque is 0.014 mNm resulting in 0.3 Am^2. The selected magnetic torquer offers a magnetic dipole moment 0.2 Am^2. The pointing accuracy is 2° and pointing knowledge of 2°. A sun sensor would improve the pointing knowledge to 0.5° [73].

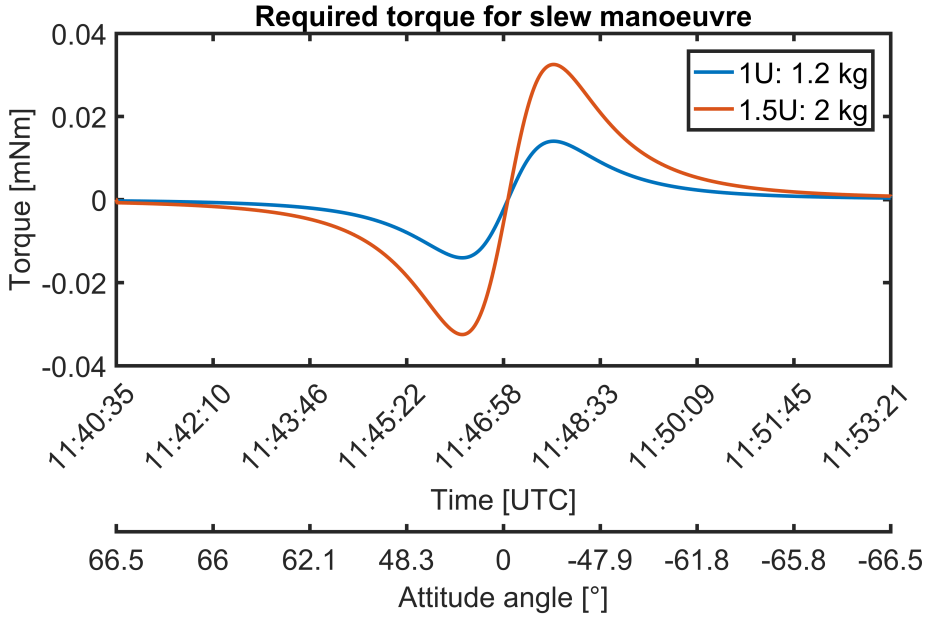

Fig. 5–10: Required torques to point the spacecraft concepts B, C at GS during the second cycle on Oct 4, 2016

5.3.2 Satellite concept ADCS (concept C)

The 1.5U CubeSat concept differs from the 1U only in the actuation of the satellite. The selected ADCS has a size of 1/2U and is manufactured by Maryland Aerospace, Inc [74]. Since no data on the pointing accuracy and pointing knowledge was available values from comparable systems were adopted. The assumed pointing accuracy is 0.5° and the assumed pointing knowledge is 0.055° [75]. The selected ADCS board comes with three magnetic torquer, three reaction wheels and two Earth horizon sensors. Due to the increased mass (2.016 kg) and increased length of 147.6 mm the moment of inertia is 0.0053 kg m^2. According to equation 5–11 a torque of 2.2×10^{-4} mNm is necessary to ensure pointing. Evaluating the attitude angle based on STK (Fig. 5–10, blue line) results in a maximum required torque of 0.0325 mNm. The maximal available torque of the fully integrated ADCS is 0.635 mNm.

5.4 Budgets

For the further analysis COTS subsystems with a complete data sheet were favored (Tab. 5–1). If data was missing it was estimated by comparison with similar components. The TRL was determined in accordance to [76]. The costs of the W-band payload need to be defined (tbd) in the design process of the instrument itself. A rough cost estimate based on the breakdown of small satellite costs [72] without propulsion states that the payload costs are 33% of the total bus costs. Based on the bus costs of the three concepts the payload costs are in the range of 20500 € to 34000 €.

5.4.1 Power

A first estimate of the power budget is presented in table 5–2. It summarizes the power consumption during one orbit and the different operation modes. The concepts based on the magnetic torquer (sec. 5.3.1) are indicated with $^{(A,B)}$. The values valid for the integrated ADCS are marked with $^{(C)}$. Each unmarked component is implemented in all versions.
Not the power consumption during the eclipse phase is critical for this mission, but the peak power during simultaneous downlink and W-band instrument operations. The battery capacity C_r was sized for a depth of discharge (DOD) of 45% (eq. 5–13). The selected lithium polymer cells ensure roughly 12000 cycles [14]. One charge/discharge cycle corresponds to one orbital revolution and results for this LEO satellite in an orbital life time of 2.2 years. The storage efficiency η_S is 0.9 for charging and discharging. Based on the operation mode and the concept (Tab. 5–2) the required power P during a typical cycle is 5.51 W for concept A, B and 7.51 W for concept C. These values include a path efficiency η_p of 0.9.

$$C_r = \frac{P t_o}{\eta_S DOD} \tag{5–13}$$

Solving the equation 5–13 for a power of 5.51 W results in a battery capacity of 13.6 Wh for concept A, B. For concept C the battery shall have a capacity of 18.5 Wh. For the dimensioning of the solar area the panels performance degradation was estimated

Tab. 5–1: Selected subsystems, their TRL and estimated costs for the three satellite concepts. Subsystems of concept A, B are indicated with $^{(A,B)}$, subsystems of concept C are marked with $^{(C)}$, unmarked subsystems are used in any of the three concepts

Subsystem	Quantity	Manufacturer	Heritage since	TRL	Cost/Unit (€)	Total Cost (€)
W-band payload	1	TUM lrt	-	2	tbd	tbd
VHF/UHF transceiver$^{(A,B)*}$	1	TUM lrt	-	5	7000	7000
VHF/UHF transceiver$^{(C)}$	1	ISIS	2012	8	8500	8500
Antenna	1	ISIS	2010	8	8250	8250
Onboard computer	1	ISIS	2014	8	9850	9850
ADCS magnetic torquer$^{(A,B)}$	1	NewSpace	2014	8	8000	8000
ADCS$^{(C)}$	1	MAI	-	7	31700	31700
EPS	1	Clyde Space	-	7	6500	6500
Deployable solar panels$^{(A,B)}$	2	EXA	2013	8	8500	17000
Single 1U solar panels$^{(A,B)}$	1	ISIS	2013	8	2500	2500
Deployable Solar Panels$^{(C)}$	4	EXA	2013	8	8500	34000
1U Bus$^{(A,B)}$	1	ISIS	2012	8	2150	2150
1.5U Bus$^{(C)}$	1	ISIS	-	8	2950	2950

* derived from MOVE-II

Concept$^{(A,B)}$	61250 €
Concept$^{(C)}$	101750 €

Tab. 5–2: Power Budget

	Mode		
Subsystem	Idle Power budget (W)	W-band operation Power budget (W)	VHF downlink Power budget (W)
W-band payload	0	6.60*	0
Communication$^{(A,B)}$	0.20	0.20	1.70
Communication$^{(C)}$	0.20	0.20	1.70
Antenna	0.04	0.04	0.04
OBC	0.40	0.55	0.55
ADCS$^{(A,B)}$	0.18	1.80	0.18
ADCS$^{(C)}$	1.13	3.2	1.13
Operating duration [min]	70.00	24.00	8.00
Concept$^{(A,B)}$ [W]	0.95	3.68	0.33
		5.51	
Concept$^{(C)}$ [W]	2.07	4.24	0.46
		7.51	

* includes 20% design maturity margin [64]

using the equation 5–14 from [14]. Since the efficiency e_{EOL} is the ratio of power produced at the end of life (EOL) over the power generated at beginning of life (BOL) it is valid to set e_{BOL} to 1. After the time span T of 2.2 years the efficiency e_{EOL} drops to 0.9. The production of the necessary electrical power depends on the solar flux Φ, the cell efficiency η_C, the orbital period t_o, the duty cycle duration t_d and the overall performance degradation (Equ. 5–15). With a cell efficiency η_C of 0.19 for the low cost cells [77] and a storage path efficiency η_{Sp} of 0.9 this results in an area 0.0319 m^2 for concept A, B and 0.0434 m^2 in concept C. Applying a scale factor of 1.2 gives the necessary solar panel area of 0.04 m^2 in the case of 1U and for the 1.5U concept it is 0.05 m^2. These values represent an upper limit for the low cost solar panel area and can be reduced by implementing the more efficient cells with an η_C of 0.3 [77].

$$e_{EOL} = e_{BOL} e^{(-0.043T)} \tag{5–14}$$

$$A = \frac{P}{\Phi} \frac{1}{\eta_C} \left(1 + \left(\frac{1}{\eta_{Sp}} \frac{t_d}{(t_o - t_d)} \right) \right) \frac{BOL}{EOL} \tag{5–15}$$

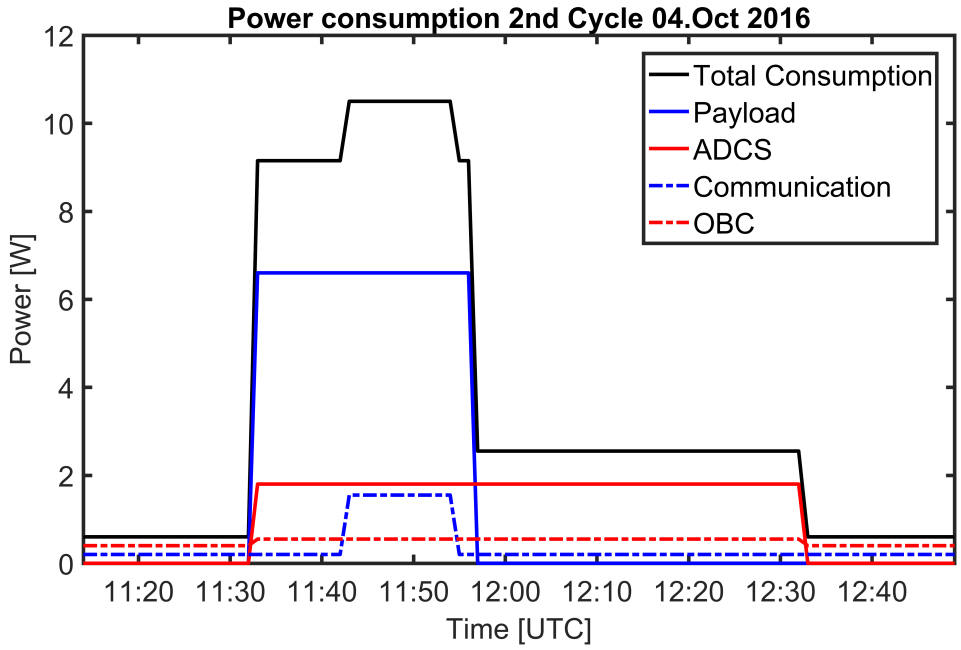

Fig. 5–11: Power consumption during the second cycle on Oct 4, 2016

5.4.2 Communication

Similar to the TUM MOVE-II, the satellite telecommand and mission plan will be uplinked via the UHF amateur band. The TT&C downlink of the telemetry and housekeeping data is performed in the amateur band of the VHF [78]. With the selected subsystem an uplink rate of 1200 b/s and a downlink rate of up to 9600 b/s can be achieved. The VHF serves also as IF for the data transmission experiment (Fig. 5–2). The active omnidirectional antenna will establish the connection from a minimum elevation of 10° onward.

5.4.3 Mass

The mass budget of the individual satellite concept was derived from the manufacturer data sheets (Tab. 5–3). According to [64] the maturity margins were applied based on the TRL of each subsystem. In all concepts the ADCS, the EPS and the solar panels belong to the heaviest components but have a TRL of at least 7. Therefore a margin of 5% is sufficient. The highest uncertainties are introduced with the W-band transmitter and the customized communication subsystem. The expected mass of the 1U concept is 1215.7 g and in the worst case 1303.3 g. For the 1.5U concept the numbers are 2016.5 g in the optimal case and 2139.9 g in the worst case.

5.5 Identification of launch opportunities

Launch providers deliver CubeSats containerized in a 3U deployer for 295000 USD as secondary payload [85] into various orbits. The major constraint is the fact that the primary payload determines the final orbit. Therefore, it seems to be difficult to find a

Tab. 5–3: Mass budgets of the 1U and 1.5U concept. Left column gives the estimated mass of the subsystem based on the manufacturers' data sheet. Margins depend on the maturity of the subsystem and the last column gives the mass including the margin

Subsystem	Mass (g)	Margin (%)	Mass incl. margin (g)	Reference
W-band payload	150.00	20.00	180.00	5.2.4
Communication$^{(A,B)}$	85.00	10.00	93.50	MOVE-II [68]
Communication$^{(C)}$	85.00	5.00	89.30	[79]
Antenna	10.00	5.00	10.50	[80]
OBC	94.00	5.00	98.70	[81]
ADCS$^{(A,B)}$	200.00	5.00	210.00	[82]
ADCS$^{(C)}$	694.00	5.00	728.70	[74]
EPS	339.00	5.00	356.00	[83]
1U Bus$^{(A,B)}$	107.70	5.00	113.10	[84]
1.5 Bus$^{(C)}$	184.50	5.00	193.70	[84]
Concept$^{(A,B)}$	1215.7		1303.3	
Concept$^{(C)}$	2016.5		2139.9	

satellite mission with exact the required orbit. More precisely, the challenge is not the LEO but to place the satellite in an orbit with the desired local time of the ascending node (LTAN) (Tab. 4–1).
In accordance to the space debris mitigation guideline the upper limit of a circular sun-synchronous orbit (SSO) for the 1U CubeSat, concept A and B, is at 650 km. The limit for the 1.5U concept is 645 km. This results from simulations in STELA with the same properties stated in section 4.1.1. Launch providers like Spaceflight Industries, Inc. [85] publish their future launch capacities on-line. For the near future, until the end of 2020, 17 launches are listed to deliver CubeSats into a SSO in an altitude range from 500–600 km (Fig. 5–12).

5.6 Discussion

It is difficult to compare the payload design of this study with existing feasibility studies because other agencies studies are not limited to CubeSat platforms in a LEO. These studies focus on channel attenuation measurements or on data transmission experiments. The WAVE-mission [7, 86] and the proposed NASA study [4] are designed to performed attenuation measurements from satellites positioned in GEO. The DAVID mission and the study by [21] are dedicated to data transmission from LEO. [21] calculated the achievable data rates for satellite antennas with a diameter of 0.5 m and 1 m. The ground station antenna diameter varied between 2 m and 6 m resulting in a mini-

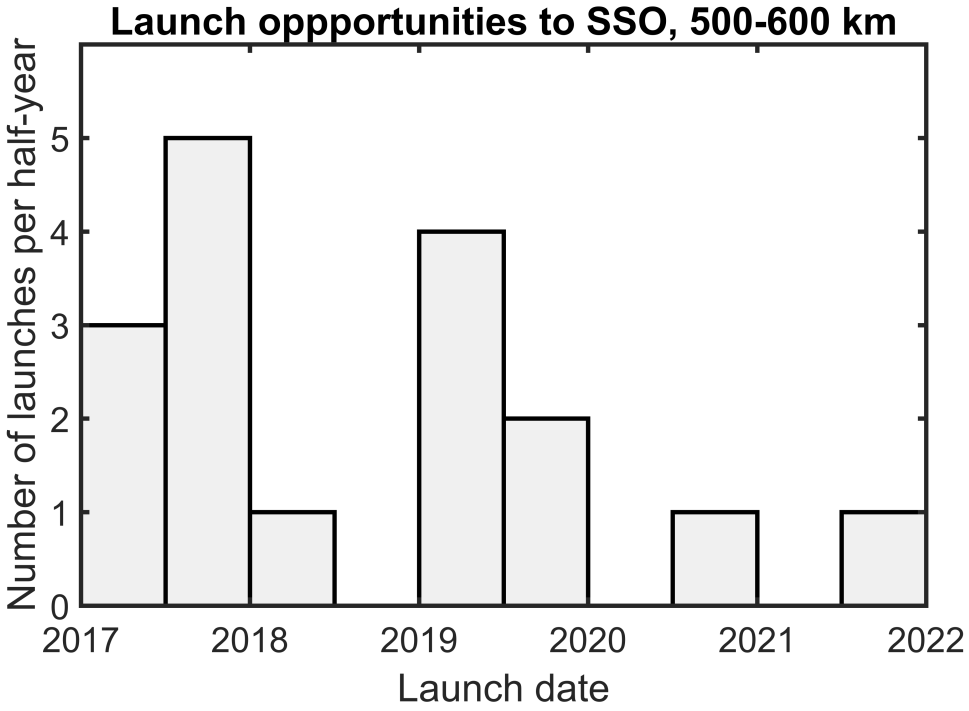

Fig. 5–12: Launch opportunities until end of 2020 to a sun-synchronous LEO in the range from 500 km to 600 km

mum data rate of 355 Mb/s to a maximum data rate of 5.0 Gb/s. These GS antennas are by a factor 6–20 larger than selected 30 cm dish and offer a larger gain. Besides the antenna dimensions the modulation scheme was different, [21] used quadrature phase-shift keying (QPSK). However, the most critical electrical hardware component is the W-band transmitter. [16] pointed out that currently no space qualified COTS for W-band communication are available at the commercial market. Therefore, existing automotive hardware operating at 77 GHz was used to demonstrate that it is technically feasible to fit the electronics and horn antenna into a CubeSat bounding box. An uncertainty for the link budget are the invalidated models in the W-band range. In the simulations this was accounted by margins. With the presented design it is possible to realize the same E_b/N_0 ensuring the required 6.9 dB for BPSK with 7/8 coding [14] and the 10 dB stated by [21]. As expected the highest data rates can be achieved under clear sky condition followed by overcast sky. The budgets prove that the payload can be supported by COTS subsystems (Tab. 5–1).
Comparing the three proposed satellite concepts shows the limitations of the magnetic torquer. The selected ADCS deliver a magnetic dipole moment of 0.2 Am^2. This is insufficient to point the payload at GS with the required magnetic moment of 0.3 Am^2. The 1.5U satellite convinces with its integrated 3-axis controllable ADCS and sensor suit. This ensures to point at the GS during the overpass. In addition the payload compartment with 96 x 90 x 37 mm^3 is larger than the required volume. The drawback of the second concept are the mass of 2.016 kg, and the high cost of the integrated ADCS.
Comparing these concepts to fully equipped CubeSat structures like EnduroSat 1U

CubeSat Platform + ADCS it is evident that the EnduroSat solution cannot deliver the required power for the instrument. To fulfill the power and the pointing requirements this platform has to be customized and equipped with sufficient EPS and ADCS so that the advantage of there larger payload compartment vanishes.

6 Data processing and validation concept

6.1 Measurement and statistics

ITU's Study Group 3 on radio-wave propagation published a list of questions concerning the planning of space communication systems [87]. They stress the need for statistic predictions of RF propagation effects for the link design of future communication satellites. Until 2019 these studies shall be completed and shall depict the temporal and spacial the distribution of atmospheric constituents like clouds, rain, water vapor and aerosols on maps [87]. These statistics are the basis for the simulation of the total attenuation that can be expected during downlink under varying weather conditions (Chapter. 3.5). The empirical models relay on these statistics. Therefore, the propagation and radiometric measurements collected during the propagation experiment are crucial to test the predictions. Storing the collected data according to international standards such as the ITU-R P.311 [48] allows to enhance existing data sets and models. To perform measurements of the tropospheric attenuation the receiver station has to be defined by location and altitude. The characteristics of the receiver antenna and spaceborne transmit antenna have to be stated as well in detail including the elevation angle as well as the satellites location in east direction. Rain gages need to measure concurrent to the attenuation measurements and have to be defined in the standardized ITU table for slant path statistics [48]. The rain gage integration time has to be one minute. ITU-R P.311 table II suggests that it is intended for fixed elevation angles of GEO satellites even though it is not clearly stated in the recommendations [48]. For each month the total duration (dt) of the experiment in days, the number of days with concurrent rain measurements (dc), the number of days with valid rain gage data (dr) and the duration of valid attenuation measurements (da) has to be provided (Tab. 6–1). P_{0e} is the probability in percent that the rain rate during an attenuation measurement exceeds 0.25 mm/h. P_{0a} indicates the probability in percent that the attenuation is larger than 0.1 dB. The exceedance percentages p in table 6–1 starts at 0.01%. It is the ratio between the exceedance time and the measurement duration (dt). On a yearly and monthly basis the threshold for exceeding the percentage have to be computed for rain rates (mm/h), excess attenuation (dB) and total attenuation (dB) and delivered for fixed and by [48] predefined exceedance percentages p.
All these measurements are a function of the climate at a certain location. As the satellite passes over Europe in cycle two, it covers 10 different climate zones [41] ranging from the Tundra climate to desert climate (Fig. 6–1). During the fly-by the instrument points at the GS. The hatched area indicates the regions where the satellite, in pointing mode (concept B, C), has direct contact to Munich. In figure 6–1 the boundaries of the 3 dB beam width define the 160 km wide swath. The narrow (33 km) one marks the boundaries of the 0.5 dB beam width. The WMO sites with operational RAOB are indicated as blue dots if they fall into the wide swath and as green dots if they lie in the narrow swath. All these climate stations carry out precipitation observations. Thus, these stations are potential locations for a mobile GS.

Tab. 6–1: ITU-R P.311 Part II, Slant path annual and monthly statistics of total attenuation, rain attenuation and rain rate

Period of year	Year	Worst month	Jan	Feb	Mar	Apr	May	Jun	Jul	Aug	Sep	Oct	Nov	Dec
dt (days)			-	-	-	-	-	-	-	-	-	-	-	-
dc (days)			-	-	-	-	-	-	-	-	-	-	-	-
dr (days)			-	-	-	-	-	-	-	-	-	-	-	-
da (days)			-	-	-	-	-	-	-	-	-	-	-	-
P_{0c} (%)			-	-	-	-	-	-	-	-	-	-	-	-
P_{0A} (%)			-	-	-	-	-	-	-	-	-	-	-	-
R 0.001 (mm/h)	-	-	-	-	-	-	-	-	-	-	-	-	-	-
A_{exc} 0.001 (dB)	-	-	-	-	-	-	-	-	-	-	-	-	-	-
A_T 0.001 (dB)	-	-	-	-	-	-	-	-	-	-	-	-	-	-
...														
R p (mm/h)	-	-	-	-	-	-	-	-	-	-	-	-	-	-
A_{exc} p (dB)	-	-	-	-	-	-	-	-	-	-	-	-	-	-
A_T p (dB)	-	-	-	-	-	-	-	-	-	-	-	-	-	-
...														

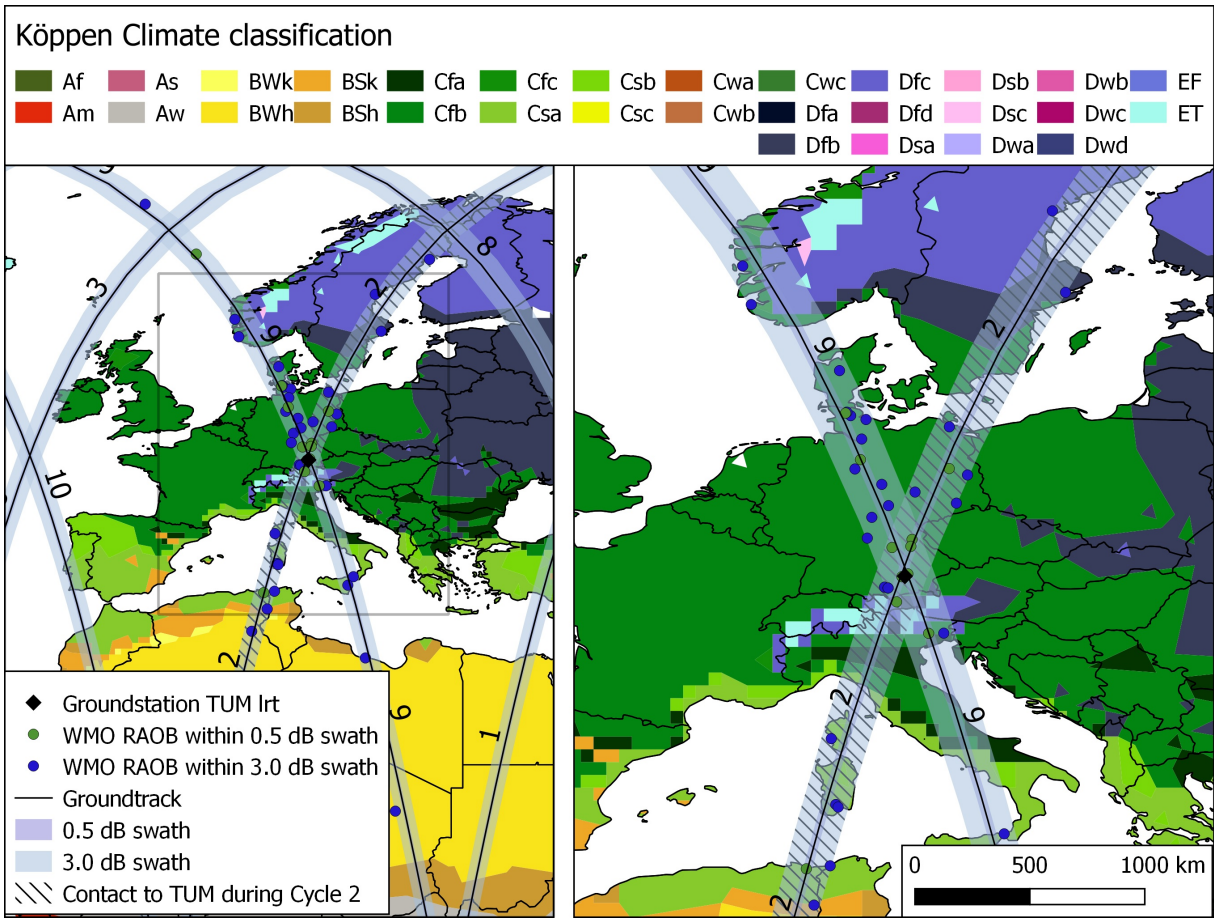

Fig. 6–1: Map of operational WMO RAOB at 00:00 UTC and 12:00 UTC, the black dashed line shows the ground track. Cycle two passes over Munich (black diamond) at 11:48:22 UTC. The narrow blue swath indicates boundaries of the 0.5 dB beam the light blue of the 3 dB.

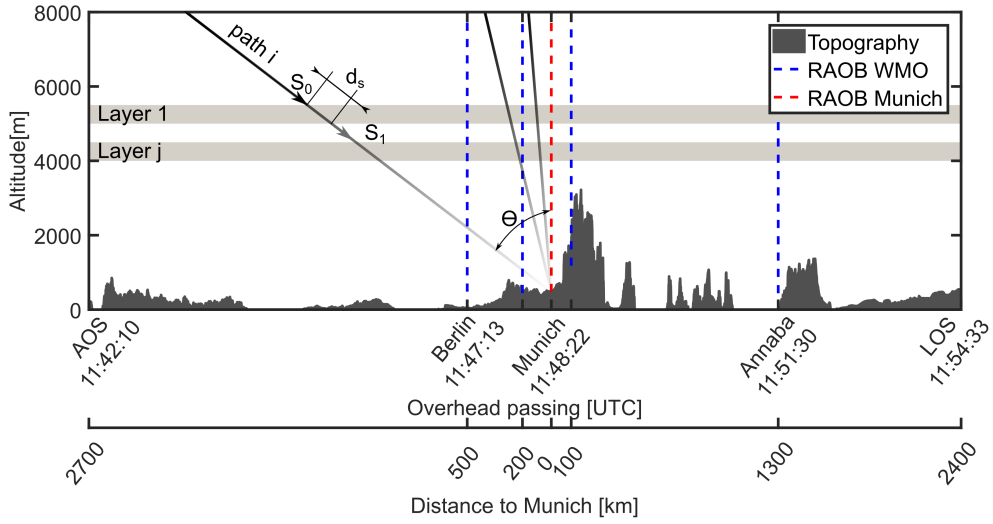

Fig. 6–2: Cross section along the ground track from AOS to LOS, RAOB are indicated by the dashed lines. Black lines indicate the carrier path through the atmospheric layers with different weighting and different optical depth τ

6.2 Separation of multiple attenuation sources

In their publications [12] and [5] state that, the W-band propagation in non-rainy conditions can be predicted reliably with current models based on physics. But further work needs to be done to develop and validate rain, cloud, depolarization and scintillation prediction models [12]. The following section describes a possible retrieval procedure to separate the integral value of the measured total attenuation $A_T(p)$ into its individual sources for validation purposes.
In atmospheric remote sensing problems the forward model F relates the physical state parameter x with the measurement y (Equ. 6–1).

$$y = F(x) \tag{6–1}$$

A proper forward model describing the attenuation of the radiation trough the atmosphere is the two stream approximation [88, 89] of the monochromatic radiative transfer equation (RTE). In this model the atmosphere is divided in plane parallel layers (Fig. 6–2). Solving analytically the two stream approximation results in a set of ordinary differential equations (Equ. 6–2), where the outgoing flux density E_+ and downward flux density E_- are coupled.

$$\begin{pmatrix} E_+(\tau_{j-1}) \\ E_-(\tau_j) \\ S_{Tx}(\tau_j) \end{pmatrix} = \begin{pmatrix} a_{11} & a_{12} & a_{13} \\ a_{21} & a_{11} & a_{23} \\ 0 & 0 & a_{33} \end{pmatrix} \begin{pmatrix} E_+(\tau_j) \\ E_-(\tau_{j-1}) \\ S_{Tx}(\tau_{j-1}) \end{pmatrix} \tag{6–2}$$

The optical properties of the layer j are specified in the coefficients a_{kl} with the following physical meaning [89]:

a_{11} : transmission coefficient for diffuse radiation

a_{12} : reflection coefficient for diffuse radiation

a_{13} : reflection coefficient for the single scattered parallel radiation

a_{23} : transmission coefficient for the single scattered parallel radiation

a_{33} : transmission coefficient for the direct parallel radiation $a_{33} = e^{-sec\Theta\tau_j}$

The flux of the direct ray $S_{Tx}(\tau_j)$ is independent of the first two equations. Since only the attenuation of the direct carrier is of interest only line three of equation is used. The first two lines might be taken into account to estimate the source term due to scattering or emission, which are noise sources within a layer. However the equation of line three is just the Lambert's law (Equ. 6–3). It states that the attenuation within one layer j (Fig. 6–2) decreases monotonically as a function of the path length d_s through the layer j [35]. In equation 6–3, N is the number of particles per unit volume and σ gives their cross section. The extinction efficiency is indicated by the dimensionless factor K_λ. In the particular case of gaseous attenuation the equation changes to the common form of equation 6–4. The air density is given by ρ, r indicates the mass of absorbing gas per unit mass of air and k_λ represents the mass absorption coefficient. The product under the integrals are refereed to as volume scattering, absorption or extinction coefficients with the unit m^{-1}. Integrating the volumetric coefficients along a path ds through the atmosphere results in the optical thickness τ (Equ. 6–5). Projecting it with $ds = sec\ \Theta\ dz$ obtains the normal optical depth, where Θ is the zenith angle. For readability the subscript indicating the wavelength dependency was omitted.

$$ln\ S_{\lambda\infty} - ln\ S_\lambda = sec\ \Theta \int_z^\infty K_\lambda N \sigma dz \tag{6–3}$$

$$ln\ S_{\lambda\infty} - ln\ S_\lambda = sec\ \Theta \int_z^\infty k_\lambda \rho r dz \tag{6–4}$$

$$\tau_\lambda = \int_z^\infty k_\lambda \rho r ds \tag{6–5}$$

The attenuation depends on the optical depth $\tau_\lambda i$ (Equ. 6–5). It is dimensionless and describes the attenuation of the radiation along the slant path. As mentioned before the optical thickness comprises absorption and scattering. Depending on the ratio of the particle radius r_P to the wavelength λ these processes can be distinguished with the size parameter χ.

$$\chi = \frac{2\pi r_P}{\lambda} \tag{6–6}$$

For ineffective scatterers ($\chi \ll 1$) the forward and backward scattering of the radiation is evenly divided [35]. This is the so-called Rayleigh regime. If $0.1 \leq \chi \leq 50$ Mie-scattering occurs and the radiation is scattered in the forward direction. For particles with $\chi > 50$ geometric optics are applicable [35]. Depending on the particle properties and the gas composition in the layer the optical depth can be split according to equation 6–7. The temperature and pressure dependence of $\tau_\lambda^{Gas}(j)$ is omitted for simplicity

[89].

$$\begin{aligned} \tau_\lambda(j) &= \tau_\lambda^{Rayleigh}(j) + \tau_\lambda^{Mie}(j) + \tau_\lambda^{Gas}(j) \\ \tau_\lambda^{Mie}(j) &= \tau_{\lambda,scat}^{Mie}(j) + \tau_{\lambda,abs}^{Mie}(j) \end{aligned} \tag{6–7}$$

The task is to derive the normal optical depth as a function of altitude. The atmosphere is represented by plane parallel layers. It is assumed that the atmospheric attenuation within a layer are independent of other layers. Each attenuating layer will have a dominant contributor (Equ. 6–7) to the optical depth. Merging the layers of the same optical properties and relating them to gas, cloud or rain allows to derive the carrier attenuation within the phenomena. These specific attenuations then can be further compared to simulation results.
The major challenge is that the attenuation measurement gives only the total attenuation along the line of sight, resulting in one optical depth for all layers. The first step is to set up a system of linear equations relating the observations with the total optical depth. It is assumed that the measured attenuation is already corrected for the free space loss. Similar to radio tomographic imaging (RTI) [90] the signal loss in path i can be expressed as by combing equation 6–3, 6–4 with equation 6–5 in discrete form:

$$A_{T_i} = \sum_{j=1}^{n} w_{ij}\tau_j + \epsilon \tag{6–8}$$

Where w_{ij} is a weighting of the optical depth τ_j in layer j. Treating each measurement at a different elevation angle as independent [48] allows to rewrite in matrix form:

$$\mathbf{A_T} = \mathbf{w}\tau + \epsilon \tag{6–9}$$

The attenuation A_{T_i} is the difference in signal strength between the entering and exiting carrier. The most critical part in solving the estimation problem 6–9 for the optical depth is the determination of the weighting or kernel matrix **w**. It indicates how strong the attenuation of a certain layer contributes to the total attenuation. This weighting matrix can be further simplified by mapping the line of sight measurement with the corresponding elevation angle into a vertical profile (Fig.6–2). Meaning that only one vertical weighting is necessary to compute the line of sight weight via trigonometric functions. But the extent of the weather phenomena and the rain measurements limit the mapping to elevation angles close to zenith. For the vertical weighting the key are the RAOB which allow to determine pressure, height, temperature, dew-point temperature and as consequence relative humidity and mixing ratio. The wind direction and strength is also presented as well as the potential temperature to determine the stability of the atmosphere. The minimum number of layers to be estimated is equal to the number of radiosonde measurements during one ascend. From DWD weather stations measurements, the humidity, cloud type and rain rate are essential to estimate the state of the troposphere. If further independent measurements are integrated such as ceilometer the layers have to be adjusted to allow intermediate vertical levels. The estimated specific attenuations can be further used to improve empirical models.
It has to be emphasized that the presented procedure is an idea to separate individual attenuation sources and that the linearization is problematic for large attenuations [91].

6.3 Discussion on data processing

As mentioned above, the key for the statistical evaluation of the attenuation measurements are concurrent rain gage observations. The satellite concept A enables to engage several mobile GS in different climate zones throughout Europe. Measurements from Berlin in the maritime temperate climate to Annaba with Mediterranean climate. With a nadir transmitting instrument only phenomena in the air column above the GS and its close surroundings are contributing to the measured attenuation. Observed rain rates can be directly linked to the measured attenuation. But the overhead pass time is in the order of seconds and the statistics are derived from time spans measured in days [48].

This is not the case for the concepts B and C. As depicted in figure 6–2 the signal is acquired at 11:42:10 UTC. This corresponds to a distance of 2700 km between the sub-satellite point and the GS. On the way through the atmosphere the carrier gets attenuated by phenomena not related to the weather at the GS in Munich. The minimum elevation angle for a valid and concurrent measurement is determined by the extent of the cloud and the rain height and varies with season and location. Under typical rainy conditions in summer the horizontal extent of the cloud ranges from 1 km to 10 km [61]. This already points out that for elevations below the critical elevation no measurements of the troposphere are available and weather reanalysis data have to be employed. The horizontal scale of the model grid of 80 km [92] is larger than the characteristic length (10 km) of a typical thunderstorm cloud in summer [61].

The exemplary spotlight-mode measurement in cycle two (Fig. 6–2) starts with acquisition of the signal at Oct 4, 2016 11:42:10 and stops at Oct 4, 2016 11:54:33. Comparing the times for acquisition on loss of signal with the overhead passing times shows that it is not possible with concept B and C to carry out nadir measurements at all radiosonde locations and perform measurements in Munich in one cycle.

7 Conclusion

The purpose of this study was to derive requirements for a W-band transmitter accommodated in a CubeSat to determine W-band propagation in the troposphere. Further, the presented mission concepts aim for a stepwise progression from attenuation measurement to the data transmission experiment. Therefore, this thesis presented a W-band transmitter concept to be supported by COTS CubeSat subsystems. It could be shown that the payload fits into the limited payload compartment of a 1U CubeSat. With the stated requirements it is possible to establish a downlink rate up to 15.8 Mb/s in the winter during clear sky conditions. In this phase 0/A study three satellite concepts were investigated:

Concept A: 1U bus stabilized by magnetic torquer with nadir looking instrument

Concept B: 1U bus pointing at GS with magnetic torquer attitude control

Concept C: 1.5U bus pointing at GS with the integrated ADCS

During the study it became clear, that for attenuation measurements only the atmospheric column above the GS can be used to derive concurrent attenuation and rain statistics. As well as for the separation of the individual attenuation sources only measurements in the vicinity of the RAOB can be inverted. Therefore measurements close to zenith are sufficient. This ensures that only phenomena linked to the atmosphere at GS are quantified. The Concept A is adequate to carry a nadir pointing instrument. But the observation time span has to be at least one year or an integer multiple of it and the observation time of concurrent measurements has to be given in days. This is hard to realize with a LEO satellite for many reasons. First, the integration time of the concurrent rain gage is one minute which is four to five times longer than the duration of the satellite pass. Second, the duration of valid rain measurements has to be expressed in days as a real number [48]. Which generates small values if the ratios for months or years are built, resulting in questionable statistics on the fades. This limitation might be overcome by a satellite constellation.
For the data transmission experiment on the other hand it is necessary to point the satellite at the GS to ensure a sufficient link window. A nadir pointing instrument at LEO has a too short link time (10 s) to transfer large amounts of data. Concept B does not maintain the required magnetic dipole moment of 0.3 Am^2 to point the instrument at the GS. The fully integrated ADCS of concept C delivers the required torques to point at the GS.
The concepts of operation of the attenuation measurement and of the data transmission experiment contradict each other because the selected EPS limits the mission lifetime to 2.2 years. All presented concepts are unable to deliver concurrent attenuation measurements at any elevation angle over days as demanded by ITU-R P.311. Therefore, it is suggested to design two separate CubeSat missions dedicated to attenuation measurements and to data transmission experiments.
To reach the required observation duration for the statistics one possibility is to design a

GEO mission with the drawback of an increased free space loss, high costs of delivery and the limitation to one elevation angle per GS, but it offers the maximum observation time. An other idea is to set up a constellation in medium Earth orbit (MEO) similar to global navigation satellite system (GNSS) constellations. From one GS several satellites would be visible enabling to estimate the attenuation at a certain elevation angle based on the independent measurements from multiple satellites. To de-orbit the satellites within 25 years they have to be equipped with propulsion systems. Additional constrains for MEO CubeSats are the higher launch costs and the stronger radiation in these orbits compared to LEO. A different approach to extend the observation time is to use a high-altitude platform station (HAPS) to reduce the free space loss. Different elevation angles can be resolved by multiple payloads pointing to mobile GS in the surroundings of Munich.
As a consequence the requirements stated in 2.2 have to be modified. Concept C (1.5U CubeSat) guarantees the required torques to orient the spacecraft towards the GS and shall be the baseline design for the data transmission experiment. The abbreviation TAM will be used in table 7–1 to indicate the tropospheric attenuation measurements and DTE marks the data transmission experiment. Requirements not applicable (n/a) to the dedicated mission are indicated as well as the parameters tbd.

7.1 Suggestions for further studies

Independent of the concept of operation or experiment a detailed analysis of the link budget and transmission chain has to be performed. The attenuation simulations shall be refined with RAOB data of Oberschleißheim. For the attenuation measurements an unmodulated beacon at the 75.5–76 GHz amateur frequency is sufficient to carry out the measurements. This simplifies the transmission chain omitting on-board stored science data, channel encoding, scrambling and modulation. The design of the horn antenna and electronics can be tested in ground based experiments, balloon experiments and further implemented into a CubeSat.
For such a channel characterization mission it is necessary to redefine the requirements and concept of operation for the propagation experiment and for the data transmission experiment.
The corner point of an attenuation measurement mission is the need for extended observation time since the statistics are time dependent. Therefore, the suggested alternatives shall be investigated. In the ideal case the satellite is located in GEO to reach the maximum possible observation time because the required durations are measured in days. An other possibility is to place the satellite constellation in orbits above 645 km and equip them with drag sails or propulsion system to fulfill the de-orbit regulations. The attitude can be maintained with magnetic torquers reducing the complexity of the overall system. This concept will enable GS across Europe to contribute with attenuation measurements to the ITU 311 database. A third possibility is a high-altitude platform station.
In the case of the data transmission experiment the concept C, in particular the transmission chain, has to be revised.

Tab. 7–1: Traceability Matrix: summary of the stated requirements and their modifications

ReqID	Parameter	Requirement	Remarks
R-MIS-001	Downlink frequency	75.5–76 GHz	TAM: 75.5–76 GHz DTE: 71.0–76 GHz
R-MIS-002	Modulation	BPSK	TAM: n/a
R-MIS-003	E_b/N_0	10 dB	TAM: C/N_0 tbd
R-MIS-004	EIRP	30 dB	
R-MIS-005	BER	$< 10^{-6}$	TAM: n/a
R-MIS-006	Sampling rate receiver	10 Hz	
R-MIS-007	Power stability Tx	$<$0.3 dB/day	
R-MIS-008	Gain stability Rx	$<$0.2 dB	
	Power measurement accuracy	$<$0.1 dB	
R-MIS-009	Polarization	horizontal	
R-MIS-010	System availability	99%	
R-SYS-001	Mission life time	14 months	TAM: 14 DTE: tbd
G-SYS-002	Extended Mission life time	36–60 months	TAM: integer multiple of 12 DTE: tbd
R-SYS-003	Orbit	daily revisit 12:00 UTC	DTE: tbd
R-SYS-004	Space segment	one 1U space craft	
R-SYS-005	Space segment	3 S/C constellation	DTE: n/a
R-SYS-006	Deorbit	within 25 years	
R-OGS-001	MOC	TUM Garching	
G-OGS-002	Mobile GS	across European climate zones	TAM: tbd DTE: n/a
R-OGS-003	GS equipment	total radiometer weather station	
R-OGS-004	Antenna diameter	0.3–0.5 m	
R-OGS-005	Receiver-Noise temp.	$<$ 1000 K	
R-OGS-006	Pointing error	$\leqslant 0.1^\circ$	TAM: tbd

Bibliography

[1] "DLR - Earth Observation Center - Big Data for the Environment." [Online]. Available: http://www.dlr.de/eoc/en/desktopdefault.aspx/tabid-5258/19488_read-47013/15811

[2] A. Jebril, M. Lucente, E. Re, T. Rossi, M. Ruggieri, C. Sacchi, and V. Dainelli, "Perspectives of W-Band for Space Communications." IEEE, 2007, pp. 1–12. [Online]. Available: http://ieeexplore.ieee.org/lpdocs/epic03/wrapper.htm?arnumber=4161395

[3] C. Bonifazi, M. Ruggieri, M. Pratesi, A. Salome, G. Varacalli, A. Paraboni, and E. Saggese, "The DAVID satellite mission of the Italian Space Agency: High rate data transmission to Internet at W and Ka bands," in *Communications, 2002. ICC 2002. IEEE International Conference on*, vol. 5. IEEE, 2002, pp. 3022–3026. [Online]. Available: http://ieeexplore.ieee.org/xpls/abs_all.jsp?arnumber=997394

[4] R. J. Acosta, J. A. Nessel, R. N. Simons, M. J. Zemba, J. R. Morse, and J. M. Budinger, "W/V-Band RF Propagation Experiment Design," 2012. [Online]. Available: http://ntrs.nasa.gov/search.jsp?R=20120016067

[5] E. Cianca, T. Rossi, A. Yahalom, Y. Pinhasi, J. Farserotu, and C. Sacchi, "EHF for Satellite Communications: The New Broadband Frontier," *Proceedings of the IEEE*, vol. 99, no. 11, pp. 1858–1881, Nov. 2011. [Online]. Available: http://ieeexplore.ieee.org/lpdocs/epic03/wrapper.htm?arnumber=5961601

[6] R. Emrick, P. Cruz, N. B. Carvalho, S. Gao, R. Quay, and P. Waltereit, "The Sky's the Limit: Key Technology and Market Trends in Satellite Communications," *IEEE Microwave Magazine*, vol. 15, no. 2, pp. 65–78, Mar. 2014. [Online]. Available: http://ieeexplore.ieee.org/lpdocs/epic03/wrapper.htm?arnumber=6763281

[7] A. Jebril, M. Lucente, M. Ruggieri, and T. Rossi, "WAVE-a new satellite mission in W-band," in *Aerospace Conference, 2005 IEEE*. IEEE, 2005, pp. 870–879. [Online]. Available: http://ieeexplore.ieee.org/xpls/abs_all.jsp?arnumber=1559378

[8] "O3bnetworks - The Reach of Satellite with the Speed of Fiber." [Online]. Available: http://www.o3bnetworks.com/

[9] "Intelsat | The Globalized Network." [Online]. Available: http://www.intelsat.com/

[10] "OneWeb." [Online]. Available: http://oneweb.world/

[11] "SpaceX seeks permission for 4,425-satellite internet constellation," Nov. 2016. [Online]. Available: http://www.spaceflightinsider.com/organizations/space-exploration-technologies/spacex-seeks-permission-4425-satellite-internet-constellation/

[12] C. Riva, C. Capsoni, L. Luini, M. Luccini, R. Nebuloni, and A. Martellucci, "The challenge of using the w band in satellite communication," *International Journal of Satellite Communications and Networking*, vol. 32, no. 3, pp. 187–200, May 2014. [Online]. Available: http://doi.wiley.com/10.1002/sat.1050

[13] R. Crane, “Propagation phenomena affecting satellite communication systems operating in the centimeter and millimeter wavelength bands,” *Proceedings of the IEEE*, vol. 59, no. 2, pp. 173–188, 1971. [Online]. Available: http://ieeexplore.ieee.org/lpdocs/epic03/wrapper.htm?arnumber=1450053

[14] G. Maral, M. Bousquet, and Z. Sun, *Satellite communications systems: systems, techniques and technology*, 5th ed. Chichester, West Sussex, U.K: John Wiley, 2009, oCLC: ocn317921066.

[15] F. T. Ulaby, D. G. Long, and W. Blackwell, *Microwave radar and radiometric remote sensing*. Ann Arbor, Mich: Univ. Of Michigan Press, 2014, oCLC: 870827227.

[16] M. Lucente, T. Rossi, A. Jebril, M. Ruggieri, S. Pulitano, A. Iera, A. Molinaro, C. Sacchi, and L. Zuliani, “Experimental Missions in W-Band: A Small LEO Satellite Approach,” *IEEE Systems Journal*, vol. 2, no. 1, pp. 90–103, Mar. 2008. [Online]. Available: http://ieeexplore.ieee.org/lpdocs/epic03/wrapper.htm?arnumber=4443222

[17] J. A. Bruder, J. T. Carlo, J. H. Gurney, and J. Gorman, “IEEE standard letter designations for radar-frequency bands,” *IEEE Aerospace & Electronic Systems Society*, pp. 1–3, 2003.

[18] G. M. Kizer, *Digital microwave communication: engineering point-to-point microwave systems*. Hoboken, New Jersey: John Wiley & Sons, Inc, 2013.

[19] I. Poole, “WG and WR Waveguide Dimensions and Sizes.” [Online]. Available: http://www.radio-electronics.com/info/antennas/waveguide/rf-waveguide-dimensions-sizes.php

[20] Electronic Communications Committee (ECC), European Conference of Postal and, and Telecommunications Administrations (CEPT), “The European table of frequency allocations and applications in the frequency range 8.3 kHz to 3000 GHz (ECA table),” Jun. 2016. [Online]. Available: http://www.erodocdb.dk/Docs/doc98/official/pdf/ERCREP025.PDF

[21] U. J. Lewark, J. Antes, J. Walheim, J. Timmermann, T. Zwick, and I. Kallfass, “Link budget analysis for future E-band gigabit satellite communication links (71–76 and 81–84 Ghz),” *CEAS Space Journal*, vol. 4, no. 1-4, pp. 41–46, Jun. 2013. [Online]. Available: http://link.springer.com/10.1007/s12567-013-0030-0

[22] C. Bonifazi, M. Ruggieri, and A. Paraboni, “The DAVID mission in the heritage of the SIRIO and ITALSAT satellites,” *IEEE Transactions on Aerospace and Electronic Systems*, vol. 38, no. 4, pp. 1371–1376, 2002. [Online]. Available: http://ieeexplore.ieee.org/xpls/abs_all.jsp?arnumber=1145759

[23] C. Sacchi, G. Gera, and C. S. Regazzoni, “W-band physical layer design issues in the context of the DAVID–DCE experiment,” *International journal of satellite communications and networking*, vol. 22, no. 2, pp. 193–215, 2004. [Online]. Available: http://onlinelibrary.wiley.com/doi/10.1002/sat.780/abstract

[24] A. Jebril, M. Lucente, T. Rossi, M. Ruggieri, and L. Zuliani, “Aero-WAVE: a W-band preliminary test using HAP,” in *2006 IEEE Aerospace Conference*. IEEE, 2006, pp. 6–pp. [Online]. Available: http://ieeexplore.ieee.org/xpls/abs_all.jsp?arnumber=1655988

[25] M. Lucente, E. Re, T. Rossi, E. Cianca, C. Stallo, M. Ruggieri, A. Jebril, C. Dionisio, G. Codispoti, and L. Zuliani, “IKNOW mission: Payload design for in orbit test of w band technology,” in *2008 IEEE Aerospace Conference*, pp. 1–10.

[26] J. A. Nessel, R. J. Acosta, and F. A. Miranda, “Preliminary experiments for the assessment of V/W-band links for space-earth communications,” in *2013 IEEE Antennas and Propagation Society International Symposium (APSURSI)*. IEEE, 2013, pp. 1616–1617. [Online]. Available: http://ieeexplore.ieee.org/xpls/abs_all.jsp?arnumber=6711467

[27] “ARTES Advanced Technology Statement of Work Cubesat-based W-band channel measurements Ref. 3b.033.” [Online]. Available: https://artes.esa.int/funding/cubesat-based-w-band-channel-measurements-artes-51-3b033

[28] Committee on Achieving Science Goals with CubeSats, Space Studies Board, Division on Engineering and Physical Sciences, and National Academies of Sciences, Engineering, and Medicine, *Achieving Science with CubeSats: Thinking Inside the Box*. Washington, D.C.: National Academies Press, Oct. 2016. [Online]. Available: http://www.nap.edu/catalog/23503

[29] “Nanosatellite and CubeSat Database | Constellations, Companies, Technologies, Instruments.” [Online]. Available: http://www.nanosats.eu/

[30] K. Woellert, P. Ehrenfreund, A. J. Ricco, and H. Hertzfeld, “Cubesats: Cost-effective science and technology platforms for emerging and developing nations,” *Advances in Space Research*, vol. 47, no. 4, pp. 663–684, Feb. 2011. [Online]. Available: http://linkinghub.elsevier.com/retrieve/pii/S0273117710006836

[31] W. Blackwell and K. Cahoy, “Small Satellite Constellations for Data Driven Atmospheric Remote Sensing,” in *Dynamic Data-Driven Environmental Systems Science*. Springer, 2015, pp. 3–9. [Online]. Available: http://link.springer.com/chapter/10.1007/978-3-319-25138-7_1

[32] A. Martinez and A. Petro, “Optical Communications and Sensor Demonstration,” 2015.

[33] B. R. Elbert, *Introduction to satellite communication*, 3rd ed., ser. The Artech House space applications series. Boston: Artech House, 2008.

[34] International Telecommunication Union (ITU), “Ionospheric propagation data and prediction methods required for the design of satellite services and systems,” *Recommendation ITU-R P.531-13*, 2016.

[35] J. M. Wallace and P. V. Hobbs, *Atmospheric science: an introductory survey*, 2nd ed., ser. International geophysics series. Amsterdam ; Boston: Elsevier Academic Press, 2006, no. v. 92.

[36] World Meteorological Organization, Ed., *International cloud atlas*, rev. ed ed., ser. WMO [publications] ; no. 407. Geneva: Secretariat of the World Meteorological Organization, 1975.

[37] International Telecommunication Union (ITU), "Attenuation due to clouds and fog," *Recommendation ITU-R P.840-6*, 2013.

[38] H. R. Pruppacher and J. D. Klett, *Microphysics of Clouds and Precipitation: Reprinted 1980*. Springer Science & Business Media, Dec. 2012.

[39] International Telecommunication Union (ITU), "The radio refractive index: its formula and refractivity data," *Recommendation ITU-R P.453-11*, 2015.

[40] ——, "Radio noise," *Recommendation ITU-R P.372-8*, no. 8, 2003. [Online]. Available: https://www.itu.int/dms_pubrec/itu-r/rec/p/R-REC-P.372-8-200304-S!!PDF-E.pdf

[41] M. Kottek, J. Grieser, C. Beck, B. Rudolf, and F. Rubel, "World map of the köppen-geiger climate classification updated," vol. 15, no. 3, pp. 259–263.

[42] "World Weather Information Service - Muenchen." [Online]. Available: http://worldweather.wmo.int/en/city.html?cityId=58

[43] "Deutscher Wetterdienst CDC (Climate Data Center)." [Online]. Available: ftp://ftp-cdc.dwd.de/pub/CDC/observations_germany/climate/monthly/kl/historical/

[44] T. S. Glickman and American Meteorological Society, Eds., *Glossary of meteorology*, 2nd ed. Boston, Mass: American Meteorological Society, 2000.

[45] International Telecommunication Union (ITU), "Propagation data and prediction methods required for the design of Earth-space telecommunication systems," *Recommendation ITU-R P.618-12*, 2015.

[46] M. G. L. Frecassetti, *E-Band and V-Band-Survey on status of worldwide regulation*. 06921 Sophia Antipolis CEDEX, France: ETSI, Jun. 2015. [Online]. Available: http://www.etsi.org/images/files/ETSIWhitePapers/etsi_wp9_e_band_and_v_band_survey_20150629.pdf

[47] J. M. Garcia-Rubia, e. Riera, P. Garcia-del Pino, and A. Benarroch, "Attenuation Measurements and Propagation Modeling in the W-Band," *IEEE Transactions on Antennas and Propagation*, vol. 61, no. 4, pp. 1860–1867, Apr. 2013. [Online]. Available: http://ieeexplore.ieee.org/document/6392207/

[48] International Telecommunication Union (ITU), "Acquisition, presentation and analysis of data in studies of radiowave propagation," *Recommendation ITU-R P.311-15*, 2015.

[49] PC/104 Embedded Consortium, "PC/104 Specification," Oct. 2008. [Online]. Available: http://pc104.org/hardware-specifications/pc104/

[50] ESA Space Debris Mitigation WG, *ESA Space Debris Mitigation Compliance Verification Guidelines*, ser. ESSB-HB-U-002. Noordwijk, The

Netherlands: European Space Research and Technology Centre, Feb. 2015. [Online]. Available: http://www.iadc-online.org/References/Docu/ESSB-HB-U-002-Issue1(19February2015).pdf

[51] The MathWorks, Inc., *MATLAB version 9.1.0.441655 (R2016b) RF Toolbox*, Natick, Massachusetts, United States, 2016.

[52] BayernAtlas. [Online]. Available: http://www.bayernatlas.de

[53] International Telecommunication Union (ITU), "Reference standard atmospheres," *Recommendation ITU-R P.835-5*, 2012.

[54] ——, "Attenuation by atmospheric gases," *Recommendation ITU-R P.676-10*, 2013.

[55] H. Häckel, *Meteorologie*, 6th ed., ser. UTB Geowissenschaften, Agrarwissenschaften. Stuttgart: Ulmer, 2008, no. 1338, oCLC: 244628657.

[56] International Telecommunication Union (ITU), "Characteristics of precipitation for propagation modelling," *Recommendation ITU-R P.837-6*, 2012.

[57] ——, "Rain height model for prediction methods," *Recommendation ITU-R P.839-4*, 2013.

[58] ——, "The concept of "worst month"," *Recommendation ITU-R P.581-2*, 1990.

[59] Analytical Graphics Inc., *Systems Tool Kit (STK) Version 11.0*, Exton, Pennsylvania, United States, 2016. [Online]. Available: http://www.agi.com/products/stk/

[60] Centre national d'études spatiales CNES, *Semi-analytic Tool for End of Life Analysis software (STELA) 3.0*, Paris, France, 2015. [Online]. Available: https://logiciels.cnes.fr/content/stela?language=en

[61] J. Smagorinsky, "Global atmospheric modeling and the numerical simulation of climate," *Weather and climate modification*, pp. 633–686, 1974.

[62] "75.5-81.5 GHz - International Amateur Radio Union - Region 1." [Online]. Available: http://www.iaru-r1.org/index.php/spectrum-and-band-plans/ehf/755-815-ghz

[63] K. W. Kark, *Antennen und Strahlungsfelder: elektromagnetische Wellen auf Leitungen, im Freiraum und ihre Abstrahlung ; mit 80 Tabellen und 128 Übungsaufgaben*, 3rd ed., ser. Studium. Wiesbaden: Vieweg + Teubner, 2010, oCLC: 496272021.

[64] SRE-FM, SRE-P, ESOC & D-TEC, *Margin philosophy for science assessment studies*, 2nd ed., ser. SRE-PA/2011.097/. Noordwijk, The Netherlands: European Space Research and Technology Centre, Dec. 2014.

[65] "Radar für Sensorik und Materialprüfung - Fraunhofer IAF." [Online]. Available: http://www.iaf.fraunhofer.de/de/leistungsangebot/elektronik/radar-sensorik-materialpruefung.html

[66] “Continental Industrial Sensors -ARS 300 Long Range Radar Sensor 77 GHz.” [Online]. Available: http://www.conti-online.com/www/industrial_sensors_de_en/themes/ars_300_en.html

[67] “FMCW Radar front end.” [Online]. Available: http://siversima.com/products/radar-sensors/

[68] M. Langer, personal communication, Oct. 2016.

[69] Dassault Systèmes, *CATIA Version 5.19*, Vélizy-Villacoublay, France, 2008.

[70] E. Decrossas, T. Reck, C. Lee, C. Jung-Kubiak, I. Mehdi, and G. Chattopadhyay, “Evaluation of 3d printing technology for corrugated horn antenna manufacturing,” in *Electromagnetic Compatibility (EMC), 2016 IEEE International Symposium on*. IEEE, 2016, pp. 251–255.

[71] EnduroSat, “EnduroSat 1u CubeSat Platform + ADCS | CubeSat by EnduroSat.” [Online]. Available: https://www.endurosat.com/capabilities-and-products/endurosat-1u-cubesat-platform-adcs/

[72] J. R. Wertz and W. J. Larson, Eds., *Space mission analysis and design*, 3rd ed., ser. Space technology library. El Segundo, Calif. : Dordrecht ; Boston: Microcosm ; Kluwer, 1999.

[73] CubeSatShop.com, “nanoSSOC-D60 digital sun sensor,” Jun. 2016. [Online]. Available: https://www.cubesatshop.com/product/nanossoc-d60-digital-sun-sensor/

[74] I. Maryland Aerospace, “MAI-400 Attitude Determination and Control Systems.” [Online]. Available: http://maiaero.com/components/

[75] Clyde Space Ltd., “Attitude Determination and Control System.” [Online]. Available: https://www.clyde.space/products/51-attitude-determination-and-control-system

[76] ESA TRL Working Group, *Guidelines for the use of TRLs in ESA programmes*, 1st ed., ser. ESSB -HB -E-002, Aug. 2013. [Online]. Available: https://artes.esa.int/sites/default/files/ESSB-HB-E-002-Issue1(21August2013).pdf

[77] CubeSatShop.com, “Deployable solar panels DSA/1a,” Jul. 2016. [Online]. Available: https://www.cubesatshop.com/product/solar-panels/

[78] M. Langer, N. Appel, M. Dziura, C. Fuchs, J. Gutsmiedl, M. Losekamm, D. Me\s smann, T. Pöschl, and C. Trinitis, “MOVE-II–der zweite Kleinsatellit der Technischen Universität München,” *Deutscher Luft-und Raumfahrtkongress (DLRK) 2015*, 2015. [Online]. Available: https://www.researchgate.net/profile/Martin_Losekamm/publication/305610780_MOVE-II_--_der_zweite_Kleinsatellit_der_Technischen_Universitat_Munchen/links/57953fc008aeb0ffccf75e90.pdf

[79] Innovative Solutions In Space, “VHF downlink/UHF uplink full duplex transceiver - ISIS,” Feb. 2016. [Online]. Available: https://www.isispace.nl/product/vhf-downlink-uhf-uplink-full-duplex-transceiver/

[80] ——, “Dipole antenna,” Apr. 2016. [Online]. Available: https://www.isispace.nl/product/dipole-antenna/

[81] ——, “ISIS on board computer,” Feb. 2016. [Online]. Available: https://www.isispace.nl/product/on-board-computer/

[82] NewSpace Systems, “NewSpace Systems – Lean Engineering.” [Online]. Available: http://www.newspacesystems.com/

[83] Clyde Space Ltd., “CS 1u Power Bundle A: EPS + 10whr Battery.” [Online]. Available: https://www.clyde.space/products/15-cs-1u-power-bundle-a-eps-10whr-battery

[84] Innovative Solutions In Space, “CubeSat Structures.” [Online]. Available: https://www.isispace.nl/product-category/satellite-products/structures/

[85] “Small Satellites, Launch, and Network Services.” [Online]. Available: http://www.spaceflight.com/schedule-pricing/

[86] A. Jebril, M. Lucente, M. Ruggieri, and T. Rossi, “W-band satellite transmission in the WAVE mission,” in *International Conference on Telecommunications & Multimedia*, 2006. [Online]. Available: http://www.temu.gr/2006/sessions%5C6%5C2%20ID%200402.pdf

[87] International Telecommunication Union (ITU), “Radiometeorological data required for the planning of terrestrial and space communication systems and space research application,” *Question 201-6/3*, 2016.

[88] W. E. Meador and W. R. Weaver, “Two-Stream Approximations to Radiative Transfer in Planetary Atmospheres: A Unified Description of Existing Methods and a New Improvement,” *Journal of the Atmospheric Sciences*, vol. 37, no. 3, pp. 630–643, Mar. 1980. [Online]. Available: http://journals.ametsoc.org/doi/abs/10.1175/1520-0469%281980%29037%3C0630%3ATSATRT%3E2.0.CO%3B2

[89] W. Zdunkowski, T. Trautmann, and A. Bott, *Radiation in the atmosphere: a course in theoretical meteorology*. Cambridge University Press, 2007.

[90] J. Wilson and N. Patwari, “Radio Tomographic Imaging with Wireless Networks,” *IEEE Transactions on Mobile Computing*, vol. 9, no. 5, pp. 621–632, May 2010. [Online]. Available: http://ieeexplore.ieee.org/document/5374407/

[91] H. Rott, personal communication, Nov. 2016.

[92] European Centre for Medium-Range Weather Forecasts, “Documentation and support | ECMWF - Atmospheric and Ocean-wave reanalysis Cycle 31r2.” [Online]. Available: http://www.ecmwf.int/en/forecasts/documentation-and-support

A First Appendix

With the Matlab built-in functions the atmospheric attenuation was simulated in accordance to the ITU recommendations.

A.1 Atmospheric simulations

```
% ITU simulations for atmospheric attenuation
% Description: In this script the attenuation due to atmospheric gases,
% clouds and rain is computed. The specific attenunation [dB/km] is
   calculated with the Matlab R2016b built in functions
% which rely on the ITU Recommendations. The input variables are defined in
% a seperate csv table covering summer and winter state of the atmosphere
% over Munich.
%
%   Author Stefan Scheiblauer
%   Date 15.Sept.2016
%   Matlab R2016b (use of built in RF propagation modules)
clear all
close all

%% Declaration of constants:
h_S=500;% Station height [m] from Bayer Atlas, asumed building height of 25
   m
freq_range=[76];%[GHz]
freq = freq_range*1E9;% conversion to Hz for Matlab functions
elev=90; % Elevation [deg]
D=0.6; % physical diameter (m) of the earth-station antenna 0.3m is the
   worst case diameter lower attenuation at 0.6m
p=1; % [%] time percentage, p, in the range between 0.01%<p<50%, also for
   rain outage

pltswitch =0; % turn on plot function=1 turn of plot function =0
AttCalc=3; % 0...computes only tropospheric attenuation, 1...total
   attenuation (free space loss and tropospheric att), enter any other
   integer number to skip the attenuation calculation
cnt=0; % counter
% Att=zeros(12,5,length(freq));
elevcount=0;

for elev=[10:1:90];
    elevcount=elevcount+1;
for ScNr=[1:5]; % loop through selected scenarios min(1),max(5)
for Month=[7]; % loop through selected months min(1),max(12)
    cnt=cnt+1;
% Scenario,ScNr,Temperature,AirPressure,WVPressure,absHumidity,WaterDensity
   ,Rainrate
fid = fopen(['C:\Users\Stefan Scheiblauer\LRZ Sync+Share\MasterThesis\
   Document\chapters\chapter02\table\Input_Variables_ITU_P_Simulation_',
   num2str(Month),'.csv'],'r');
```

```
DataImport = textscan(fid,'%s %f %f %f %f %f %f %f %f %f %f','headerlines'
   ,1,'delimiter',',');
fclose(fid);
Scenario = DataImport{1};
T_S = DataImport{3}; % Temperature at surface DWD climate station [degC]
T_d = DataImport{4}; % Dewpoint Temp at surface [degC]
p_S = DataImport{5}; % Surface AirPressure [hPa]
e_S = DataImport{6}; % Surface Water VapourPressure [hPa]
rou = DataImport{7}; % absolute humidity in [g/m3] 15 degC =7.5g/m3
cloud = [DataImport{9},DataImport{10},DataImport{8}]; % VertExtent [km] %
   HoriExtent [km] %  Liquid water density in clouds [g/m3] 0.05-0.5
rainrate = DataImport{11}; %[mm/hr] 1 light rain 50 thunderstorm
clear DataImport

[Att_gas,h_RP] = Gas_Attenuation(freq,elev,Month); % o2 water vapour
[Att_cloud] = Cloud_Attenuation( h_S,elev,freq,T_S(ScNr),T_d(ScNr),cloud(
   ScNr,:) ); % 4 types of clouds, and clear sky
[Att_rain] = Rain_Attenuation ( freq,elev,rainrate(ScNr),h_RP,h_S,p ); %
   call function for rain attenuation
[Att_scin] = scintillation ( T_S(ScNr),e_S(ScNr),freq,elev,D,p );

%% computation of total attenuations
Att_total = Att_gas + ((Att_rain+ Att_cloud).^2 + Att_scin.^2).^0.5;
% AttGas(elevcount,ScNr)=Att_gas;
% AttRain(elevcount,ScNr)=Att_rain;
% AttCloud(elevcount,ScNr)=Att_cloud;
% AttScin(elevcount,ScNr)=Att_scin;
%% Noise temperature ITU 618
Att4NoiseCalc = Att_gas + ((Att_rain+ Att_cloud).^2 ).^0.5;
T_mr = 37.34 + 0.81*(273+T_S(ScNr)); %[K]
T_sky(elevcount,ScNr+1)=T_mr*(1-10^(-Att4NoiseCalc/10))+(2.7*10^(-
   Att4NoiseCalc/10));

% attenuation as a function of elevation
if AttCalc==0; Att(elevcount,ScNr)=Att_total; elseif AttCalc==1;
Orbit_height=[570.5/sind(elev)];
Att(elevcount,ScNr)=Att_total+10.*log10((4.*pi.*Orbit_height.*1000./(3e8./
   freq)).^2);
else;end

if pltswitch==1
% % plot figure
h(cnt)=figure;
if ScNr==1
    semilogy(freq_range,Att_gas,'b-',freq_range,Att_scin,'b--',freq_range,
       Att_total,'k-','linewidth',2)
    legend('O_2 Water Vapour','Scintillation','Total','Location','SouthEast
       ')
elseif ScNr==4 |ScNr==5
    semilogy(freq_range,Att_gas,'b-',freq_range,Att_cloud,'g-',freq_range,
       Att_rain,'r-',freq_range,Att_scin,'b--',freq_range,Att_total,'k-','
       linewidth',2)
    legend('O_2 Water Vapour','Clouds','Rain','Scintillation','Total','
       Location','SouthEast')
else
```

```
    semilogy(freq_range,Att_gas,'b-',freq_range,Att_cloud,'g-',freq_range,
       Att_scin,'b--',freq_range,Att_total,'k-','linewidth',2)
    legend('O_2 Water Vapour','Clouds','Scintillation','Total','Location','
       SouthEast')
end
xlim([min(freq_range) max(freq_range)]);
ylim([1E-2 1E2]);
xlabel('Frequency [GHz]')
ylabel('Attenuation [dB]')
title(Scenario(ScNr))
% hold on
text(gca,'String',[num2str(p),'% outage, ',num2str(elev),' elevation'],'
   Position',[72 10^-1.7]);
saveas(h(cnt),['C:\Users\Stefan Scheiblauer\LRZ Sync+Share\MasterThesis\
   Document\chapters\chapter02\figures\Scenario_',num2str(ScNr),'_M',
   num2str(Month),'_e',num2str(elev),'p',num2str(p),'_',datestr(now,'
   yyyymmdd'),'.fig'])
saveas(h(cnt),['C:\Users\Stefan Scheiblauer\LRZ Sync+Share\MasterThesis\
   Document\chapters\chapter02\figures\Scenario_',num2str(ScNr),'_M',
   num2str(Month),'_e',num2str(elev),'p',num2str(p),'_',datestr(now,'
   yyyymmdd'),'.jpg'])
else; end
%
end
end
end;
% EOF
```

A.1.1 Gaseous attenuation

```
function [Att_gas,h_RP] = Gas_Attenuation(freq,elev,Month);
% ITU simulations for gaseous atmospheric attenuation
% Description: In this script the attenuation due to atmospheric gases,
% the Matlab R2016b built in functions which rely on the ITU
   Recommendations. The input variables are defined in
% a seperate csv table covering summer and winter state of the atmosphere
% over Munich.
%
%   Author Stefan Scheiblauer
%   Date 15.Sept.2016
%   Matlab R2016b (use of built in RF propagation modules)
%   Rec.  ITU-R  P.676-10
% Input:
% freq: frequency in Hz
% elev: elevation angle in deg
% Month: number of month int
%
% Output:
% Att_gas: attenuation of the whole atmosphere from 0 to 100km height due
   to gas in dB
% h_RP rain parameter: rain height; pressure and water vappour density at
   that level

delta=(1E-4)*exp(([1:922]-1)/100); % devide the atmosphere in layers Rec.
```

```
    ITU-R P.676-10 Eq 21
[n,T,rho,P,h_RP]=VertProfile(Month,cumsum(delta)); % standard atmosphere
    based on height profile according to Rec. ITU-R P.835-5 for high
    latitude lat >45deg
r=ones(size(delta))*6371;% km radius of the earth
beta=ones(size(delta))*degtorad(90-elev); %complemetary angle of elevation
gamma_gas=zeros(size(delta));
alpha=zeros(size(delta));
a=zeros(size(delta));
Att_gas=zeros(size(freq));

for j=1:length(freq); %loop throug all frequencies
    for i=1:length(delta)-1; %loop throug all atmospheric layers
        a(i)=-r(i)*cos(beta(i))+0.5*(4*r(i)^2*(cos(beta(i)))^2+8*r(i)*delta
            (i)+4*delta(i)^2)^0.5; % a_n is  the  path  length  through
            layer n eq 17
        alpha(i)=pi-acos((-2*a(i)^2-2*r(i)*delta(i)-delta(i)^2)/(2*a(i)*r(i
            )+2*a(i)*delta(i))); %ITU-R P.676-10 Eq 18
        gamma_gas(i) = gaspl(1000,freq(j),T(i),100*P(i),rho(i)); % ITU-R
            P.676-10 Eq 1 = Matlab built in function for spcific gaseous
            atteuation
        beta(i+1)=asin((n(i)/n(i+1))*sin(alpha(i))); % Rec. ITU-R P.676-10
            Eq 19
        r(i+1)=r(i)+delta(i); % Rec. ITU-R P.676-10 See Figure 4 in Rec.
            ITU-R P.676-10
    end

Att_gas(j)=sum(gamma_gas.*a); % total attenuation Rec. ITU-R P.676-10 Eq 20
end

end
%EOF
```

A.1.2 Cloud attenuation

```
function [ Att_cloud ] = Cloud_Attenuation( h_S,elev,freq,T_S,T_d,cloud );
%Cloud_Attenuation: Attenuation due to clouds and fog Rec. ITU-R P.840-6
%   Author Stefan Scheiblauer
%   Date 15.Sept.2016
%   Matlab R2016b (use of built in RF propagation modules)
%
% Input:
% h_S: Station height [m]
% freq: frequency in Hz
% elev: elevation angle in deg
% T_S: Temperature at surface DWD climate station [degC]
% T_d:Dewpoint Temp at surface [degC]
% cloud: % VertExtent [km] % HoriExtent [km] %  Liquid water density in
    clouds [g/m3] 0.05-0.5
%
% Output:
% Att_cloud: attenuation due to clouds as a function of cloud type def. in
    cloud.
```

```
% set cloud attenuation to zero dB in clear sky conditions
if cloud(1)==0&cloud(2)==0; Att_cloud=zeros(size(freq)); else

h_S=h_S*1E-3; % altitude of groundstation
h_LCL=.122*(T_S-T_d); % Computation of lifting condensation level LCL 100%
    rH Hackel, Meteorologie page 92
T_LCL=T_S-(h_LCL*(9.8));% Temperature at LCL = ambient temperature for
    function fogpl

% pathlength computation, depending on vertical and horizontal extent of
% the cloud; funct(cloud_typ)
crit_el=atand(cloud(1)/cloud(2));
if elev>crit_el &elev<=90
    pathlength=cloud(1)/sind(elev);
elseif elev==crit_el;
    pathlength=(cloud(1)^2+cloud(2)^2)^.5;
elseif elev>=0&elev<crit_el;
    pathlength=cloud(2)/cosd(elev);
else
end

Att_cloud = fogpl(pathlength*1E3,freq,T_LCL,cloud(3)); % Matlab Built in
    Function based on Rec. ITU-R P.840-6 Eq 1 16 deg ambient temp
end
end
% EOF
```

A.1.3 Rain attenuation

```
function [ Att_rain ] = Rain_Attenuation ( freq,elev,rainrate,h_RP,h_S,p )
% Rain_Attenuation: Computation of attenuation due to rain according
% Rec. ITU-R P.618-12
%    Author Stefan Scheiblauer
%    Date 22.Sept.2016
%    Matlab R2016b (use of built in RF propagation modules)
%
% %INPUT VARIABLES
%    freq: frequency (GHz), where 4 GHz < f < 20 GHz
%    elev: elevation [deg]
%    h_RP: rain parameter: rain height; pressure and water vappour density
    at that level
%    h_S: altitude oof groundstation [m]
%    rainrate: 0,5,40(0.01% outage Rec.  ITU-R  P.837-6) [mm/h]
% %OUTPUT:
%    Att_rain: attenuation due to rain depending on rain rate [dB]

if rainrate>0;
%% CONSTANTS:
Re=8500; % effective radius of the Earth (8 500 km).
h_S=h_S*1E-3; % conversion from [m] to [km],
% phi=48.266149; % [deg] latitude of the earth station (degrees)
tau=0; % Tilt angle of polarization ellipse, 0 = horizontal worst case

%% CALCULATIONS:
```

```
% Step 1: Determine the rain height, hR, as given in Recommendation ITU-R
   P.839 (input to function computed in VertProfile acc ITU-R P.839-4

% Step 2: For elev > 5 deg compute the slant-path length, L_s, below the
% rain height from, If hR -hs is less than or equal to zero, the predicted
   rain attenuation for any time percentage is zero
% and the following steps are not required.
if (h_RP(1)-h_S)>0

    if elev>=5
        L_S=(h_RP(1)-h_S)/sind(elev); % slant-path length, L_s [km]
    elseif elev <5 & elev >=0
        L_S=2*(h_RP(1)-h_S)/(((sind(elev))^2+(2*(h_RP(1)-h_S)/Re))^0.5+sind
            (elev)); % slant-path length, L_s [km]
    else
    end

% Step 3: Calculate the horizontal projection, LG, of the slant-path length
    from:
L_G=L_S*cosd(elev); %[km]

% Step 5: Obtain the specific attenuation, gamma_rain [dB/km] using the
   frequency-dependent coefficients given in Recommendation ITU-R P.838 and
    the rainfall rate, R0.01, determined from Step 4, by using:
% ~16 dB/km acc. to nomogram at 40mm/h and 70 GHz Maral, Satellite
   Communication p205
% ~17 dB/km acc. to nomogram at 40mm/h and 80 GHz Maral, Satellite
   Communication p205
gamma_rain = rainpl(1000,freq,rainrate,0,tau); % [dB/km] Rec. ITU-R P.618
   -12 Eq 4; computation of specific rain attenuation with malab built in
   based on Recommendation ITU-R P.838-3, input 1000m and zero ellevation


% Step 6: Calculate the horizontal reduction factor, r, for 0.01% of the
   time:
r=(1+(0.78.*((L_G.*gamma_rain)./freq).^0.5)-0.38.*(1-exp(-2.*L_G))).^-1; %
   Rec. ITU-R P.618-12 Eq 5

% Step 7: Calculate the vertical adjustment factor, v0.01, for 0.01% of the
    time:
xi=atand((h_RP(1)-h_S)./(L_G.*r));

if xi>elev
    L_R=(L_G.*r)./cosd(elev); %[km]
else
    L_R=(h_RP(1)-h_S)./sind(elev); %[km]
end
v001=( 1+ (((sind(elev)).^.5 ).*(31.*(1-exp(-elev)).*(((L_R.*gamma_rain).^0
   .5)./(freq.^2))-0.45))).^-1;

% Step 8: The effective path length is:
L_E=L_R.*v001; %[km]

% Step 9: The predicted attenuation exceeded for 0.01% of an average year
   is obtained from:
```

```
A001=gamma_rain.*L_E;  % [dB]

% Step 10: The estimated attenuation to be exceeded for other percentages
   of an average year, in the range 0.001% to 5%, is determined from the
   attenuation to be exceeded for 0.01% for an average year:
% If p > 1% or |phi| >= 36 deg: beta = 0 Equation 8

Att_rain=A001.*(p./0.01).^(-(0.655+0.033*log(p)-0.045*log(A001)));


else; Att_rain=zeros(size(freq));end;
else; Att_rain=zeros(size(freq));end;
```

A.1.4 Scintillation

```
function [ Att_scin ] = scintillation ( T,e,f,elev,D,p )
% scintillation: Computation of attenuation due to scintillation according
% to Rec. ITU-R  P.618-12 https://www.itu.int/dms_pubrec/itu-r/rec/p/R-REC-
   P.618-12-201507-I!!PDF-E.pdf
% and Rec. ITU-R  P.453-11 http://www.itu.int/dms_pubrec/itu-r/rec/p/R-REC-
   P.453-11-201507-I!!PDF-E.pdf
%    Author Stefan Scheiblauer
%    Date 19.Sept.2016
%    Matlab R2016b (use of built in RF propagation modules)
%
% %INPUT VARIABLES
%    T average surface ambient temperature (deg C) at the site for a period
     of one month or longer
%    H average surface relative humidity (%) at the site for a
   period of one month or longer
%    e water vapour pressure (hPa) from DWD climatstations
%    f frequency (GHz), where 4 GHz < f < 20 GHz
%    theta free space elevation angle theta >5deg
%    D physical diameter (m) of the earth-station antenna
%    eta antenna efficiency; if unknown,eta =0.5 is a conservative estimate
%
% %OUTPUT:
%    Att_scin

%% CONSTANTS:
h_L =1000; % the height of the turbulent layer, is 1000m
eta =0.5; % eta antenna efficiency; if unknown,eta =0.5 is a conservative
   estimate

%% Conversions:
f=f*(1E-9); % conversion from Hz to GHz
T=T+273; % conversion from deg C to K

%% CALCULATIONS:

% Step 2:Compute the wet term of the radio refractivity
N_wet=(72.*(e./T))+((3.75E5).*(e./(T.^2))); % wet term of the radio
   refractivity Rec. ITU-R  P.453-11 Equ 4
```

```
% Step 3:Calculate the standard deviation of the reference signal amplitude
sigma_ref=(3.6E-3)+((1E-4).*N_wet); % [dB] standard deviation of the
    reference signal amplitude; ITU-R  P.618-12 Equ 43

% Step 4:Calculate the effective path length L
L=(2.*h_L)./(((((sind(elev)).^2)+2.35E-4)^0.5)+sind(elev)); % [m] Calculate
     the effective path length L [m] ITU-R  P.618-12 Equ 44

% Step 5:Estimate  the  effective  antenna  diameter
D_eff=((eta)^0.5)*D; % [m] effective antenna diameter

% Step 6:Calculate the antenna averaging factor
x=1.22.*D_eff.*(f./L);
    tmp=(((3.86.*((x.^2+1).^(11./12))).*(sin((11./6).*(atan(1./x)).^(-1))))
        -(7.08.*x.^(5./6)));
    tmp(tmp < 0)= 1E-12; % If the argument of the square root is negative,
        the predicted scintillation fade depth for any time percentage is
        zero and the following steps are not required
g_x=tmp.^0.5; % antenna a veraging factor

% Step 7:Calculate the standard deviation of the signal for the applicable
    period and propagation path
sigma=sigma_ref.*(f.^(7/12)).*(g_x./(sind(elev).^1.2));

% Step 8:Calculate the time percentage factor, a(p), for the time
    percentage, p, in the range between 0.01%<p <50%
a_p=(-0.061.*(log10(p)).^3)+(0.072.*(log10(p)).^2)-(1.71.*(log10(p)))+3;

% Step 9:Calculate the fade depth, A(p), exceeded forp% of the time:
Att_scin=a_p.*sigma;

end
% EOF
```

A.1.5 Standard atmosphere

```
function [n,T,rho,P,h_RP]=VertProfile(Month,h_profile)
% Standard Summer, winter atmosphere for lat >45 deg acc to ITU REC-P.835
% http://www.itu.int/dms_pubrec/itu-r/rec/p/R-REC-P.835-5-201202-I!!PDF-
    E.pdf
%    Author Stefan Scheiblauer
%    Date 22.Sept.2016
%    Matlab R2016b (use of built in RF propagation modules)
%
% %INPUT VARIABLES
% Month of the year integer number  1-12; 1 = Jan
% h_profile: vertical spacing of layers in km
%
% %OUTPUT:
% n refractive index as function of h_profile
% T temperature as function of h_profile [K]
% rho water vapour density [g/m3]
% P pressure as function of h_profile [hPa]
% h_RP rain parameter: rain height; pressure and water vappour density at
```

```
    that level

h=h_profile;
if Month >3 &Month <=9; % Summer High latitude Profile
    for i=1:length(h);

%% The temperature T(K) at height h(km) in SUMMER is given by Rec.  ITU-R
    P.835-5 section 4
    if h(i) >=0 & h(i) <10;
         a=-0.1402;
        b=-4.7805;
        c=286.8374;
        T(i)=c+b*h(i)+a*h(i)^2;
        h_0=2.7751; %bilinear interpolated from map ITU R-REC-P.839-4
        h_RP(1)=h_0+0.36;  % height of zero deg isotherm [km]above mean sea
            level,hR
    elseif h(i)>=10 &h(i)<23;
        T(i)=225;
    elseif h(i)>=23 &h(i)<48;
        T(i)=225*exp((h(i)-23)*0.008317);
    elseif h(i)>=48 &h(i)<53;
        T(i)=277;
    elseif h(i)>=53 &h(i)<79;
        T(i)=277-(h(i)-53)*4.0769;
    elseif h(i)>=79 &h(i)<=100;
        T(i)=171;
    else
        T(i)=nan;
    end

%% The  pressure P(hPa):  at height h(km) in SUMMER is given by Rec.  ITU-R
     P.835-5 section 4
    if h(i)>=0 & h(i) <=10;
        P(i)= 1008.0278-113.2494*h(i)+3.9408*h(i)^2;
        h_RP(2)= 1008.0278-113.2494*h_RP(1)+3.9408*h_RP(1)^2;
    elseif h(i)>10 & h(i) <=72;
        P(i)=(1008.0278-113.2494*10+3.9408*10^2)*exp(-0.140*(h(i)-10));
    elseif h(i)>72 & h(i) <=100;
        P(i)=(1008.0278-113.2494*10+3.9408*10^2)*exp(-0.140*(72-10))*exp(-0
            .165*(h(i)-72));
    else
        P(i)=nan;
    end

%% The  water vapour (g/m3):  at height h(km) in SUMMER is given by Rec.
    ITU-R  P.835-5 section 4
    if h(i)>=0 & h(i) <=15;
        rho(i)=8.988*exp(-0.3614*h(i)- 0.005402*h(i)^2-0.001955*h(i)^3);
        h_RP(3)=8.988*exp(-0.3614*h_RP(1)- 0.005402*h_RP(1)^2-0.001955*h_RP
            (1)^3);
    elseif h(i)>15
        rho(i)=0;
    else
        rho(i)=nan;
    end
```

```
    end; %end for loop

elseif (Month >=1 &Month <=3)|(Month >9 &Month <=12); % Winter High
    latitude Profile
    for i=1:length(h);

%% The temperature T(K) at height h(km) in WINTER is given by Rec.  ITU-R
    P.835-5 section 4
    if h(i) >=0 & h(i) <8.5;
         a=0.08473;
        b=-1.5479;
        c=2.3474;
        d=257.4345;
        T(i)=d+c*h(i)+b*h(i)^2+a*h(i)^3;
        h_0=2.7751; %bilinear interpolated from map ITU R-REC-P.839-4
        h_RP(1)=h_0+0.36;  % height of zero deg isotherm [km]above mean sea
            level,hR
    elseif h(i)>=8.5 &h(i)<30;
        T(i)=217.5;
    elseif h(i)>=30 &h(i)<50;
        T(i)=217.5 + (h(i) - 30)*2.125;
    elseif h(i)>=50 &h(i)<54;
        T(i)=260;
    elseif h(i)>=54 &h(i)<100;
        T(i)=260 - (h(i) - 54)*1.667;
    else
        T(i)=nan;
    end

%% The  pressure P(hPa):  at height h(km) in WINTER is given by Rec.  ITU-R
     P.835-5 section 4
    if h(i)>=0 & h(i) <=10;
        P(i)=1010.8828 -122.2411*h(i) + 4.554*h(i)^2;
        h_RP(2)=1010.8828 -122.2411*h_RP(1) + 4.554*h_RP(1)^2;
    elseif h(i)>10 & h(i) <=72;
        P(i)=(1010.8828 -122.2411*10 + 4.554*10^2)*exp(-0.147*(h(i)-10));
    elseif h(i)>72 & h(i) <=100;
        P(i)=((1010.8828 -122.2411*10 + 4.554*10^2)*exp(-0.147*(72-10)))*
            exp(-0.150*(h(i)-72));
    else
        P(i)=nan;
    end

%% The  water vapour (g/m3):  at height h(km) in WINTER is given by Rec.
    ITU-R  P.835-5 section 4
    if h(i)>=0 & h(i) <=10;
        rho(i)=1.2319*exp(0.07481*h(i)-0.0981*h(i)^2 + 0.00281*h(i)^3);
        h_RP(3)=1.2319*exp(0.07481*h_RP(1)-0.0981*h_RP(1)^2 + 0.00281*h_RP
            (1)^3);
    elseif h(i)>10
        rho(i)=0;
    else
        rho(i)=nan;
    end
```

```
    end; %end for loop

else
end

%% compute based on temperature profile vatervapour profil, profile of
   refractive index
e=(rho.*T)./216.7;
N=77.6.*(P./T)-5.6.*(e./T)+(3.75E5).*(e./T.^2);
n=1+N*1E-6;
end
%EOF
```

A.2 Payload design

The budget calculations for the payload design were based on textbooks and on the results of the attenuation computations and the STK simulations.

A.2.1 Link budget

```
% Antenna Parameters
% Description: This script is used to calculate thelink budget for the
% W-band payload. Calculations are performed for the modulated and
% unmodulated up and downlink. Attmospheric attenuation is derived with
% the script ITU_Simulations.m the orbit height was computed with STK.
%
%   Author Stefan Scheiblauer
%   Date 10.Oct.2016
%   Matlab R2016b (use of built in RF propagation modules)

% to find satellite transmit power via EIRP
% clear all

%% CONSTANTS:
c=3e8; % [m/s] velocity of lght
k=-228; % Boltzman constant
elev=[90]';
%% REQUIREMENTS:
f=[76]*1e9; % [Hz] Downlink 76  / Uplink frequency 86Ghz
Orbit_height=[570.5./sind(elev)]; % [km] STK Simulation
DR=10.*log10([1e6 10e6]); % [dB] datarate of 1Mbps and 10Mbps
D_T=0.03; % [m] antenna horn diameter satellite / transmit
D_R=0.3; % [m] antenna dish Ground Station /receive 0.3 like Nasa paper
EIRP=30; % [dBW] req acosta
EbNoReq=10; % [dB] the energy per bit to noise power spectral density ratio
    Lewark 2013, maral states 6.9dB for BPSK and 7/8 coding
%% ASSUMPTIONS DATA SHEET
Margin_ESA=3;% [dB] Additional margin of 3dB ESA Margin philosophy for
   science assessment studies 2.0
Tsys=30; %System Noise Temperatuer noistem GS from Lucente 2008 30 dB/
   acostaa 2012 1200K =30.8dBK
eta=0.5; % efficiency satellite equipment / Ground equipment
```

```
% Att_trop_Jan=[0.413844471225595 1.01173372655112 2.94949005357670 2
    .39355839512870 11.4945546292648]; % January,90 elevation
% Att_trop_Jul=[0.827562696374450 3.94455465722990 9.51690611834385 5
    .23158447708745 17.7350661759560]; % July,90 elevation
%
% Att_trop=Att_trop_Jan';
% minimum elevation berechnen

%% Caclculations
Space_Loss=10.*log10((4.*pi.*Orbit_height.*1000./(c./f)).^2); % [dB] maral
    172
theta3dB(1)=2.*asind((0.5662*(c/f))./D_T) % 3 DB antenna beam width for
    horn antenna Kark 2010 Equ 14.60 in the more stringent E-Plane
theta3dB(2)=70.*(3e8./(f.*D_R)) % 3 DB antenna beam width Maral 2009 eq 5
    .4b

Depointing=2+sum(12.*(0.1./theta3dB).^2) % max pointing error <0.1 deg
    Ciana 2011 plus 2db savety margin
G_Tmax=24.8011;%[dBi] hornantenna diameter 40mm length of 131mm; 24.8011
    dBi for 30 mm diametera nd length of 74 mm acc to Kark 2010
% G_Tmax=10.*log10(eta.*((pi.*D_T.*f)./c).^2) % maximum Tx antenna gain
    Maral 2009 eq 5.3
G_Rmax=10.*log10(eta.*((pi.*D_R.*f)./c).^2);  % maximum Rx antenna gain
    Maral 2009 eq 5.3

% assumed values
G_Rmax=45;
Depointing=2.4;

DR=10.*log10(10e6);
scen=2;
for scen=2:2;
if scen==1;
    % January;
    load('LTrop_inkl_Lfs_allscenarios_1.mat')
    tit={'Maximum data rate January'};
    leg={'Clear sky',' Stratus St','Nimbostratus Ns','Moderate rain St','
       Heavy rain Ns'}
elseif scen==2;
    % July;
    load('LTrop_inkl_Lfs_allscenarios_7.mat');
    tit={'Maximum data rate July'};
    leg={'Clear sky','Cumulus Cu','Cumulonimbus Cb','Moderate rain Cu','
       Heavy rain Cb'};
end

% P_T=EIRP-G_Tmax % [dB] subtract from the required (Acosta) EIRP the gain
    to get the power
P_TCalc=(EbNoReq+Att+Depointing-G_Tmax-G_Rmax-228+Tsys+DR+Margin_ESA) % [dB
    ] P_TCalc is the power reqired based on the requirement of min 10 dB
    EBNo; Messerschmid 2011 EQU. 12.6
EbNo_Calc=EIRP-Att-Depointing+228-DR+G_Rmax-Margin_ESA % [dB] EbNo_Calc is
    the actual EbNo with the reqired 30 dB EIRP; Messerschmid 2011 EQU. 12.6
CNo=EbNo_Calc+DR;  % [dB] Carrier to noise ratio based on EIRP of 30 dB and
    min 10 dB EbNo; Messerschmid 2011 EQU. 12.7
```

```
% Critical_Att=EbNoReq+10.*log10([1e6 10e6])-EIRP-G_Rmax+Tsys-228+
    Margin_ESA;
Critical_Att=EIRP-(EbNoReq+Depointing-G_Rmax-228+Tsys+10.*log10([1e6 10e6])
    +Margin_ESA);


DR_felev=(10.^((EIRP-EbNoReq-Att-Depointing+G_Rmax+228-Tsys-Margin_ESA).
    /10));
figure
plot([10:90],DR_felev/1e6)
xlim([10 90])
ylim([0 15])
grid on
legend(leg)
title(tit)
xlabel('Elevation [deg]')
ylabel('Data rate [Mbit/s]')
end
```

A.2.2 Power Budget

```
% Power Budget
% estimate of solar panel area and battery capacity
%   Author Stefan Scheiblauer
%   Date 10.Nov.2016
%   Matlab R2016b (use of built in RF propagation modules)

% computation of solar panel area: Messerschmid eq 8.9
OrbLifeTime=2.2; %years assumed (SMAD DOD) even STK shows lifetime of 8.2
    years
phi=1371; %W/m2
te=2114.936; % [s] STK orbit 2
to=24*60; % [s] STK orbit 2

tu=5760; %[s] STK orbit 2
etaEVA=0.19; % from EXA
etaSp=0.9; % assumed
DOD=0.45; % depth of discharge
BOL=1; % from Clyde Space
EOL=BOL*exp(-0.043*OrbLifeTime); % no info; esteimate from Maral Equ: 10.26
P=[5.51 7.51];
A=(P./phi).*(1./etaEVA).*(1+(1./etaSp).*(to./(tu-to))).*(BOL./EOL); %
    computation of solar panel area: Messerschmid eq 8.9

Wsp=P./(etaSp.*DOD);
% Amph=Wsp/5
% EOF
```

A.2.3 Optimum conical horn

```
% Horn Antenna dimensions
% comparison between length and diameter of optimum conical horn antenna
% with resulting antenna gain and transmit power for an EIRP of 30 dB
```

```
%   Author Stefan Scheiblauer
%   Date 10.Nov.2016
%   Matlab R2016b (use of built in RF propagation modules)

close all

EIRP=30; % R-MIS-005
diameter=[10:1:90]; %R-SYS-004

length=(diameter.^2)./(3.127*3.9);
gain=7.08+20.*log10(diameter/3.9); %[dB]
P_Tx=EIRP-gain; %[dB]

Theta_E=2.*asind((0.5662*3.9)./diameter); % Kark 2010 Equ 14.60
Theta_H=2.*asind((0.6639*3.9)./diameter); % Kark 2010 Equ 14.60

% label ticks
diameter_label=[10:10:90];
length_label=(diameter_label.^2)./(3.127*3.9);
gain_label=7.08+20.*log10(diameter_label/3.9); %[dB]
P_Tx_label=EIRP-gain_label; %[dB]


figure;
% axis for length
b=axes('Position',[.1 .15 .75 1e-12]);
set(b,'Units','normalized');
set(b,'Color','none');

% axis for diameter
a=axes('Position',[.1 .3 .75 .6]);
set(a,'Units','normalized');
plot(a,diameter,gain)

% set limits and labels
set(a,'xlim',[min(diameter) max(diameter)]);
set(b,'xlim',[min(diameter) max(diameter)]);
xlabel(a,'diameter [mm]')
xlabel(b,'length [mm]')
set(b,'xtick',diameter_label,'Xticklabels',round(length_label))

ylabel(a,'gain [dBi]');
yyaxis right
set(gca,'ylim',[min(gain) max(gain)],'Ytick',gain_label,'Yticklabels',round
    (10.^(P_Tx_label./10),1))
ylabel('transmit power [W]')
title(a,'Gain of conical horn antenna for EIRP =30 dBi')
grid on
% EOF
```

A.2.4 Estimated downlinked data volume

```
% Max DataVolume
% estimation of the maximum downlink data volume for the best case in
```

```
% January and the worst case in July. Conversion of the data volume from Gb
% with the coding rate to MB. Elevation angles of the GS antena taken from
% STK during pointing.
%   Author Stefan Scheiblauer
%   Date 04.Jan.2017
%   Matlab R2016b (use of built in RF propagation modules)

Month=7;    % 1=January;    7=July;
Pointing=0; % 1=on;         0=off=nadir;
if Month==1;
    load('MaxDataRateJan.mat')
    MaxDataRate=MaxDataRateJan;
    clear MaxDataRateJan
elseif Month==7;
    load('MaxDataRateJul.mat')
    MaxDataRate=MaxDataRateJul;
    clear MaxDataRateJul
else;
end;

if Pointing==1;
    % elevation angles pointing; duration of the elevation angle
    EleDataRate= [3 60;8 60;14 60;23 60;39 60;70 60;66 60;37 60;22 60;13
       60;7 60;2 60];
elseif Pointing==0;
    % elevation angles angles nadir; duration of the elevation angle
    EleDataRate=[80 2;85 2;90 2;85 2;80 2];
else;end;

dt=mean(EleDataRate(:,2)); %time step in seconds
[n,m]=ismember(EleDataRate(:,1),MaxDataRate(:,1));
ind=m(m>0);

Gb=round((sum(MaxDataRate(ind,[2:6]).*dt*1e-9)),1) %Gigabit [Gb]
Mb=round((sum(MaxDataRate(ind,[2:6]).*dt*1e-6)),1) %Megabit [Mb]
MB=round((sum(MaxDataRate(ind,[2:6]).*dt.*1e-9))*(1000/8)*(7/8),1) %
   Megabyte [MB]
% EOF
```

A.2.5 Bit error rate for BPSK

```
% BER Analysis
% estimation of the BER for BPSK depending on Eb/No and Coding rate rho
% Script based on Maral, Satellite Comm.
%   Author Stefan Scheiblauer
%   Date 25.Jan.2017
%   Matlab R2016b (use of built in RF propagation modules)
close all

rho=[1 7/8 3/4 2/3 1/2]'; % Coding Rates
EbN0=2:0.1:11; % EbNo

EcN0_dB=zeros(length(rho),length(EbN0));
EcN0=zeros(size(EcN0_dB));
```

```
BER=zeros(size(EcN0_dB));

figure
EcN0_dB = EbN0-10.*log10(rho); %Maral equ. 4.13
EcN0 = 10.^(EcN0_dB/10);
BER = 1/2.*erfc(sqrt(EcN0)); %Maral tab. 4.3
semilogy(EbN0,BER);
grid on
ylabel('BER')
xlabel('E_b/N_0 (dB)')
title('Bit Error Rate for Binary Phase-Shift Keying')
legend(num2str(rho))
%EOF
```